Ministry of Higher Education and Scientific Research

University of Baghdad

Institute of Laser for Postgraduate Studies

Study the Effect of ZnO, Ag Nanoparticles on Bacteria with and without 410 nm Diode Laser

A Thesis Submitted to the Institute of Laser for Postgraduate Studies, University of Baghdad in Partial Fulfillment of the Requirements for the Degree of Master of Science in Laser / Physics

By

Hiba Taqi Saleh

B.Sc. Medical Physics – 2008

Supervisor

Asst. Prof. Dr. Zainab Fadhil Mahdi

2020 A.C **1442 A.H**

بســم الله الرحمــن الرحيـم

﴿ وَمَا تَوْفِيقِي إِلا بِاللَّهِ عَلَيْهِ تَوَكَّلْتُ وَإِلَيْهِ أُنِيبُ ﴾

صدق الله العظيم

سورة هود الاية " 88 "

الاهـــداء

إلى من أحمل أسمـه بكل فخـر.. إلى من غرسـني ولم يشـهـد آوان عطائي .. إلى عـزيز قلبي

والـدي العزيـز (رحمه الله)

إلى مـن ركـع العطاء أمـام قدمـيها .. إلى مـن أعـطت من دمهـا وروحهـا وعمرها حبا وتصميمـا لغد اجمـل .. إلى من كان دعـائها سـر نجاحي ...الى أغـلى الاحبـة

أمـــي الحـبيبـة

إلى الشمعــة المتقـدة التي تنيــر دربـي .. إلى مـن آنسني دراستـي وشـاركني همـومـي .. إلى من بوجـوده اكتسـب قـوه ومحبـة لاحـدود لها

أخـــي الغـالـي

هبـــة

Acknowledgement

First of all, I begin with immeasurable gratitude to Almighty **Allah** who has sustained me, gave me the strength to pass my way successfully.

I would like to express my grateful, appreciation, and sincere thanks to my supervisor **Dr. Zainab Fadhil Mahdi**, for guidance, help and valuable advice in all stages of this work.

I would like to give special thanks to Dean of the Institute of Laser for Postgraduate Studies **Prof. Dr. Hussein Ali Jawad**, for his support during the study and research work.

I would like to express my deep gratitude and appreciation to **Dr. Mohamed K. Dhahir** for paternal support, kind advice, encouragement and help through this work. My thanks to **Mr. Sinan A. Muhi**, in Iraqi National Monitoring Authority (INMA), for his help and continuous support during the period of study. Also, I introduce my thanks to **Miss. Hiba K.Wahhib**, for his help and support.

In particular, I am also eternally grateful to **my father** soul and **my mother** the source of inspiration and a pillar of strength in every aspect of my life. Special Gratitude is due to my brother **"Ahmed"** whose dedication, affection and persistent confidence in me, has taken the load off my shoulder.

Finally, I would like to express my thanks to **"my friends",** for their never ending moral support.

Hiba

September 2020

Abstract

The green synthesis method was used as a faster metallic nanoparticle production by offering an environmentally friendly, simple, non-toxic, economical, and reproducible approach. In this method, an extract plant root Withania Somnifera (Ashwagandha) with silver and zinc oxide nanoparticles was utilized as an antibacterial activity.

In this research, the structure, and characterization of silver and zinc oxide nanostructured material were examined using X-ray diffraction (XRD) analysis were analyzed for identifying and measure the crystainality and particle size of them. The structural results approved a face-centered cubic structure (FCC) of silver and a hexagonal wurtzite structure of ZnO, while the crystalline size is 21 nm, 29 nm for silver and zinc oxide respectively. The existence of Ag and ZnO was clarified by FTIR،where the peak at 495 cm^{-1} corresponds to metal confirms the formation of (Ag), while the peaks between 400 cm^{-1} to 600 cm^{-1} to the metal-oxygen (M–O).

The optical properties were examined using a UV-VIS spectrophotometer, where the absorption spectrum of Ashwagandha root extract was at 286 nm. Broad absorption spectra for AgNPs between 375 and 450 nm. The strong absorption peak at 300 nm, which is a characteristic signature for ZnONPs.

The topological properties of the Ashwagandha roots extract were investigated used Atomic Force Microscopy (AFM) with an average particle size of the sample equals to 72.24 nm.

EDX illustrates that the chemical composition and quantity of the Ashwagandha roots completely matched with the basic used material, where the EDX spectrum proves that the Ashwagandha roots were composed of Calcium, Copper, Carbon, and Oxygen. The FESEM results revealed that the

prepared samples existed in the shape of flowers of ZnO formed from concentrated rods structure for Ashwagandha roots and zinc oxide nanoparticles with a length of rod (40 mm) and width diameter (5 mm), also the Ashwagandha roots appear as a rod shape, while the silver nanoparticle was spherical particles shape with width diameter is (5.06 mm).

Bacterial isolates were identified by a combination of cultural characteristics, Gram stain appearance, and finally confirmed by Vitek 2 compact system.

The antibacterial activity of green synthesis nanoparticles was performed on the growth of Gram-negative and Gram-positive. Also, the effect of 410 nm diode laser irradiation on the growth of Gram-negative *Escherichia coli* and Gram-positive *Staphylococcus aureus* .Following irradiation, Colony-forming unit (CFU/ml) was calculated, by using Enzyme-linked immunosorbent assay (ELISA).

Laser Irradiation experiments showed that the number of CFU/ml of *E.coli* and *S. aureus* was significantly reduced with increasing exposure times, reaching a100% bacterial mortality at 15 min for Gram-negative *(E.coli)*, while the exposure time (15 minutes) for Gram-positive *S.aureus* no significant differences in the number of log CFU/ml, just at the exposure time 3 minutes number of log CFU/ml was a significant reduction ($P<0.01$) compared with the control group.Accordingly, the blue laser irradiation seems to have a more bactericidal effect on Gram-negative *(E.coli)* than Gram-positive bacteria *(S. aureus)*.

From all that was mentioned earlier, the silver and zinc oxide nanoparticles by using the green synthesis method and diode laser 410 nm irradiation on the growth of Gram-negative and Gram-positive is an efficient method for antibacterial activity.

List of Contents

List of Tables

List of Figures

List of Symbols and Abbreviations

Symbol	Meaning	Unit
WS	Withania Somnifera	---
AgNPs	Silver Nanoparticles	---
ZnO	Zinc Oxide	---
$AgNO_3$	Silver Nitrate	---
ZND	Zinc Nitrate Hexahydrate	---
ZAD	Zinc Acetate Dehydrate	---

PVA	Polyvinyl Alcohol	---
HMT	Hexamethylenetetramine	---
IPA	Isopropyl alcohol	---
DI	De-ionized Water	---
CBD	chemical bath deposition	---
a ,b ,c	Lattice Constant	Angstroms
D	Crystallite size	---
θ	Braggs diffraction angle	Degree
Eg	Energy gab	electron- volt
λ	Wavelength	nanometer
k	Crystallite shape factor	---
βFWHM	Full-Width at Half-Maximum	---
XRD	X-ray Diffraction	---
FTIR	Fourier Transformation Infrared Spectrometer	
AFM	Atomic Force Microscopy	---
EDX	Energy Dispersive X-ray	---
CFU	Colony Forming Units	
FESEM	Field Emission Scanning Electron Microscope	
MSA	Mannitol Salt Agar	---
UCA	Uti Chrom Agar	---
MCA	MacConkey Agar	---
LB	Luria Bertani Broth	---

Chapter One

Introduction and Basic Concepts

1.1 Introduction

In this chapter, some definitions and concepts of Enzyme-Linked Immunosorbent Assay (ELISA), Green Nanotechnology, Withania Somnifera (Ashwagandha), Gram-negative and Gram-positive Bacteria and laser in addition to some review of literature survey will be introduced.

1.2 Enzyme Linked Immunosorbent Assay (ELISA)

ELISA is a biochemical assay that uses antibodies and enzyme-mediated color changes to detect the presence of any antigen (proteins, peptides, hormones, etc.) or antibodies in a given sample [1]. The ELISA analysis is based on the solid-phase ELISA principle, which uses spectroscopic color reaction detection. Performed on plastic plates that each have 96 small wells.

Each well is coated with an antibody (AB1) that is specific for the hormone being assayed. Samples or standards are added to each of the wells, followed by a second antibody (AB2) that is also specific for the hormone, but binds to a different site of the hormone molecule. A third antibody (AB3) that is added recognizes AB2 and is coupled to an enzyme that converts a suitable substrate to a product that can be easily detected by colorimetric or fluorescent optical methods. Because each molecule of enzyme catalyzes the formation of many thousands of product molecules, even small amounts of hormone molecules can be detected. In contrast to competitive radioimmunoassay methods, ELISA methods use excess antibodies so that all hormone molecules are captured in antibody-hormone complexes.

Therefore, the amount of hormone present in the sample or in the standard is proportional to the amount of product formed [2]. The basic steps of ELISA described in Figure (1.1).

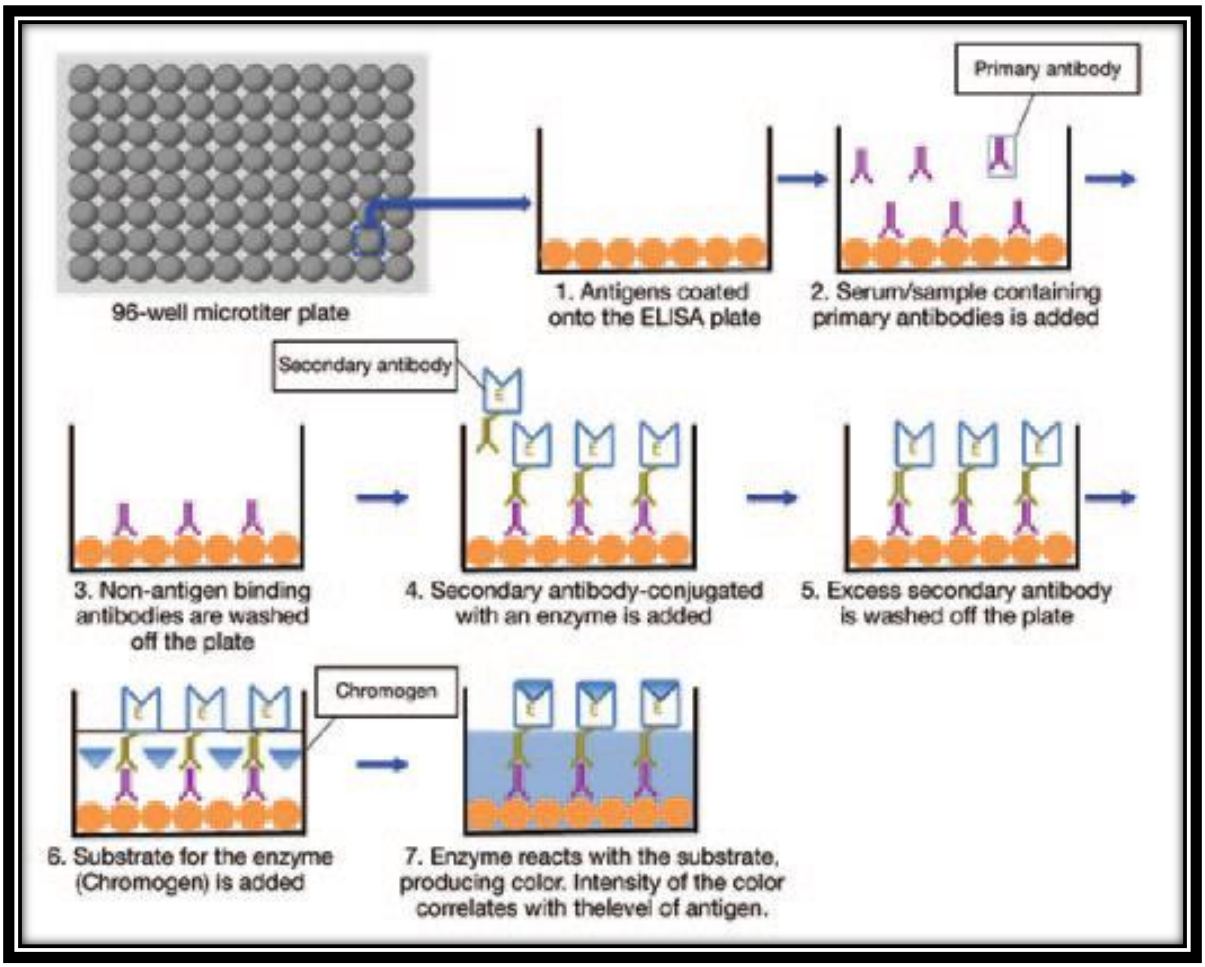

Figure (1.1):Enzyme-Linked Immunosorbent Assay (ELISA) Technique Used to Detect an Antigen in A Given Sample [1].

1.3 Nanotechnology

Nanotechnology is the term given to those areas of science and engineering where phenomena that take place at the dimensions in the nanometer scale are utilized in the design, characterization, production and application of materials, structures, devices and systems [3].

The rapidly developing nanotechnology is the interdisciplinary research and development field of biology, chemistry, physics, food, medicine, electronics, aerospace, medicine, etc., which examines the design, manufacture, assembly, characterization of materials that are smaller than100 nanometers in scale, as well as the application of miniature functional systems

derived from these materials [4]. The development of a metal nanoparticle is an increasing interest due to its distinctive properties and this leads to many significant applications in the field of multi-disciplinary research activities [5,6].

Noble metal nanoparticles have found widespread applications in catalysis, bio sensing, drug delivery, antibacterial activity, anticancer activity, and gene therapy [7]. Among the noble metals, silver nanoparticles have attracted increasing interest due to their distinctive physical-chemical properties, including a high electrical and thermal conductivity, surface-enhanced Raman scattering, chemical stability, catalytic activity and nonlinear optical behavior [8]. In addition, Nano silver in powder form, as well as suspensions, is a safe and effective antibacterial metal as it's non-toxic to animal cells and highly toxic to bacteria such as Escherichia coli and Staphylococcus aureus, and the cost-effectiveness of AgNPs products is that one gram of silver nanoparticles is all that is needed to give antibacterial properties to a hundred of square meters of substrate material [9] .

1.4 Nanomaterials

Nano science is the study of materials (which are at least one external dimension in the size range from approximately 1-100 nanometers) that exhibit remarkable properties, functionality, and phenomena due to the influence of small dimensions. This science has become one of the most important sciences at the present time because these material properties have unique properties and several applications [10].

Nanomaterials, which are the mainstay of nanotechnology that serve our lives for many years thanks to the contributions of many sciences, can be classified according to their origins, dimensions and structural configurations. According to their origin; nanomaterials are classified into two main groups:

natural nanomaterials that are found in nature such as viruses, proteins, enzymes and minerals, and artificial nano-materials, which are not found in nature and require some processes for their production.

According to their dimensions, nanomaterials are examined under four classes:

1-Nano- sized nanocrystals, also known as zero dimensions, including metallic and semiconductor nanoparticles.

2. One- dimensional nanomaterials are nanowires and nanotubes.

3.Two-dimensional nanomaterials such as nanocomposites and nanoplates.

4. Three-dimensional nanomaterials, bulkers

According to their structural configurations, nanomaterials are studied under four main groups as metallic nanomaterials, carbon-based nanomaterials, dendrimers, and composites [11]. Figure (1.2) shows some types of nanoparticles used in nanotechnology.

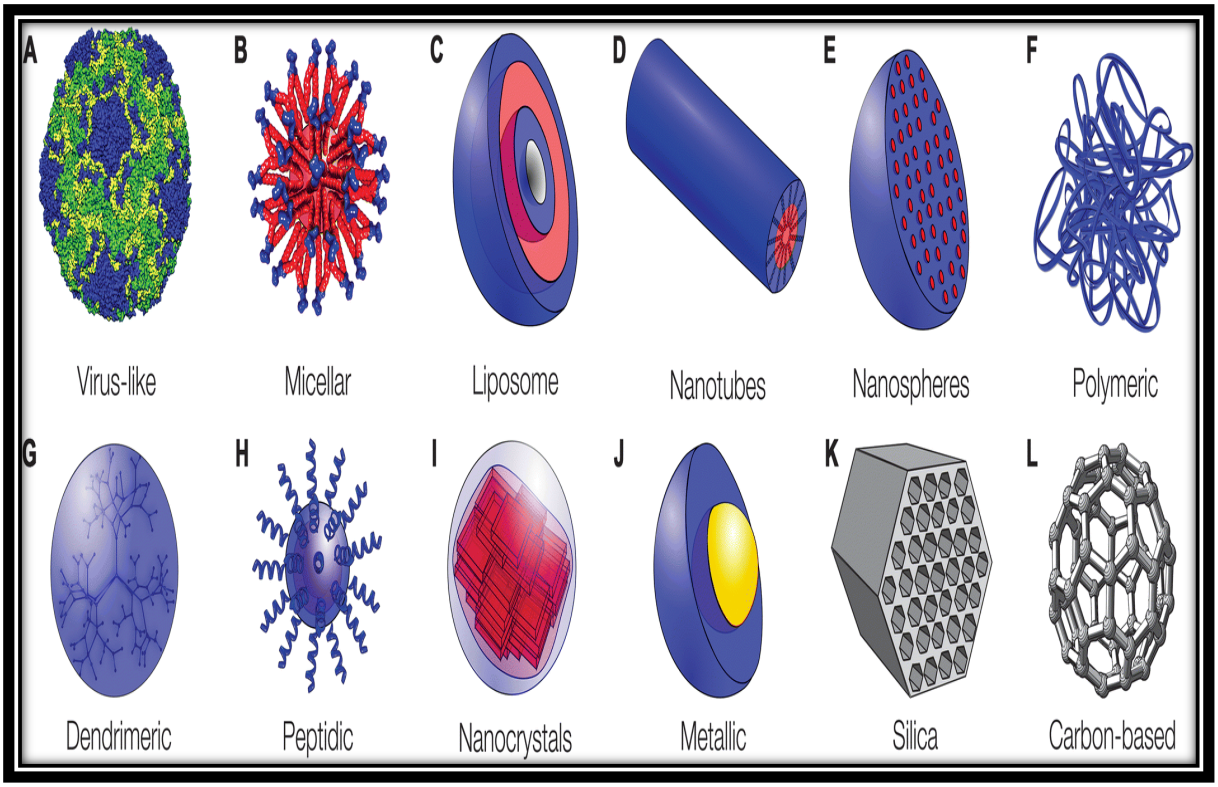

Figure (1.2): Types of nanoparticles used in nanotechnology [11]

Nanoparticles (NPs) can be synthesized using a variety of methods, including physical, chemical, biological techniques. Figure (1.3) shows different methods of Nanoparticles. Nanoparticles (NPs) can be synthesized using two approaches, the top-down (Physical) approach and the bottom-up (Chemical and biological) approach [12].

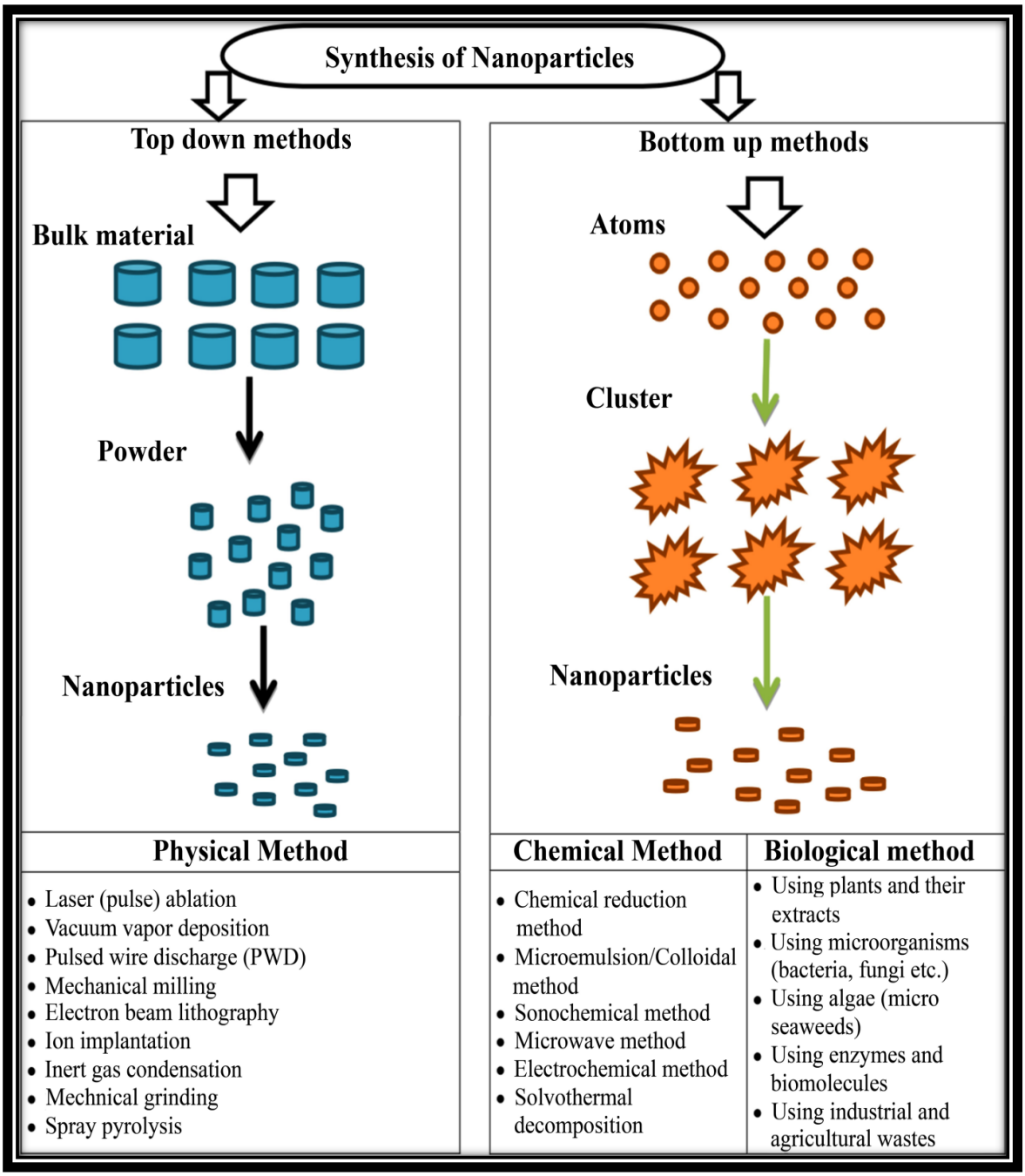

Figure (1.3): Different methods used for the synthesis of NPs [12].

- **Top-down approach:** The concept behind this approach is that bulk materials are broken down into nano-sized dimensions using cutting, grinding, and scraping techniques, i.e. nanomaterials are created from larger materials without atomic-level control. Physical techniques for NP synthesis include laser ablation (pulse), vacuum vapor deposition, pulsed wire discharge (PWD), and mechanical milling.
- **Bottom-up approach:** Bottom-up self-assembly refers to the formation of an atom by atom, molecule by molecule, or cluster by cluster structure. A simple example of a bottom-up approach is colloidal dispersion that is used for nanoparticle synthesis. Atoms, molecules or clusters make up the structure of NPs. Chemical reduction, non-chemical reduction, electrochemical, microwave-assisted, and hydrothermal micro-emulsion (colloid) techniques. Plants (inactivated plant tissue, plant extracts and living plants), enzymes and microorganisms are used in the biological synthesis of NPs (especially Cu-NPs) [12].

In the biomedical field, metallic nanoparticles developed by biological methods are used for purposes such as protection against harmful microorganisms, bioimaging, drug transport, cancer treatment, medical diagnosis, and sensor construction due to their unique properties, such as isolation, optics, antimicrobial, antioxidant, anti-metastasis, biocompatibility, and stability.

Metallic nanoparticles can be used in the industrial field due to their catalytic activity, are of great importance nowadays. Figure (1.4) shows where metallic nanoparticles obtained through biological methods are used in detail [11].

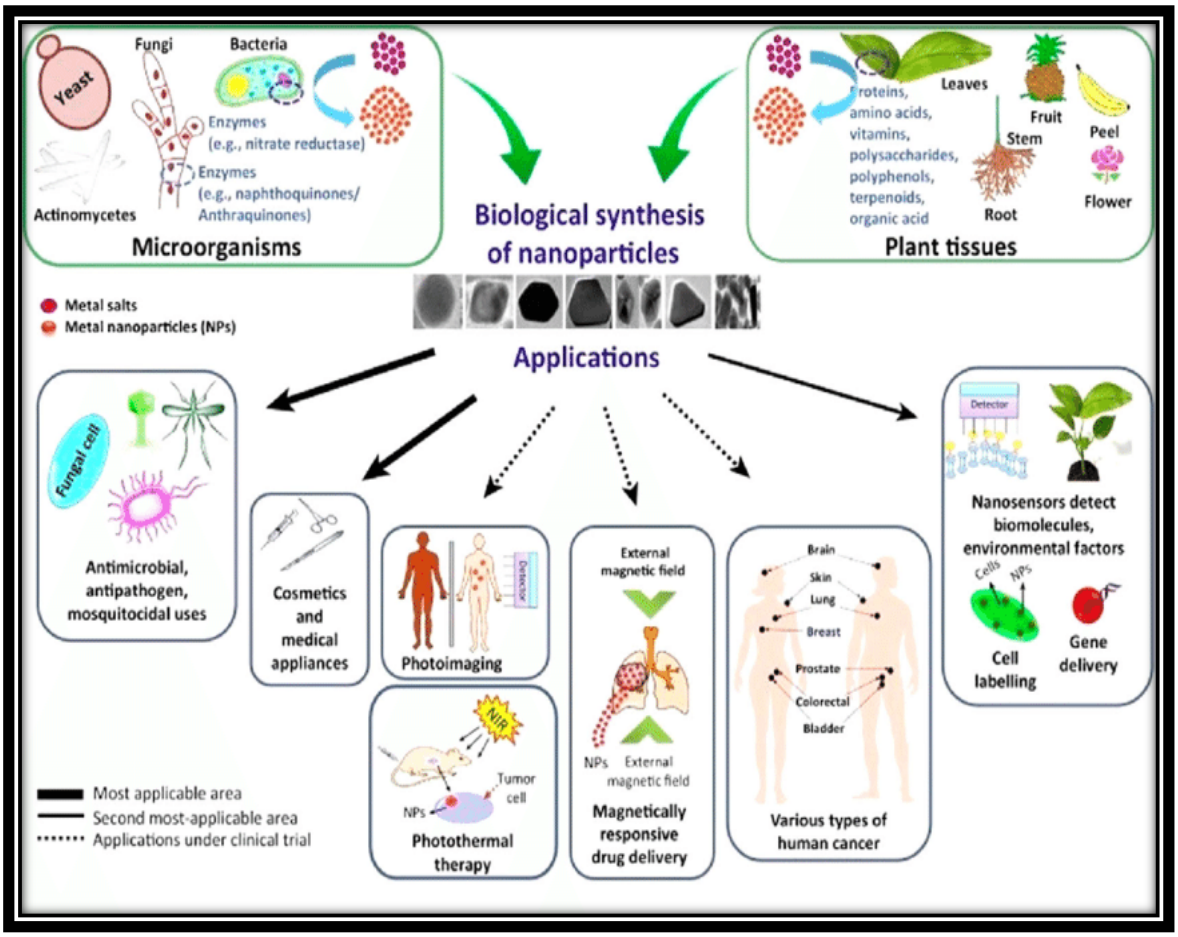

Figure (1.4) :Application areas of metallic nanoparticles synthesized by biological methods [11].

1.5 Silver Nanoparticles (Ag-NPs):

Silver Nanoparticles (Ag-NPs) are one of the highly utilized nanomaterials due to their distinctive properties, such as good conductivity, chemical stability, catalytic activity, and antimicrobial activity [13].

Due to the high degree of commercialization, silver nanoparticles have a range of applications that enable them to be used in many applications, such as biosensors, catalysts, antimicrobials, optical limiters, pharmaceuticals, cosmetics, medical devices, apparel and textile industries [14]. Also, AgNPs been effective in the purification of drinking water/ effluent water through the efficient removal of waterborne pathogens [15].

1.6 Synthesis of Silver Nanoparticles.

Generally, the methods for synthetic AgNPs can be classified into three broad categories: physical, chemical, and biological (or green) synthesis [16] which illustrated in figure (1.5). Each of these methods has different process efficiency and accompanying technological limitations. Parameters of obtaining nanoparticles, such as shape, diameter or longest dimension, stability, are closely related to the choice of methods leading to their receipt [17].

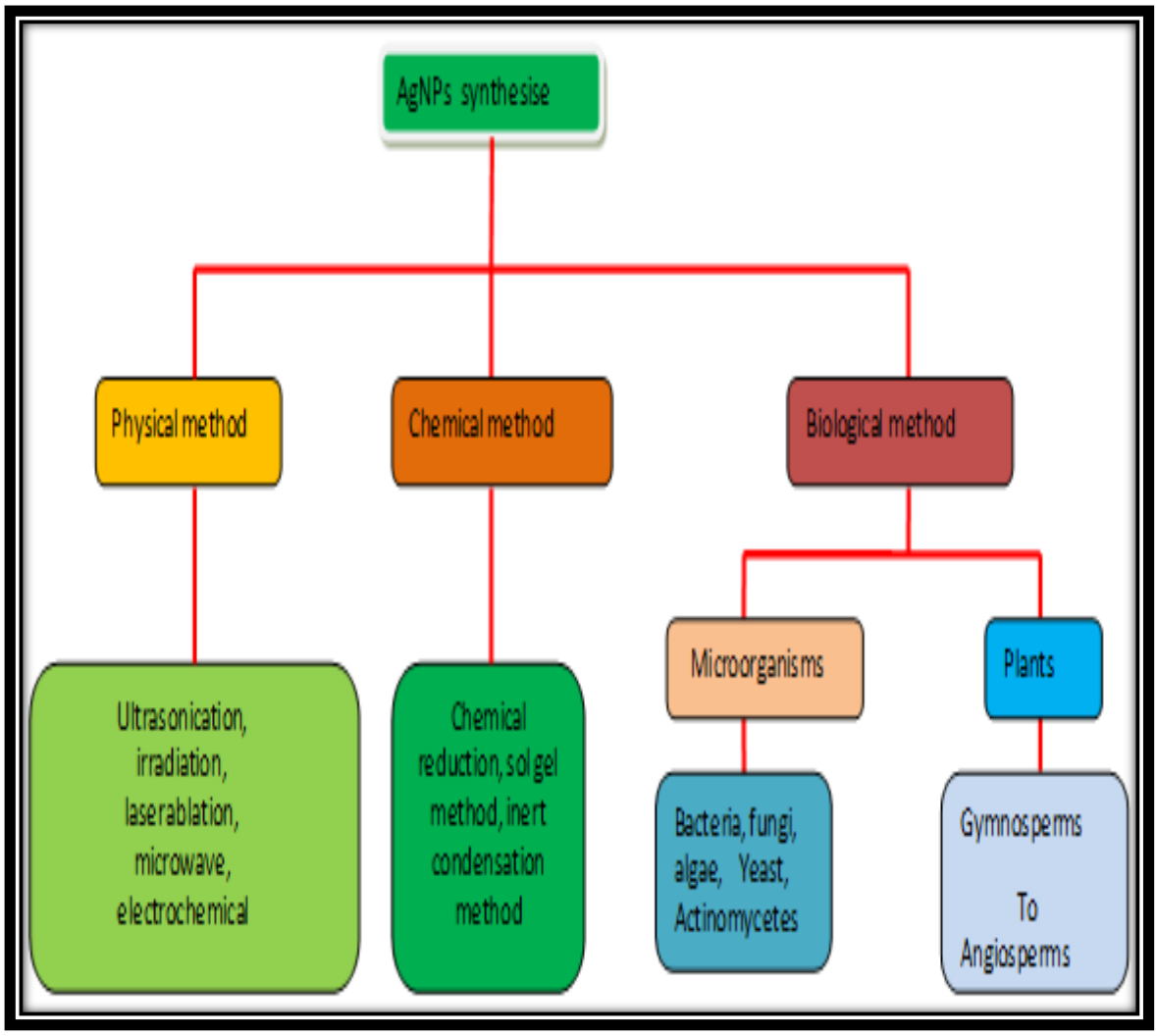

Figure (1.5) :Illustrates the methods of synthesizing AgNPs [16].

1.7 Antibacterial activity of AgNPs

Silver has been widely used as a therapeutic agent for a wide range of diseases since ancient times. Until antibiotic treatment, silver was used as an antiseptic agent to treat burns and open wounds [18]. For gram-negative and gram-positive bacteria, the antibacterial activity of AgNPs is not comparable, but competes with each other [19].

The antibacterial activity of AgNPs against gram-negative and gram-positive bacteria are drawn from conflicting conclusions. Some researchers have indicated that gram-negative bacterial strains are more susceptible to AgNP than gram-positive bacterial strains [20-22]. The cell membrane of the bacteria is negatively charged and the AgNPs are positively charged, and when these positively charged AgNPs accumulate on a negatively charged membrane, they cause structural changes in the membrane, making the membrane of the bacteria more permeable. Unregulated transport across the cytoplasmic membrane contributes to cell death [23].

AgNPs can harm the genetic material inside the bacterial cell by binding to it, resulting in inhibition of transcription and translation [24]. Two types of antibacterial activity can be characterized by AgNPs: inhibitory action and biocidal action. The antibacterial activity of AgNPs depends strongly on numerous factors, including pH, temperature, bacterial forms, the concentration of $AgNO_3$ [25].

However, due to the large area to volume ratio, AgNPs could have much better performance. Potential mechanisms for intervention are as follows:

1. Nanometer-scale silver provides an incredibly wide bacteria-contact surface area, enhancing interaction with the microorganism. Nanoparticles bind to the cell membrane and bacteria are also penetrated by them.

2. Bacterial membranes contain sulfur-containing proteins, and AgNPs can interact with them to inhibit activity, such as Ag^+, as well as compounds containing phosphorus, such as DNA. Silver (nanoparticles or Ag^+) can attack the respiratory chain of bacterial mitochondria and lead to cell death.

3. AgNPs may have sustained release of Ag^+ once (in a lower pH environment) into bacterial cells, which can generate free radicals and induce oxidative stress, further enhancing their bactericidal activity, as shown in Figure (1.6) [26].

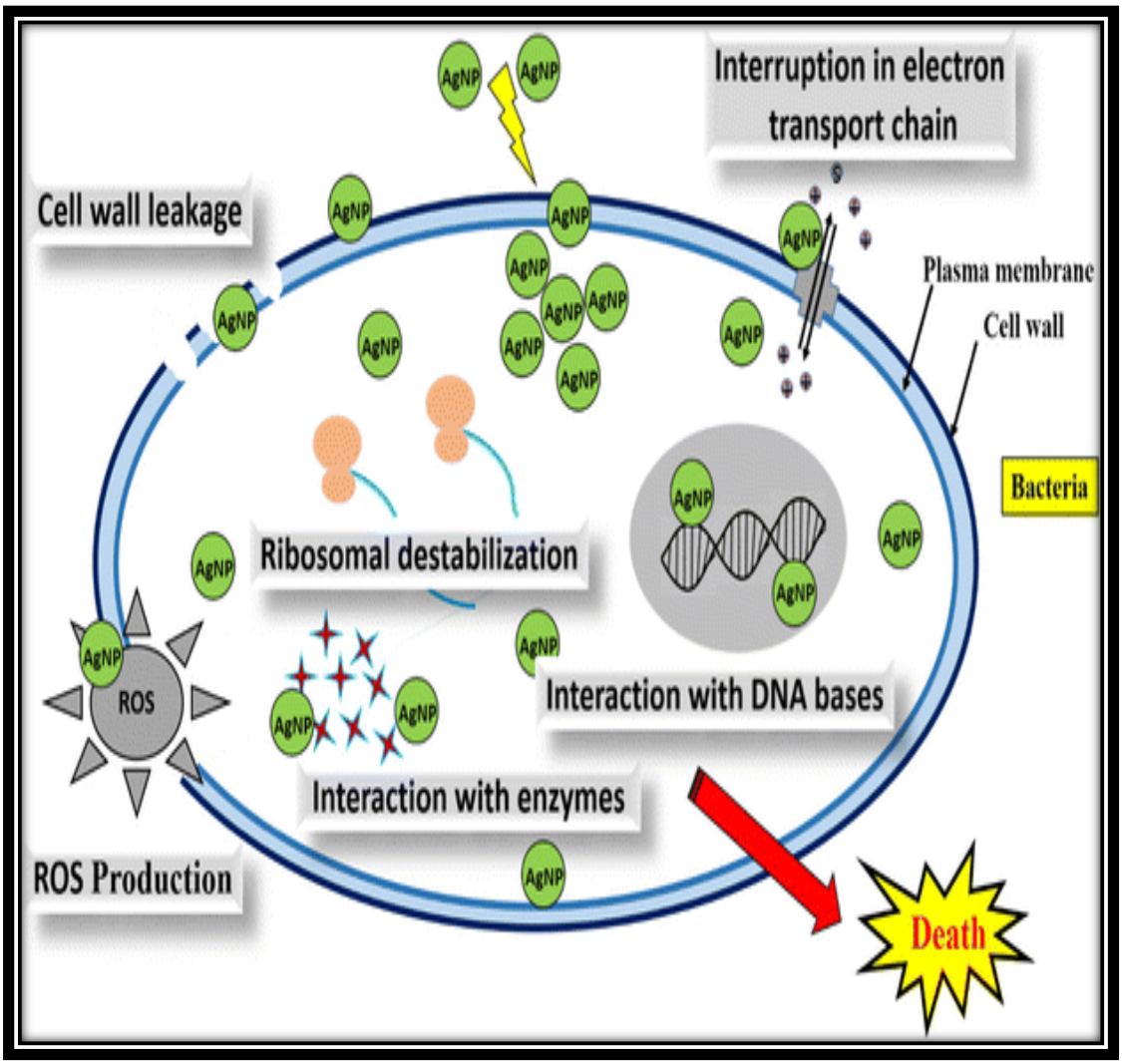

Figure (1.6): Schematic diagram showing the different antibacterial activity mechanisms of silver nanoparticles [26].

1.8 Zinc Oxide (ZnO).

In Nanotechnology, Zinc oxide is one of the most significant semiconductive metal oxide materials. ZnO, which occurs in two stable forms, the hexagonal wurtzite and the blend of cubic zinc. Under ambient conditions, the wurtzite structure is the most stable structure and has a hexagonal structure with a = b=0.3296 nm,and c=0.520 nm lattice parameters. The ZnO structure can simply be described as a number of alternating planes consisting of tetrahedrally coordinated O^{2-} and Zn^{2+} ions, as shown in Figure (1.7) [27].

Zinc oxide has attracted considerable attention in electronics, optics, and Photonics applications due to its promising properties, including a wide band gap of 3.2 eV, a large binding energy of 60 meV, low toxicity, high electron mobility high chemical stability, good transparency and photochemical stability [28].

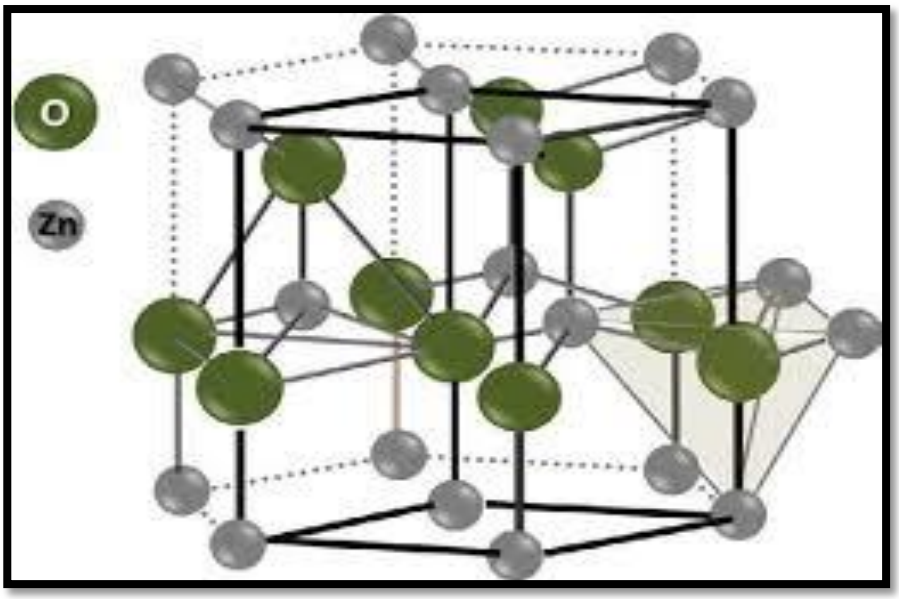

Figure (1.7): Crystal structure of a hexagonal wurtzite ZnO [27]

Zinc oxide nanoparticles are currently used in some devices, such as biosensors, gas sensors, and solar cells, as it is relatively easy to shape ZnO nanostructures, that has good charge-carrier transport properties and high crystalline quality. ZnO nanostructures can be synthesized using a wide range

of chemical, physical and green methods. ZnO nanoparticles are also good antibacterial agents for Gram-positive and Gram-negative bacteria [29-31].

The mechanism of antibacterial behavior of ZnO nanoparticles can be associated with a combination of more than one phenomenon, such as:

(a) The mechanical effect due to the physical interaction of ZnO nanoparticles on the membrane, resulting in deformation and rupture, blockage of critical ion channels, penetration of extremely small nanoparticles interacting effectively with multiple compound cells components, and cause oxidative stress, resulting in extensive protein and DNA damage.

(b) Membrane lipid peroxidation formed by reactive oxygen as a result of the interaction with culture media of photo-excited electrons and holes in ZnO NPs that could lead to the cell wall breakup and leakage of cellular material, as shown in Figure (1.8).

(c) Dissolution of NPs to yield toxic amounts in culture media of $Zn2^{+}$ ions [32].

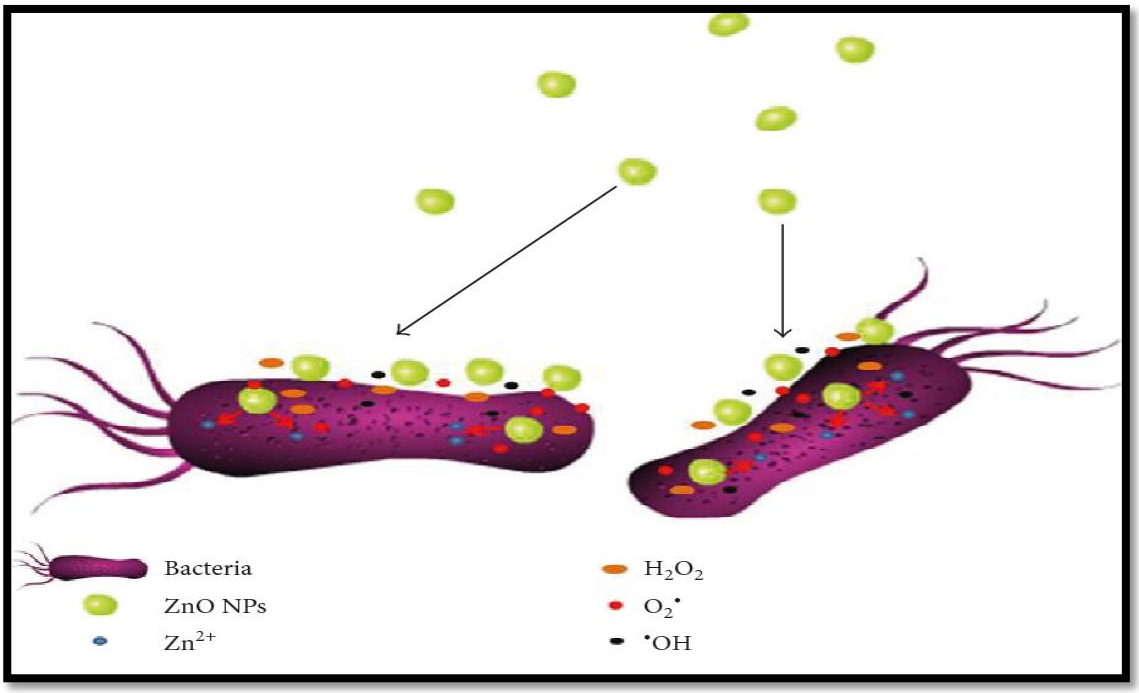

Figure(1.8):Schematic illustration of antibacterial activity of ZnO NPs[33].

1.9 Green Nanotechnology

The concept of green technology or green nano-biotechnology is currently a part of the important objective of facilitating the development of nanotechnology-based products that are simple, fast, low-cost, environmentally friendly, and safe for all beings. Owing to their peculiar optical, biochemical, photochemical and electronic properties, the "green synthesis" of metal nanoparticles receives a great deal of interest [34,35].

Green Nanobiotechnology synthesizes using plant extracts, have attracted more attention than chemical and physical methods, as well as the use of microbes. The method is acceptable for nanoscale metal synthesis due to the lack of any need to maintain an aseptic environment. This can only be done by benign biological synthesis procedures using biotechnological techniques that are considered healthy and environmentally sound for the production of nanomaterials production as an alternative to conventional physical and chemical methods [36].

1.10 Withania Somnifera (Ashwagandha)

Withania Somnifera (WS) is a vital herb, which is commonly known as Ashwagandha or Winter Cherry. In Ayurveda, it is defined as "Indian ginseng", one of the most strong medicinal plants that have been used for more than 3000 years. Ashwagandha root extract has a wide variety of pharmacological activities due to the presence of many biologically active metabolites.

Due to the existence of natural, antioxidants acting as reducing, agents, free radical scavengers, and singlet oxygen, quenchers, Ashwagandha has therapeutic potential [37,38]. Figure (1.9) shows a plant Withania Somnifera.

Scientific classification

Kingdom: Plantae

Order: Solanales

Family: Solanaceae

Genus: Withania

Species: Somnifera

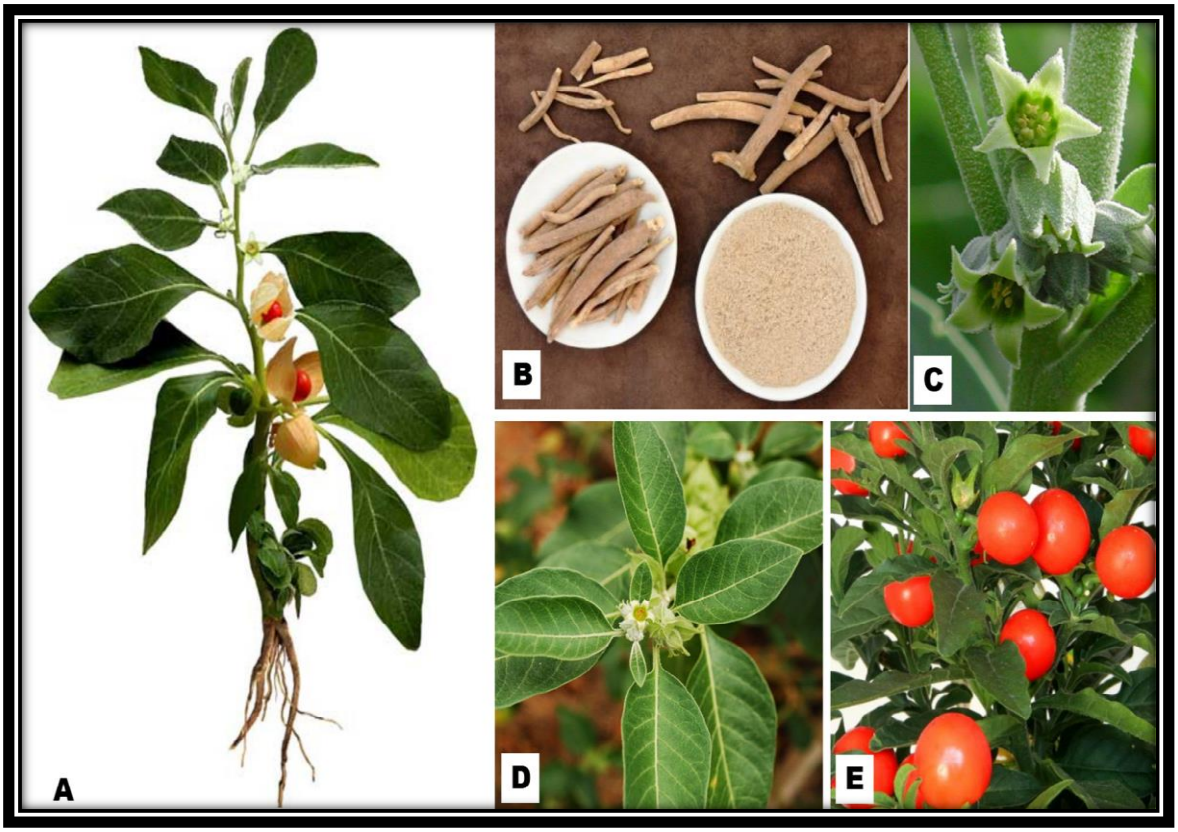

Figure (1.9) Withania somnifera plant: (A) plant; (B) roots and root powder; (C) flowers; (D) leaves; and (E) and fruits [39]

Withanolides are the most active components of W. Somnifera, isolated from its roots and leaves. The two primary Withanolides, Withaferin A and Withanolide D contribute to the majority of W.Somnifera's biological activity [39].

1.11 Chemical Composition for Ashwagandha

The chemical components of Withania Somnifera are almost 35 chemical components found in the roots of Withania Somnifera [40]. Biologically active chemical constituents are alkaloids (isopellertierine ,anferine), steroidal lactones (Withanolides, Withaferins), saponins containing additional acyl (sitoindoside VII and VIII), and Withanoloids containing glucose at carbon 27 (sitonidoside XI and X) as shown in Figure (1.10).

Withania Somnifera is also iron-rich. The major constituents of ashwagandha are alkaloids and steroidal lactones. Withanone and Withaferin are the main components of the alkaloids, and Withanolide is the main component of the steroidal lactones found in the leaves. The roots of Withania Somnifera consist mainly of compounds known as Withanolides which are believed to be responsible for their exceptional medicinal properties [41].

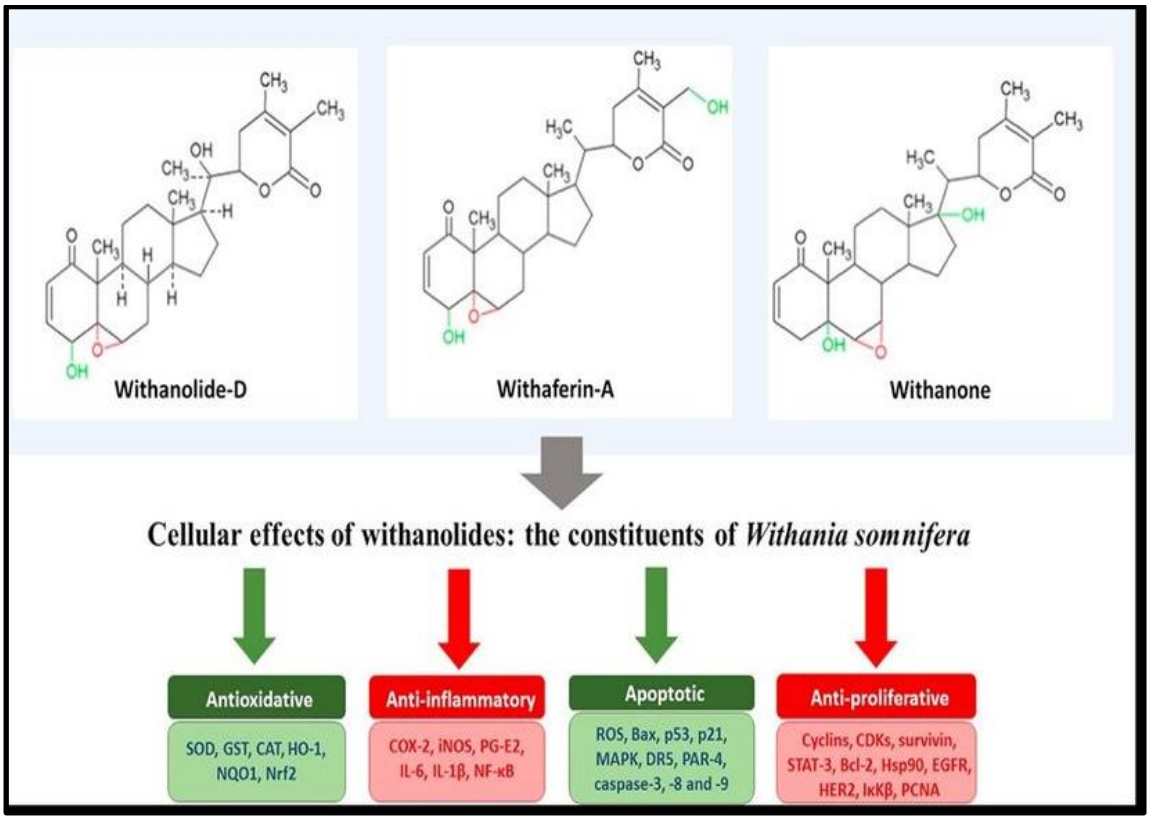

Figure (1.10):Principal biochemical constituents of Withania somnifera [39].

1.12 Pharmacological Activity for Ashwagandha

Withania Somnifera has a variety of pharmacological activities as shown in Figure (1.11), such as antibacterial activity, antifungal activity, antiviral activity, antitumor activity, immunomodulatory activity, anti-stress /adaptogen activity, etc. [42].

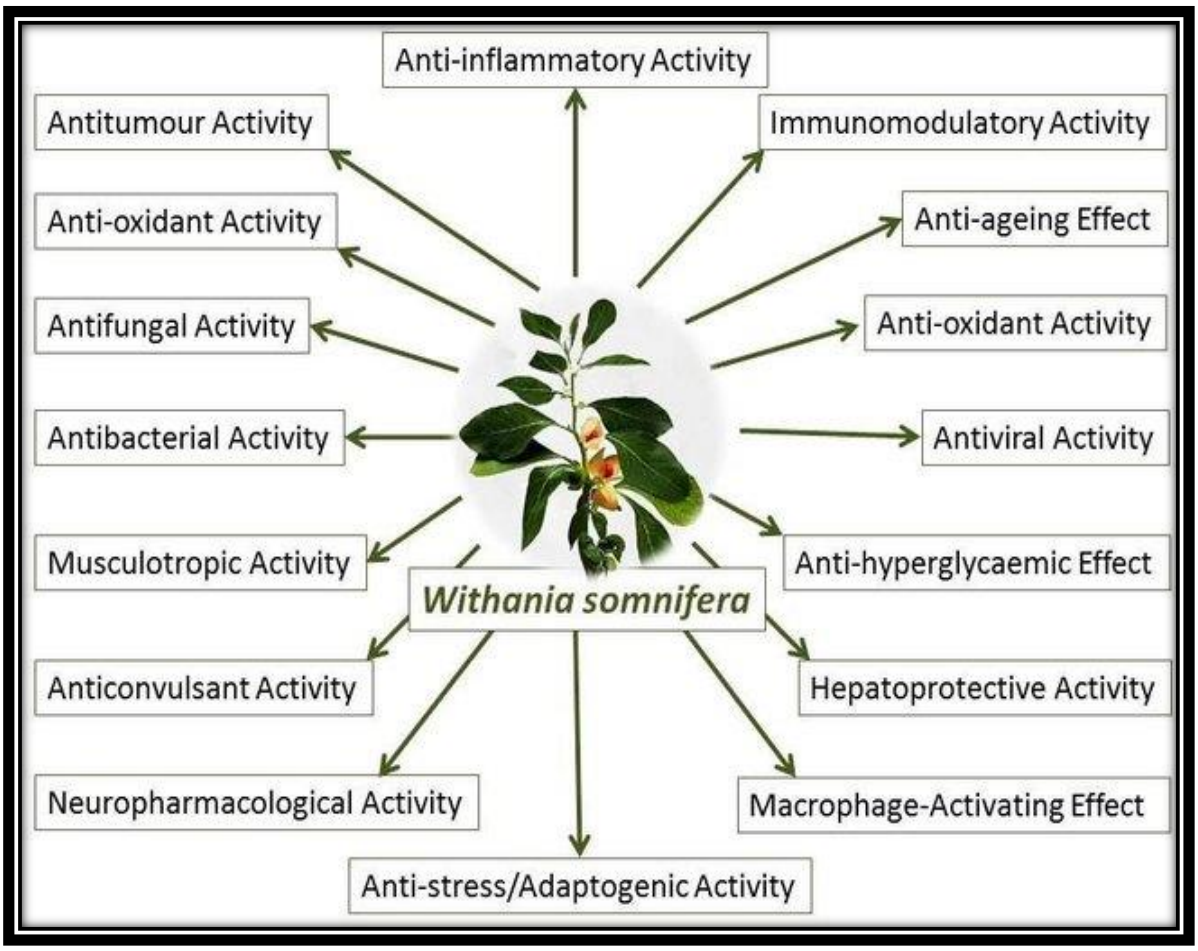

Figure (1.11) :Pharmacological activities of Ashwagandha (W. somnifera) [42].

1.13 Gram-negative and Gram positive Bacteria

Bacteria can be classified into two broad categories: gram-negative and gram-positive. They have similar internal structures, but have somewhat different external structures, as shown in Figure (1.12) [43].

Gram-positive bacteria (such as Streptococcus, Staphylococcus, Clostridium, Listeria, etc.) have a thick layer of peptidoglycan (20-40 layers) containing teichoic and lipoteichoic acids covering the cell membrane. Gram-negative bacteria, on the other hand, have only a thin layer of peptidoglycan covering the cell membrane (such as Escherichia, Salmonella, Pseudomonas, Legionella, Helicobacter, etc.),and are further surrounded by an external outer membrane containing lipopolysaccharide, phospholipids, and proteins.

In the periplasmic space between the cytoplasmic and outer membranes, transportation, degradation, and cell wall synthetic proteins are found. The outer membrane is connected to the cytoplasmic membrane at adhesion points, and lipoprotein connections are attached to the peptidoglycan membrane [43].

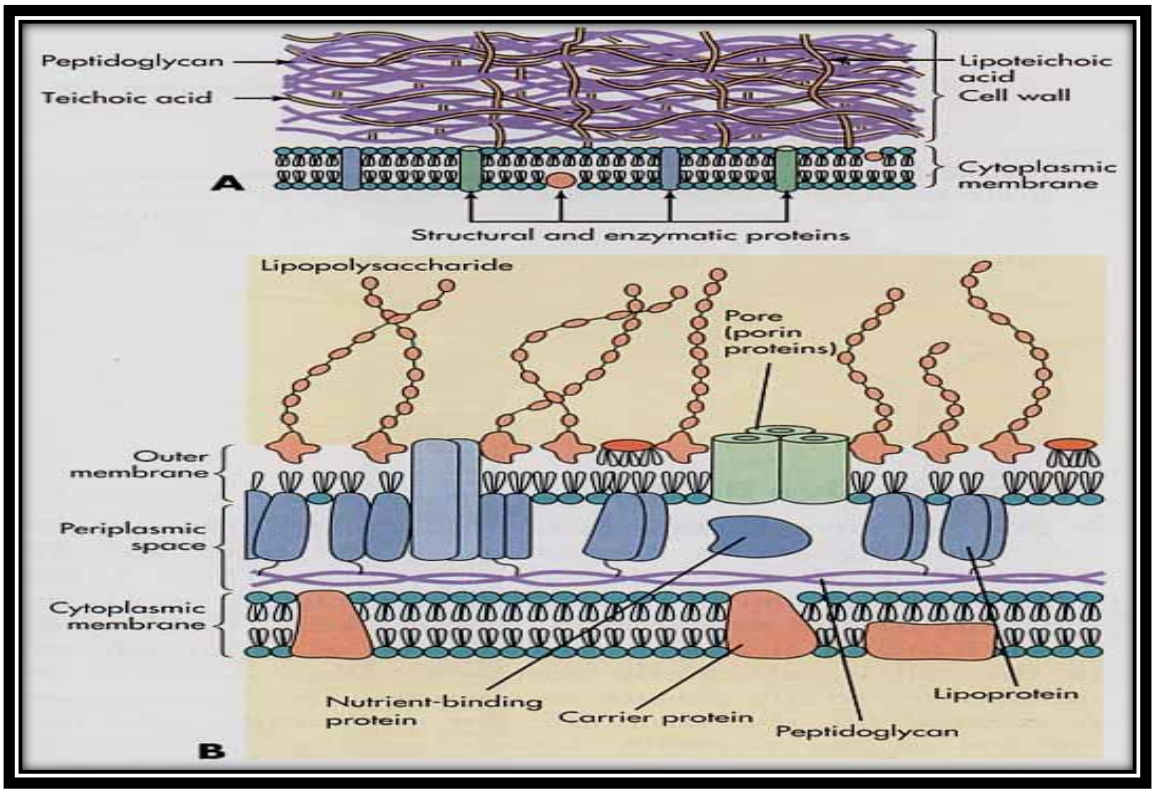

Figure (1.12): Comparison of Gram-positive and Gram-negative bacterial cell walls. Cross-section view of cell envelope (A) Gram-positive bacteria (B) Gram-negative bacteria [43].

Gram-positive bacterial walls are rich in peptidoglycans (protein-sugar complex), that are closely linked and allow cells to withstand decolorization. Gram-negative bacterial walls have a high lipid concentration that dissolves in the decolorizer (alcohol) and is washed away with the purple crystal. The decolorizer thus prepares gram-negative organisms the counterstain safranin or carbol fuchsine [44].

1.14 Bacteria

The isolated bacteria used in our study are *Escherichia coli*, ,*Staphylococcus.*

1.14.1 *Escherichia coli*

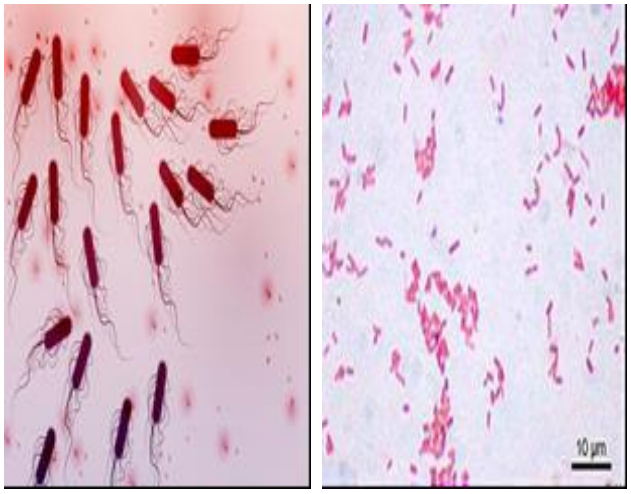

Figure (1.13) Gram stain of *E. coli*

Domain	Bacteria
Phylum	Proteobacteria
Class	Gammaproteobacteria
Order	Enterobacteriales
Family	Enterobacteriaceae
Genus	Escherichia
Species	coli

Escherichia coli is a gram-negative, facultative, rod-shaped anaerobic bacterium of the Escherichia gene commonly found in warm-blooded organisms (endotherms) in the lower intestine. Cells are typically rod-shaped and around (0.25-1 µm) in diameter and around 2 micrometers (µm) in length, with a cell volume of 0.6-0.7 μm^3, as shown in figure (1.13) [45, 46].

1.14.2 *Staphylococcus aureus*

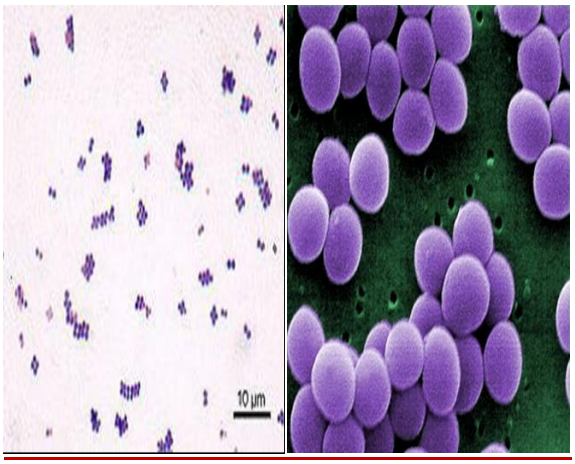

Domain	Bacteria
Phylum	Firmicutes
Class	Bacilli
Order	Bacillales
Family	Staphylococcaceae
Genus	Staphylococcus
Species	aureus

Figure (1. 14) Gram stain of *S. aureus*

Staphylococcus aureus is a gram-positive bacteria. Its cells are represented as being spherical, as shown in figure (1.14). No spores can be produced with a diameter ranging from 0.5 to 1.7 µm, unable to move (non-motile), *S.aurus* is a facultative anaerobic agent that has a temperature of 37°C and a pH of 7, 5. *S.aureus* produces white colonies that appear to change over time to a buff-golden color [47]. In particular *S. aureus*, is found predominantly on the skin in wet areas such as the nose, armpits, and thighs [48].

1.15 Laser Tissue Interaction

When the laser light strikes the surface of the biological tissue, it can be reflected, refracted, absorbed, scattered or transmitted [49]. The intensity of these processes depends on the optical properties of the tissue, such as the absorption coefficients, scattering, particle size, and reflectivity [50], as well as laser parameters, such as energy, wavelength, pulse duration,output spectral profile and operation mode [51, 52].

In the medical application of laser, refraction plays an essential role in the radiation of transparent media such as corneal tissue. The effect of refraction is normally difficult to evaluate in opaque media because of scattering and absorption [53]. The laser light that passes through the tissues presents several processes scattering processes and converts from a narrow-collimated beam to a wide-spreading beam [54]. All light impacts begin with electromagnetic radiation absorption [55]. The intensity of the incident light, by passing the medium, is decreased by the fact that the light energy is partially converted into heat movement or the particular vibrations of the absorbing material molecules.

The ability of the medium to absorb electromagnetic radiation depends on several variables, such as the wavelength of the radiation, the electronic structure of its molecules and atoms, the thickness of the absorption layer, and internal parameters, such as temperature or concentration. Two laws that have frequently been implemented, describe the effect of either density or concentration on absorption, often referred to as Beer's and Lambert's, and are expressed as:

$$I_{(z)} = I_o \exp^{-\alpha z} \quad \text{.....} \quad (1.1)$$

$$I_{(z)} = I_o \exp^{-k c z} \quad \text{.....} (1.2)$$

Where **(z)** are the optical axis, **I (z)** is the intensity at a distance **z**, **Io** is the incident intensity, **α** is the absorption coefficient of the medium, **c** is the concentration of the absorbing agent , and **k** depends on the internal parameter [53]. The most significant optical property that determined the appropriateness of a laser for a surgical operation is the penetration depth of its radiation in the tissue. It is equivalent to the inverse of the absorption coefficient (α) of the laser radiation in the tissue, and it's described as the depth at which laser

radiation intensity decreases to 37% (drops to l/e) of its peak value at the surface of the tissue. The depth of penetration changes considerably with the laser radiation wavelength [56]. The penetration depth can be significantly high in the red portion of the spectrum and near the IR region. In spectral regions with a relatively high absorption coefficient, the radiation is absorbed in a thin layer close to the surface [54,56].

In biological tissue, absorption is caused mainly by water molecules or macromolecules such as pigments and proteins. The IR region absorption of light can be credited to water molecules, while visible light and UV absorbs by pigments and proteins [57].Figure (1.15) illustrates the physical phenomenon when the laser light hits the surface of the tissue.

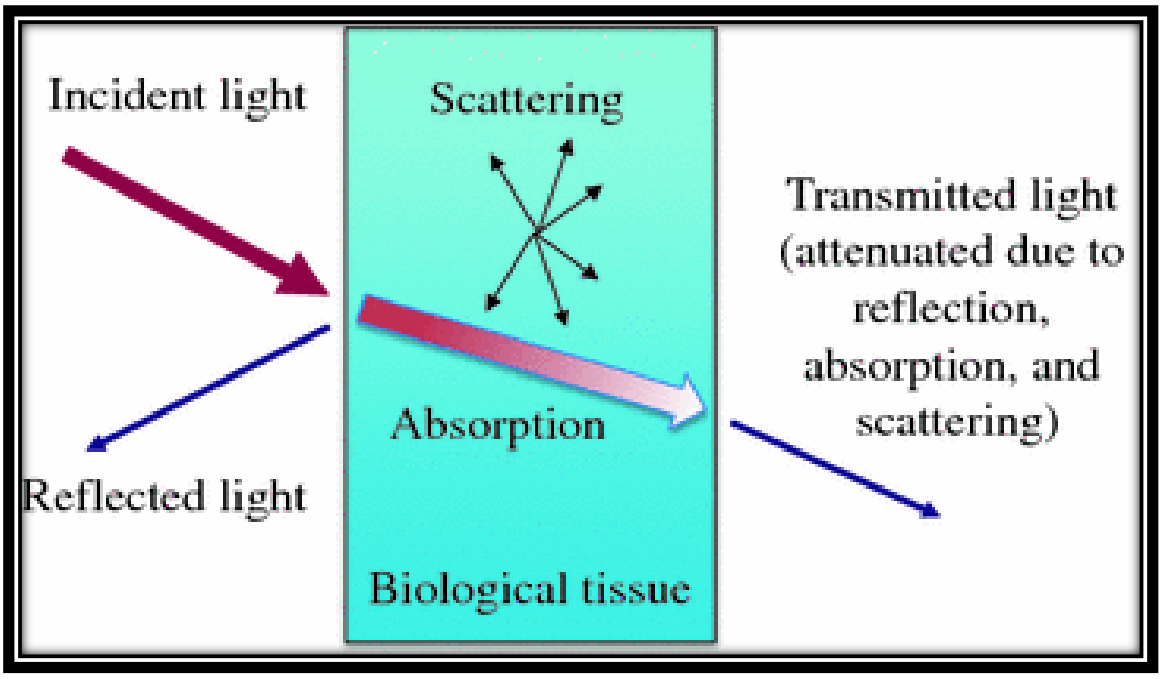

Figure (1.15) : Reflection, refracted, absorbed, scattering or transmission when laser light hits a tissue surface [50].

Depending on the nature of the tissue and the wavelength of the laser radiation, the absorbed amount of laser radiation can generate photochemical or photothermal impacts [56,57].

1.16 Literature Survey

S. K. Verma and A. Kumar (2011) [58] Found that Withania Somnifera was a medicinal plant commonly used by traditional medical practitioners in everyday practice to treat various diseases. In traditional medicines, for liver tonics, anti-inflammatory agents, and more recently for the treatment of bronchitis , asthma, ulcers, emaciation, insomnia and senile dementia, etc., several parts (leaves , stems, bulbs, roots, seeds , bark and even whole plants) of the whole plant of Withania Somnifera (known as Ashwagandha in Hindi) have been recommended. Ashwagandha's chemical preventive properties make it a potentially useful adjunct for patients with radiation and chemotherapy. Steroidal alkaloids and steroidal lactones are the main biochemical constituents of the Ashwagandha root in a class of constituents called Withanolide extract.

M. P. Srivastava et al. (2013) [59] reported using 'Withania Somnifera' medicinal plant leaf extract to establish the synthesis of silver nanoparticles and test their anti-microbial properties. To confirm the antibacterial activity of silver nanoparticles, UV-Visible spectrophotometer,Fourier Transform Infrared (FTIR), Scanning Electron Microscopy (SEM), Transmission Electron Microscopy (TEM), and Disc diffusion assay methods were used to confirm the synthesis and characterization of silver nanoparticles. Maximum absorption was demonstrated at 455 nm by the UV-Visible absorption spectra of the reaction medium containing silver nanoparticles. FTIR research has confirmed the reduction of Ag^{+} ions to Ag^{0} ions in the synthesized silver nanoparticles. The study of SEM and TEM showed that the size of the particles was between 5-40 nm, and the shape was spherical. The silver nanoparticles have shown bactericidal activity against Escherichia coli and Staphylococcus aureus.

A. K. Singh et al. (2015) [60] reported insulation of Fusarium sp. Endophytic fungus Isolated from stable Withania Sominnifera (Ashwagandha) leaves and undergoing extracellular silver nanoparticle (AgNps) biosynthesis. The synthesized AgNps were characterized by visual observation, UV-Vis spectroscopy and Transmission Electron Microscopy (TEM).Other synthesized AgNps have been tested for efficacy against bacterial pathogens such as E. Coil, S.typhi, S.aureus. AgNps formation was confirmed by visual observation of the color transition from pale white to brown and the UV-Vis spectrum was determined by the Surface Plasmon Resonance at 422 nm. TEM revealed the existence of small-scale spherical shaped nanoparticles ranging from 12 to 20 nm. Promising results were obtained for the antibacterial activity of AgNps against E.coli, S.typhi and S.aureus, showing a maximum inhibition zone of 26 mm, 26 mm and 28 mm at 60 µl of AgNps against E.coli, S.typhi and S.aureus respectively.

A. Tereshchenko et al. (2016) [61] studied the use of beneficial physicochemical properties of ZnO nanostructures in the identification of a wide range of biological compounds. As medical diagnostics require reliable , fast and inexpensive biosensors, the advantages inherent in optical detection methods are taken into account. The key points of the immobilization process responsible for the production of biosensors (biomolecule adsorption, surface properties, surface defect location, surface functionalization, etc.) are revealed along with the mechanism of interaction between biomolecules and ZnO. The latest achievements in surface-plasmon resonance (SPR), surface-enhanced Raman spectroscopy (SERS) and photoluminescent biosensors, along with new trends in the development of the ZnO biosensor system.

M. G. Mohammed and A. M. Maki (2017) [62] Studied The effect of 410 nm laser diode irradiation on the growth of Gram-negative Pseudomonas aeruginosa and Gram-positive Staphylococcus aureus was evaluated at different exposure times. These bacteria have been isolated and characterized in selective media, cultural characteristics, Gram stain morphology and biochemical tests on the basis of their growth and have finally been confirmed by the Vitek 2 compact system test. The sum of CFU / ml of P.aeruginosa and S.aureus was shown by laser irradiation studies. With-exposure periods, S. aureus decreased significantly, reaching a 100% bacterial mortality rate of 13 minutes for S.aureus and 19 minutes with P.aeruginosa. Laser diode 410 nm irradiation appears to have a more bactericidal than gram-negative(P. aeruginosa) effect on Gram-positive bacteria (S.aureus).

C. Zhou et al. (2018) [63] Studied the detection of Escherichia coli in water and juice, a fiber optic Surface Plasmon Resonance (FOSPR) sensor has been developed. AgNPs-rGO successfully performed the essential signal amplification, leading to a low detection limit of 5 to 102 cfu / mL E. Coli.

I. Uddin et al.(2018) [64] Found to develop the green synthesis of silver nanoparticles (AgNPs) of ashwagandha root aqueous extract (ARAE) and their in vitro anti-diabetic activity was produced in order to develop an eco-friendly, inexpensive and effective technique. UV-Visible spectroscopy showed a 440 nm absorption peak absent in ARAE and $AgNO_3$. FTIR spectroscopy revealed the absorption peaks of the various functional groups involved in the formation of ARAENP and further emphasized the position of ARAENP data with anolides. By scanning electron microscopy (SEM), an average ARAENP size of 123.23 nm was seen. Two peaks at 28.98^o, 39.80^o, 42.24o, 64.42^o, and 79.76^o, respctialy were observed in X-ray diffraction (XRD) studies.

S. Rahman et al. (2019) [65] Studied the successful biosynthesis analysis of AgNPs using endophytic organisms, characterization, mechanisms, and their biological activities. The microbial behavior of AgNP depends on the size, shape, concentration, and surface of the organic group that regulates the absorption and cytotoxicity of its cells. Possible biological activities of AgNPs (anti-fungal, antibacterial, kinetic destruction, antioxidants, cytotoxicity, and germination of seeds) are also possible.

B. Malaikozhundan et al. (2020) [66] Reported the first attempts to synthesize ZnO nanoparticles using extracts were investigated.W. Somnifera (NPs of Ws-ZnO).The particles, with an average size of 15.6 nm, were crystalline and hexagonal. Greater effect on E. faecalis, S. aureus is shown by Ws-ZnO NPs. After treatment with Ws-ZnO NPs, the biofilm of the examined bacteria was completely removed.

1.17 The Aim of Work

The effect of different parameters like Laser, Ashwagandha, Nanoparticles for Silver and Zinc oxide, Micro material for (Silver nitrate and Zinc acetate) and Antibiotic Meropenem (Mem) on the growth of *Escherichia coli* and *Staphylococcus aureus.*

Chapter Two

Materials & Methods

Experimental Part

2.1 Introduction:

This chapter is divided into three parts, the chemical part that includes materials, procedures, details of the characterization devices (identification techniques), and various methods of green synthesis for silver nanoparticles and zinc oxide nanoparticles. The biological part, which includes the materials and equipment used for biological samples. The last part focuses on the experimental setup of laser for *Escherichia coli* and *Staphylococcus aureus*.

The chemical part:

2.2 Materials:

The materials used in this work are:

2.2.1 The Withania Somnifera (WS)

The chemical formula of (WS) is $C_{56}H_{78}O_{12}S$. The main characteristics of it are shown in Table (2.1).

Figure (2.1) Ashwagandha root extract

Table (2.1): The main characteristics of (WS)

Name	Mol.wt	Solubility	Physical form	Supplier
Withania Somnifera (WS)	975.3 g/mol	Methanol and Distilled Water	Brown powder	Solgar, India

2.2.2. The Silver Nitrate ($AgNO_3$)

The chemical formula of is ($AgNo_3$)**.** The main characteristics of it are shown in Table (2.2).

Table (2.2): The main characteristics of Silver Nitrate ($AgNO_3$)

Name	Mol.wt	Solubility	Physical form	Supplier
Silver Nitrate ($AgNO_3$)	169.5g/mol	Distilled Water	White powder	SIGMA CHEMICAL CO.(USA)

2.2.3. The Zinc Nitrate Hexahydrate (ZND)

The chemical formula of (ZND) is ($Zn(No_3)_2.2H2O$). The main characteristics of it are shown in Table (2.3).

Table (2.3): The main characteristics of Zinc Nitrate Hexahydrate (ZND)

Name	Mol.wt	Solubility	Physical form	Supplier
Zinc Nitrate Hexahydrate (ZND)	297.49 g/mol	Distilled water	White crystalline solid	SIGMA CHEMICAL CO.(USA)

2.2.4. The Zinc Acetate Dehydrate (ZAD)

The chemical formula of (ZAD) is (Zn (CH3COO) 2.2H2O). The main characteristics of it are shown in Table (2.4).

Table (2.4): The main characteristics of The Zinc Acetate Dehydrate (ZAD).

Name	Mol.wt	Solubility	Physical form	Supplier
Zinc Acetate Dehydrate (ZAD)	219.50 g/mol	Alcohol and Distilled water	White powder	Central Drug Hose India

2.2.5. The Polyvinyl Alcohol (PVA)

The chemical formula of (PVA) is ($CH_2CH(OH)$).The main characteristics of it are shown in Table (2.5).

Table (2.5): The main characteristics of Polyvinyl Alcohol (PVA)

Name	Mol.wt	Solubility	Physical form
Polyvinyl Alcohol (PVA)	44.5 g/mol	Distilled water	White powder

2.2.6. The Hexamethylenetetramine (HMT)

The chemical formula of (HMT) is $(CH_2)_6N_4$ **.** The main characteristics of it are shown in Table (2.6) .

Table (2.6): The main characteristics of Hexamethylenetetramine (HMT)

Name	Mol.wt	Solubility	Physical form
Hexamethylenetetramine (HMT)	140.186 g/mol	Distilled water	White powder

2.2.7. Isopropyl alcohol (IPA)

Isopropyl alcohol commonly called isopropanol or propanol. The chemical formula of (IPA) is (CH3CHOHCH3). The main characteristics of it are shown in Table (2.7) .

Table (2.7): The main characteristics of Isopropyl alcohol (IPA)

Name	Mol.wt	Solubility	Physical form
Isopropyl alcohol (IPA)	60.1 g/mol	Distilled water, benzene, chloroform, ethanol and ether.	Colorless

2.2.8. De-ionized Water (DI)

De-ionized Water (DI) is water that has the ions removed and it's purer than distilled water.

2.3 Sample Preparation:

In the present work, using green synthesis:

2.3.a Preparation of plant extract

The extract was prepared by the freshly Ashwagandha root extract. The root powder was weighed about (5 g) and mixing with distilled water (100 ml) on a magnetic stirrer with a hot plate then the solution was boiling at 50 ^{o}C for 15 minutes. The plant extract was filtered through filter paper after cooling, and the filtered extract was stored for further experiments at a temperature of 4 °C.

2.3.b Green synthesis of Silver Nanoparticles

The Silver nitrate solution was freshly prepared about (0.09g) with distilled water (100 ml) under dark conditions. Prepared root extracts were used to reduce Ag^{+} to Ag^{0} by combining it with silver nitrate solution ($AgNO_3$) at a ratio of 1 to 1 mol. These plant extracts and $AgNO_3$ mixtures have been kept under 27 ° C with continuous stirring.

Reduction of silver ions in solution was monitored by a visible change in the color. This indicates the initial confirmation that Ashwagandha was formed as silver nanoparticles (As-Ag Nanoparticles) , as shown in figure (2.2).

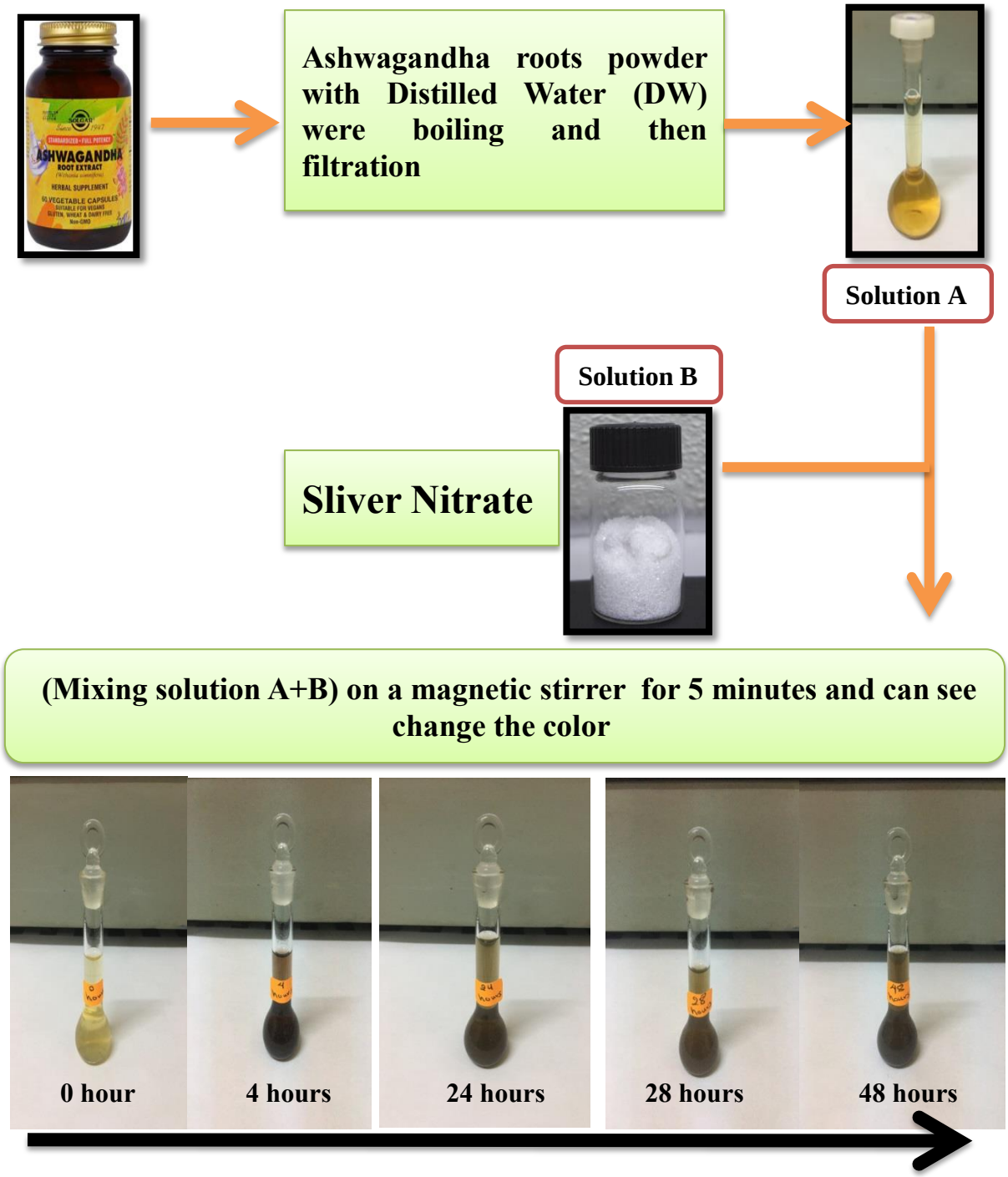

Figure (2.2): Block diagram of Green synthesis of Silver Nanoparticles using extract roots

2.3.c Thin Films preparation of Silver Nanoparticles

AgNPs thin films were deposited onto the microscope glasses by dropping coating at room temperature. The glass slides which had cleaned before using for the deposition process. The ultrasonic cleaner was used for 15 minutes to wash the slides in isopropanol (IPA) bath, then dried in the air before being used.

The coating steps are: immersing the substrate into the sample, the solution prepared by adding (mixed solution of $AgNO_3$ with Ashwagandha) to hexamethylenetetramine (HMT). The molar ratio of AgNPs to HMT was fixed in 1:1. The mixtures were stirred on a magnetic stirrer in DI water. The cleaned glass slides were dipping in the mixtures solution by ingrown via chemical bath deposition (CBD) method were placed in glass beakers containing 80 ml of the growth solution for 16 hours at 85°C. The glass slides were dried for 5 minutes, the resulting thin film added drops of mixed solutions (AgNPs 48 hours), and then allowed to cool at the room temperature.

2.3.d Green synthesis of Silver Nanoparticles

Using the Ashwagandha plant extract roots and their antibacterial activity evaluation, as shown in figure (2.3).

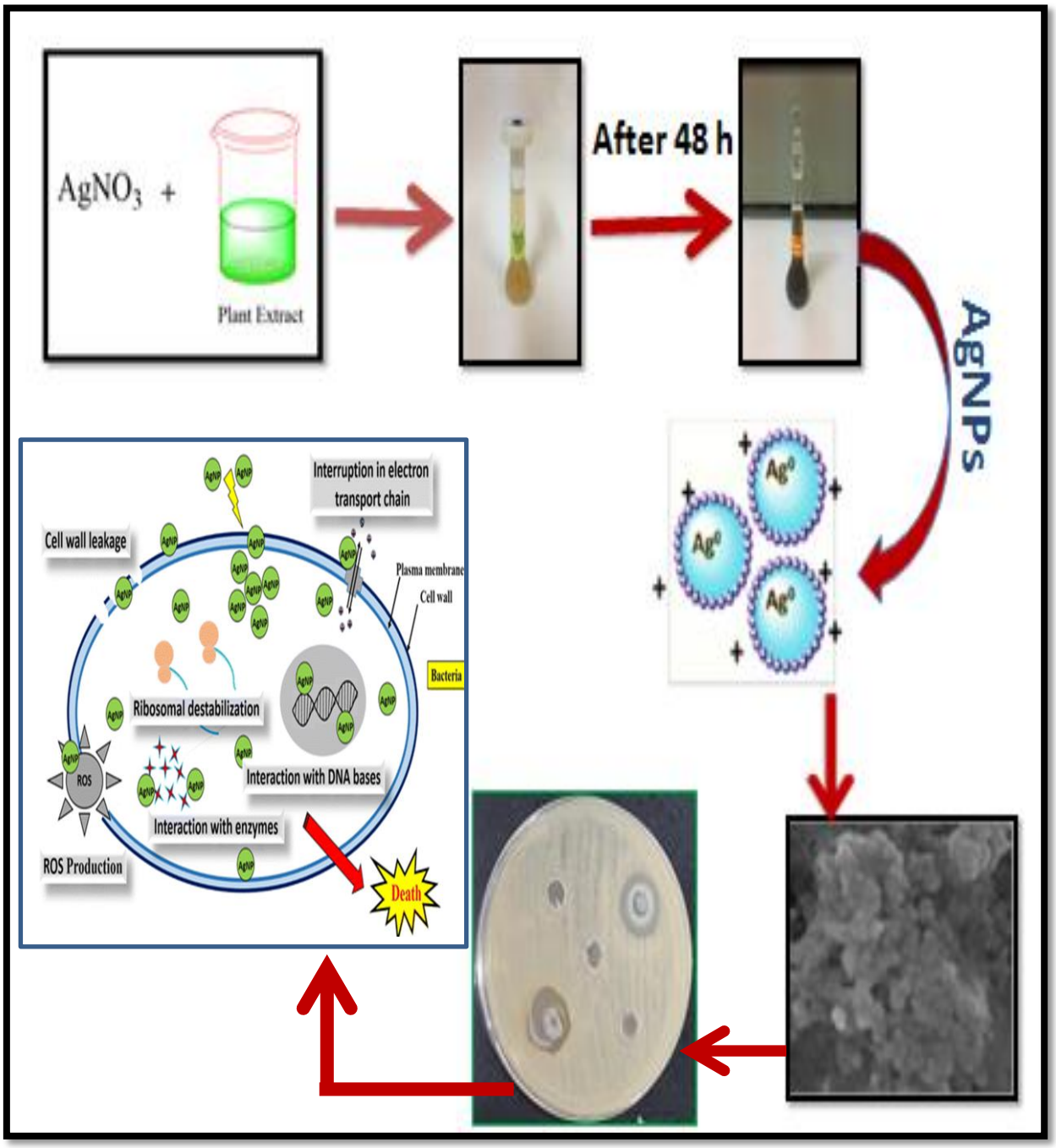

Figure (2.3): Block diagram of Biosynthesis for Silver Nanoparticles using extract roots

2.4. Preparation for Growing ZnO Nanoparticles

Preparation of plant extracts of Ashwagandha root extract was described in Section 2.3.a.

The thin films were made on glass microscope slides, which had cleaned before being used for the deposition process. They were used to create a seeding layer on the surface of the substrate by spin coating. Two different solutions for seeding have been prepared. The first solution (ZA) was formed by dissolving 2.195 g of zinc acetate in 10 ml of deionized water (DI) and magnetic stirring for 2 hours to produce a seed solution of 1 M.

The second solution (ZAP) has the same concentration of zinc acetate by adding 0.6 g polyvinyl alcohol (PVA) in a 10 ml solution with increased viscosity. To compensate for the difference in viscosity, the coating of the first solution (ZA) was spun for 30 s at a lower spin speed 300 rpm while the coating of the second solution (ZAP) was spin at the spin speed 800 rpm.

The thin film-coated samples were annealed in a furnace at 350 ° C for an hour. This temperature was maintained to remove PVA and convert zinc acetate to ZnO nanocrystal seeds. In a nutrient solution consisting of a molar ratio of 1:1 of zinc nitrate hexahydrate , hexamethylenetetramine(HMT), and ashwagandha root extract in DI water, vertically aligned ZnONTs and NRs were grown using the CBD method. In the growth solution the final concentration of Zn^{2+} was 1 M. The glass slides were put in glass beakers containing 80 ml of the growth solution at 85 ° C for 16 hours. Samples allowed to cool down at room temperature.

2.5 Biosynthesis route of ZnO nanostructures

Using the Ashwagandha plant extract roots and their antibacterial activity evaluation, as shown in ,as shown in figure (2.4) .

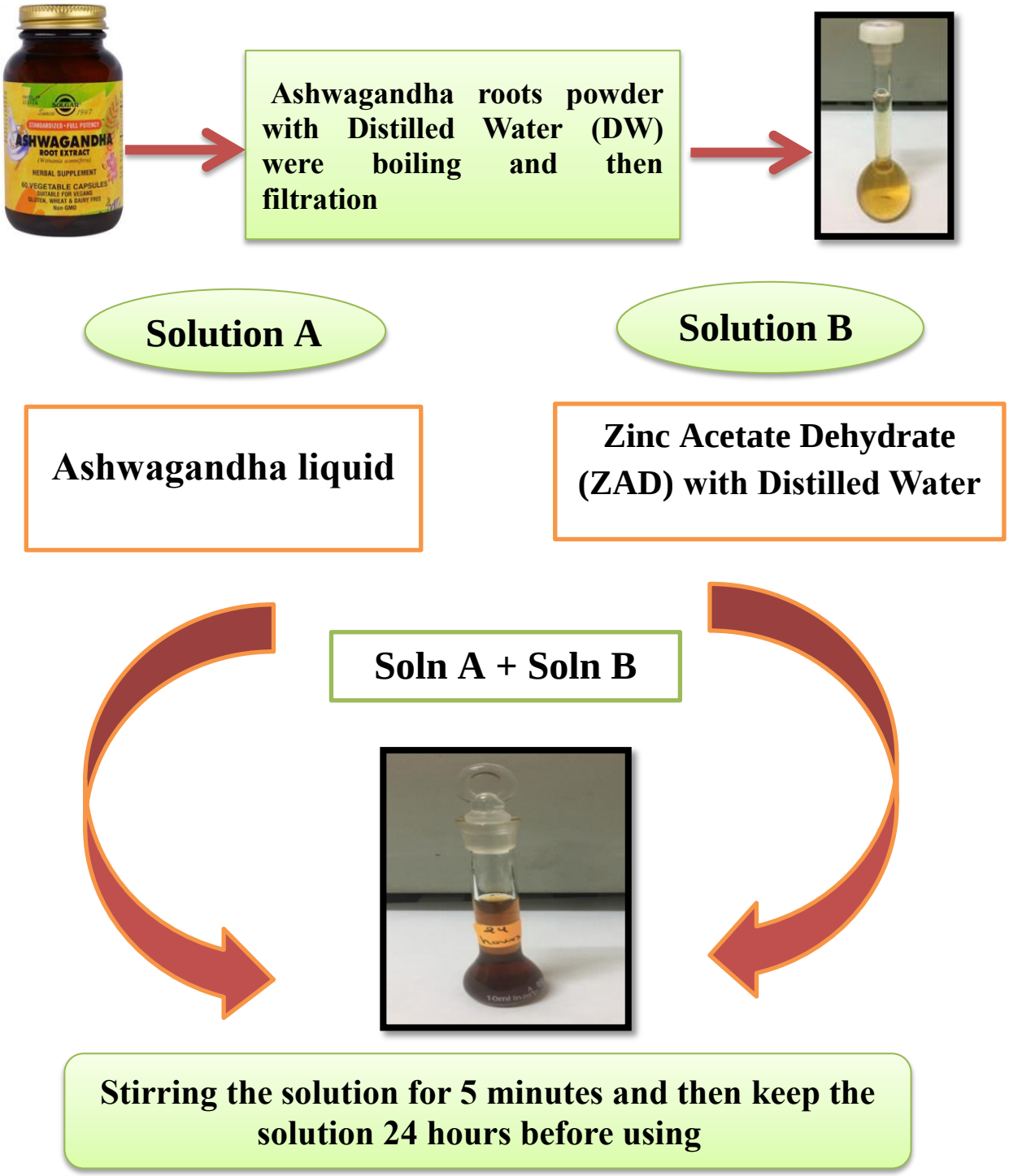

Figure (2.4):Block diagram of Biosynthesis for ZnO nanostructures using extract roots

2.6 Identification Techniques

The characterizations of nanoparticles and structural measurements are important for the realization and control of nanoparticle synthesis and their applications. A variety of different techniques are used , as shown in figure (2.5):

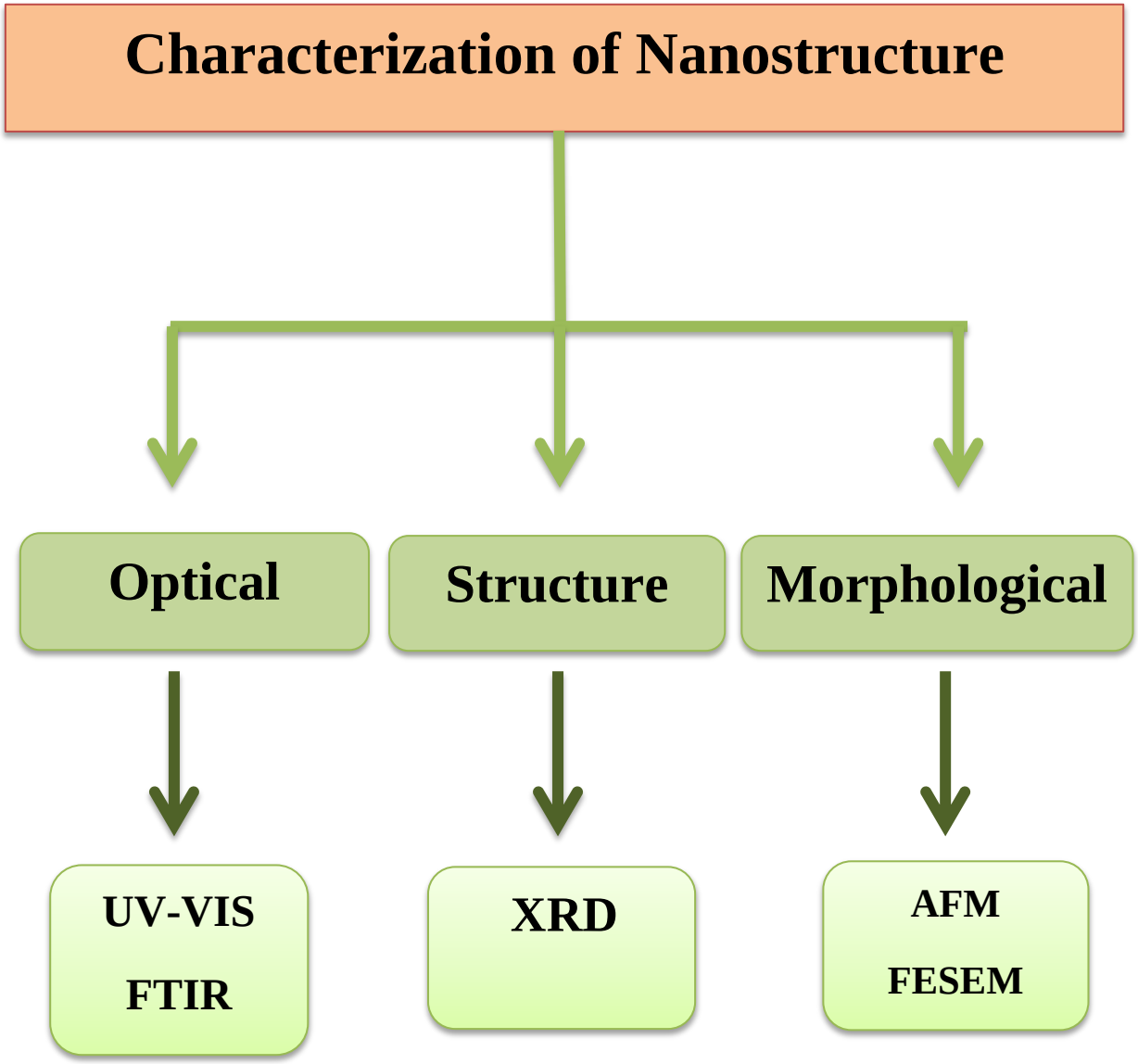

Figure (2.5): Block diagram of the Characterization of nanoparticle synthesis

2.6.1 X-ray Diffraction (XRD)

All XRD patterns for synthesized AgNPs and ZnO were recorded and analyzed using a (SHIMADZU LabX) XRD-6000 (Baghdad University, Ibn Al Haitham College of Education, Central Service Laboratory) with a copper anode emitting at 1.5406 A^0 and analyzed by the MDI/JADE6 software as shown in Figure (2.6) to determine the crystalline size. The sample was placed on the sample holder and scanned in the range from 20° to 80°.

X-ray diffraction is a valuable method for studying the structure of the compounds and investigating the effects of thermal treatment on improved crystalline samples. This is a useful method for calculating the average distance between layers or rows of atoms. The average size of the crystalline was calculated from XRD peak broadening according to Debye–Scherer relation (2.1) as shown below [67] :

$$D = (K\lambda) / (\beta FWHM \cos\theta) \quad \text{.....(2-1)}$$

Where:

D: The crystallite size.

***K*:** Crystalline shape factor of a good approximation of (0.9).

λ: The wavelength of the incident X-ray (λ = 0.154056 nm).

***βFWHM* :** The Full-Width at Half-Maximum (FWHM) of the XRD.

θ: The Bragg angle.

Figure(2.6) : X-ray Diffractometer

2.6.2 UV-VIS Spectrophotometer

UV – Vis spectroscopy has been used to verify the formation of silver nanoparticles and zinc oxide nanoparticles. The UV-VIS absorption spectrum of all prepared nano-solution samples, measured using the SHIMADZU UV-VIS 1800 spectrophotometer, covers an average of (190 – 1100) nm (Baghdad University, College of Science , Department of Chemistry), as shown in Figure (2.7). The instrument was computerized with a CRT screen and a keyboard to control the input value. The UV-VIS spectrophotometer specifications are shown in Table (2.8).

Figure (2.7) :The UV-VIS Spectrophotometer.

Table (2.4) :shows the specification of the UV-VIS Spectrophotometer [68]

Specification	
Wavelength Rang	190 nm – 1100 nm
Spectral Band Width (Resolution)	1 ± 0.2 nm
Wavelength accuracy	±0.1nm at (656.1nm D2), ±0.3nm (All region)
Photometric system	Double Beam
Light source	20W halogen lamp and deuterium lamp
Detector	Silicon photodiode
Operating temperature	40 ^{0}C

2.6.3 Fourier Transformation Infrared Spectrometer (FTIR)

The Fourier-transform infrared spectra was obtained using SHIMADZU 8400S corporation FTIR spectrophotometer (Baghdad University, College of Science, chemistry department) as shown in Figure (2.8).This technique was used to investigate the molecular structure of the Ashwagandha roots , sliver nanoparticles and zinc oxide nanoparticles. This analytical device used in the range of 400 to 4000 cm^{-1} mid-infrared radiation with a wave number $\bar{\nu}$.

Figure (2.8): Fourier transformation infrared Spectrometer.

2.6.4 Atomic Force Microscopy (AFM)

The topological properties of the Ashwagandha roots were studied by contact mode of Atomic Force Microscopy (AFM, modal AA 3000 scanning probe microscope from Angstrom Advanced Inc., USA), (Baghdad University, College of Science, Chemistry department) of resolution 0.26 nm laterals and 0.1 nm vertical as presented in figure (2.9). The advantage of AFM measures three-dimensional images so that particle height and its volume can be measured and surface roughness of the grown samples.

Figure (2.9):The Atomic Force Microscopy

2.6.5 Field Emission Scanning Electron Microscope (FESEM)

The Morphological characterization of the prepared AgNPs and ZnoNPs thin films and particle size measurements were studied using Field Emission Scanning Electron Microscopes (FESEM), modal TESCAN MIRA from TESCAN Essence™ multiuser software, France),(Ferdowsi University, College of Science, Iran) with the resolution of 1.0 nm at 25 kV, as shown in Figure (2.10).

Figure (2.10): Field Emission Scanning Electron Microscope

2.6.6 Energy Dispersive X-ray Analysis

Energy Dispersive X-ray (EDX) analysis of Ashwagandha roots was performed using scanning electron microscopy (SEM; INSPECT S50), as shown in figure (2.11). The EDX gives quantity and quality of the distribution of elements in the sample.

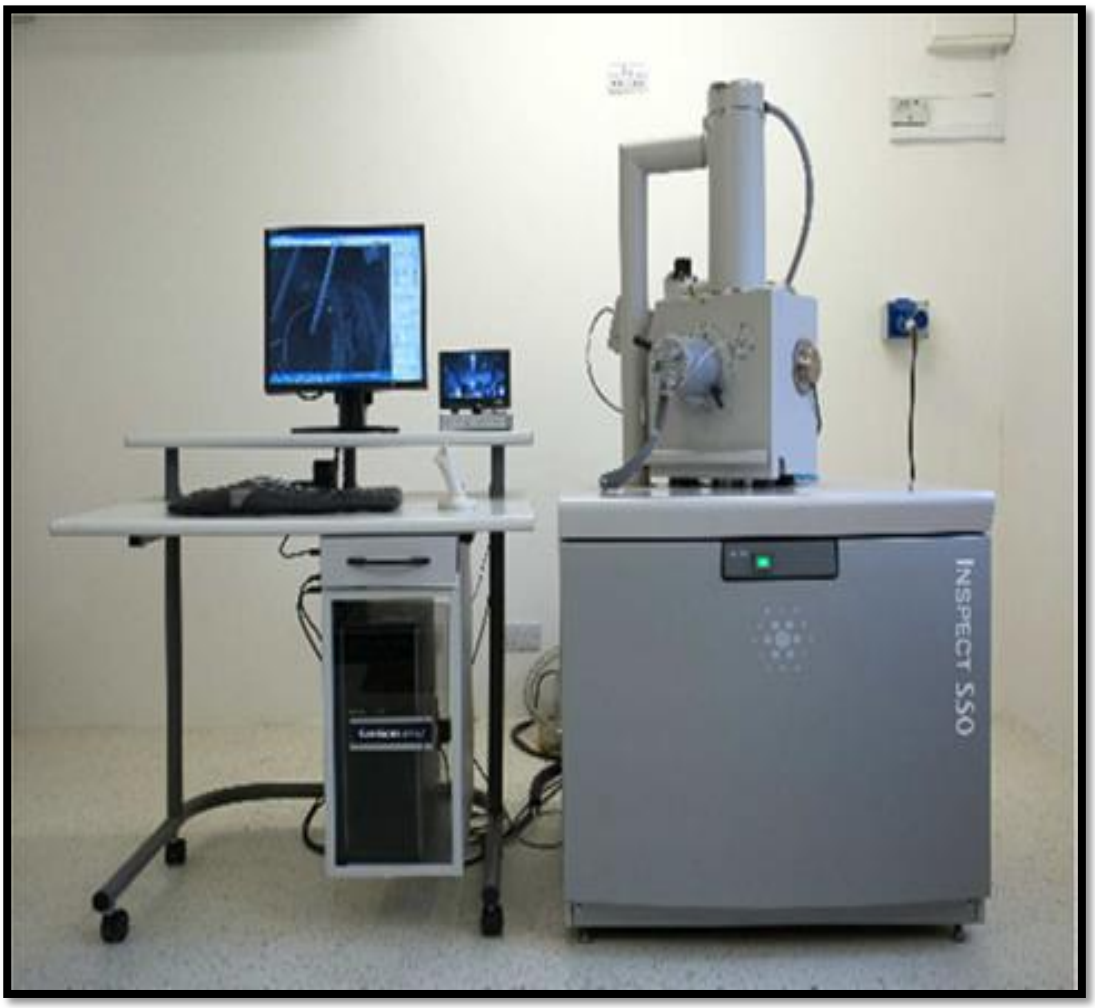

Figure (2.11): The Energy Dispersive X-ray Analysis

2.7 The biological part: Materials and Methods

2.7.1 Apparatuses and Equipment

The apparatus and equipment used for this study are listed in Table (2.5). The list involves the provider company and its origins.

Table (2.5): Apparatuses and equipment used.

Apparatus and Equipment	Company	Origin
Autoclave	CRYSTE	Korea
Incubator	Thermo	USA
Hood cabinet	CRYSTE	Korea
Micropipette and Tips	Danish	Denmark
Burner	Amal	Turkey
Eppendorf tube	Eppendorf	Germany
Vitek2 compact system	BioMérieux	France
Micropipette	Dragon lab	China
Balance	Ohaus	Switzerland
Tips	Gilson	USA
Loop	Himedia	India
VITEK®2 GN(to identified gram negative)	BioMerieux®	France
VITEK®2 GP(to identified gram positive)	BioMerieux®	France
Hot plate with Magnetic stirrer	Heidolph	Germany
Densichek Plus	BioMerieux®	France
Diode Laser (410 nm)		China
Microplate reader LT-4000	Labtech	UK

2.7.2 Biological and Chemical Materials

The biological and chemical materials used in this study are listed in Table (2.6), with the supplier company and origin.

Table (2.6): The biological and chemical materials used.

Materials	Company	Origin
Mannitol Salt Agar (MSA)	Condalab	Spain
Uti chromagar (UCA)	Himedia	India
MacConkey Agar (MCA)	Himedia	India
Luria Bertani Broth (LB)	Himedia	India
NaCl (Sodium Chloride)	Fluka	Germany

2.7.3 Antibiotic

The antibiotic used for detecting the sensitivity of *E.coli* and *S.aureus* isolates is meropenem Abbreviations for antibiotic (Mem) .

2.8 Culture Media

The ready-made media used in this study were prepared based on the information specified in the containers about the manufacturing company. They were then sterilized by autoclave at 121°C for 15 minutes.

2.8.1 Prepared Media

2.8.1.1. Mannitol Salt Agar (MSA)

Mannitol Salt Agar (MSA) was prepared by dissolving 111grams of the medium in one liter of distilled water. The suspension was then heated with constant agitation and boiled for a minute to dissolve the medium completely, then sterilized for 15 minutes at 121 ° C by autoclaving. When cooled to 45-50 ^{o}C and thoroughly mixed before pouring into sterile Petri-dishes. This medium has been used to detect bacterial ability for *staphylococci* isolation and enumeration.

2.8.1.2. Uti chromagar (UCA)

Uti chromagar (UCA) was prepared by dissolving 56.8 grams in 1000 ml of distilled water. The suspension was then heated with regular agitation and boiled for one minute to dissolve the medium completely, then sterilized for 15 minutes at 121 ° C by autoclaving. UTI Agar is a differential medium for the presumptive detection of micro-organisms, primarily causing infections of the urinary tract, most commonly known as *Escherichia coli*.

2.8.1.3. MacConkey Agar (MCA)

MacConkey Agar was prepared by dissolving 49.53 grams of the dehydrated medium in 1000 ml filtered distilled water. The suspension was then heated with regular agitation and boiled for a minute to fully dissolve the media, then autoclaved at 121 ° C for 15 minutes. Well mixing media and then cooling up to 45-50 ° C, before pouring to sterile Petri dishes. The surface of the media should be dry upon inoculation. This media helped detect the isolation of *Escherichia coli.*

2.8.1.4. Luria Bertani Broth

Luria Bertani Broth had been prepared by dissolving 25 grams of distilled water in 1000 ml. The suspension was heated regularly and boiled for one minute to dissolve the medium completely, then sterilized at 121°C for 15 minutes by autoclaving.

2.9 Bacteria counting

The instrument DensiCHEK Plus 21255-P1ML1 was used to measure the optical density (OD) of a microorganism suspension as shown in Figure (2.12). It is used to adjust bacterial suspension turbidity, consisting of four tubes (0.0 McFarland, 0.5 McF, 2.0, and 3.0 McF), providing values proportional to concentrations of microorganisms in McFarland units. The device is indicated for use with glass and polystyrene test tubes.

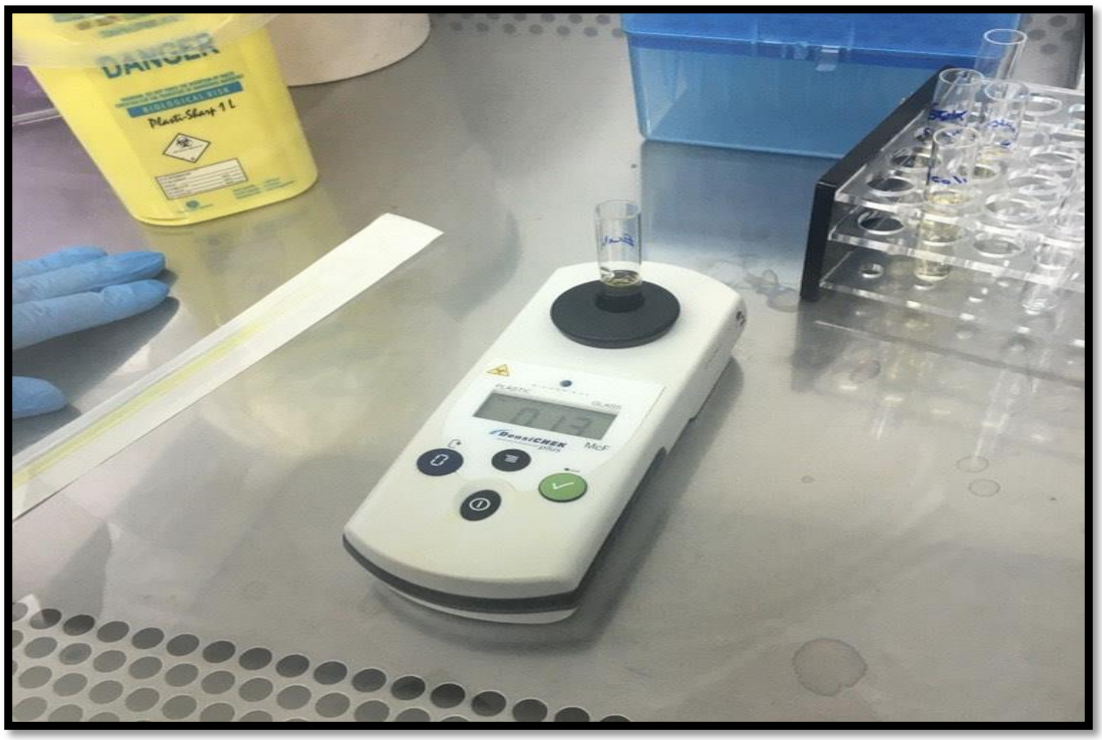

Figure (2.12):Densichek Plus

2.10 Gram Stain Solutions

Gram stain solutions include iodine, crystal violet, ethanol, and safranin stains the following solutions for bacterial identification.

2.11 Isolation and Identification of *E.coli* and *S.aureus*.

Bacterial isolates of both bacteria were identified by a combination of growth on selective media, cultural characteristics, Gram stain morphology, and finally confirmed by Vitek 2 compact system.

2.11.1 Growth on Selective Media (Uti Chrom Agar for *E.coli* and Manitol Salt Agar for *S. aureus*)

Uti Chrom Agar, MacConkey Agar was used to isolating and identifying E.coli. Each swab sample was cultured on (UCA) and(MCA) by streaking and incubated aerobically overnight at 37°C. The presence of growth is indicative of positive results.

Mannitol salt agar (MSA) can be used to isolate staphylococci as a selective, differential medium. This medium distinguishes bacteria by their ability to ferment mannitol sugar, the medium's only carbohydrate. Accordingly, this selective medium was used to plate the streaking method to culture the swabbed samples. The inoculated plates were incubated at 37oC for 24 hours to obtain isolated staphylococcal colonies. The colonies of Mannitol ferments Staphylococcus appear as yellow with yellow zones in the media (positive), while non-mannitol fermenters appear pink to red colonies with no yellow color change in the medium (negative).

2.11.2 Cultural Characteristics

Visual examination of the color, consistency, odor, colony appearance of the bacterial growth, and the effect on the selective media for *E.coli* and *S. aureus* was carried out.

2.11.3Gram Stain Morphology Gram stain was used to identify

Bacterial response to the stain in addition to the examination of shape, size, and arrangement of cells with each other. A gram stain reaction was performed by placing a drop of distill water on a clean microscopic slide. A minute amount of pure bacterial colony was transferred and mixed with the water using a sterile cool loop.

A smear was prepared, air-dried, and heat-fixed by passing the slide over a gentle flame. The smear was stained with Gram's stains and then examined using a light microscope under 100X oil-immersion objective.

2.11.4 VITEK® 2 Compact System Test for *E.coli* and *S. aureus.*

VITEK systems are automated microbial identification systems using technology based on development. It can be used for microbial identification (ID) (bacteria and yeast), antibiotic susceptibility testing (AST), and detection of resistance mechanisms.

The system is available in three variants (VITEK 2 compact, VITEK 2, and VITEK 2 XL), which vary in the capacity and automation levels. All three systems are equipped with the same calorimetric reagent cards which are automatically incubated and interpreted. In this analysis, the VITEK 2 compact system (Figure 2.13) was used for its precision in the identification of bacterial isolates.

In order to calculate and change the turbidity of the bacterial cell count per 1 ml, which must be equal to 0.5 OD by DensiCHEK Plus, three to five well-isolated.Colonies of each isolate were transferred to a glass tube containing 3 ml distal water.

The sample entered the VITEK 2 compact system for transfer to the bacterial suspension of the cassette by negative pressure, then incubate the cassette for completion of the biochemical reaction within 12 hours. Interpreting the results was done using VITEK 2 compact system special software for the identification of bacterial species and strains.

Figure (2.13) VITEK 2 Compact System

2.12 Enzyme-Linked Immune Sorbete Assay (ELISA) techniques.

ELISA is a biochemical technique using in this study for measurements the number of bacteria colonies (1ml), by used plate blank 96 well of Coated Streptavidin Plate from Applied Biosystems AB. USA kits , as shown in figure (2.14).

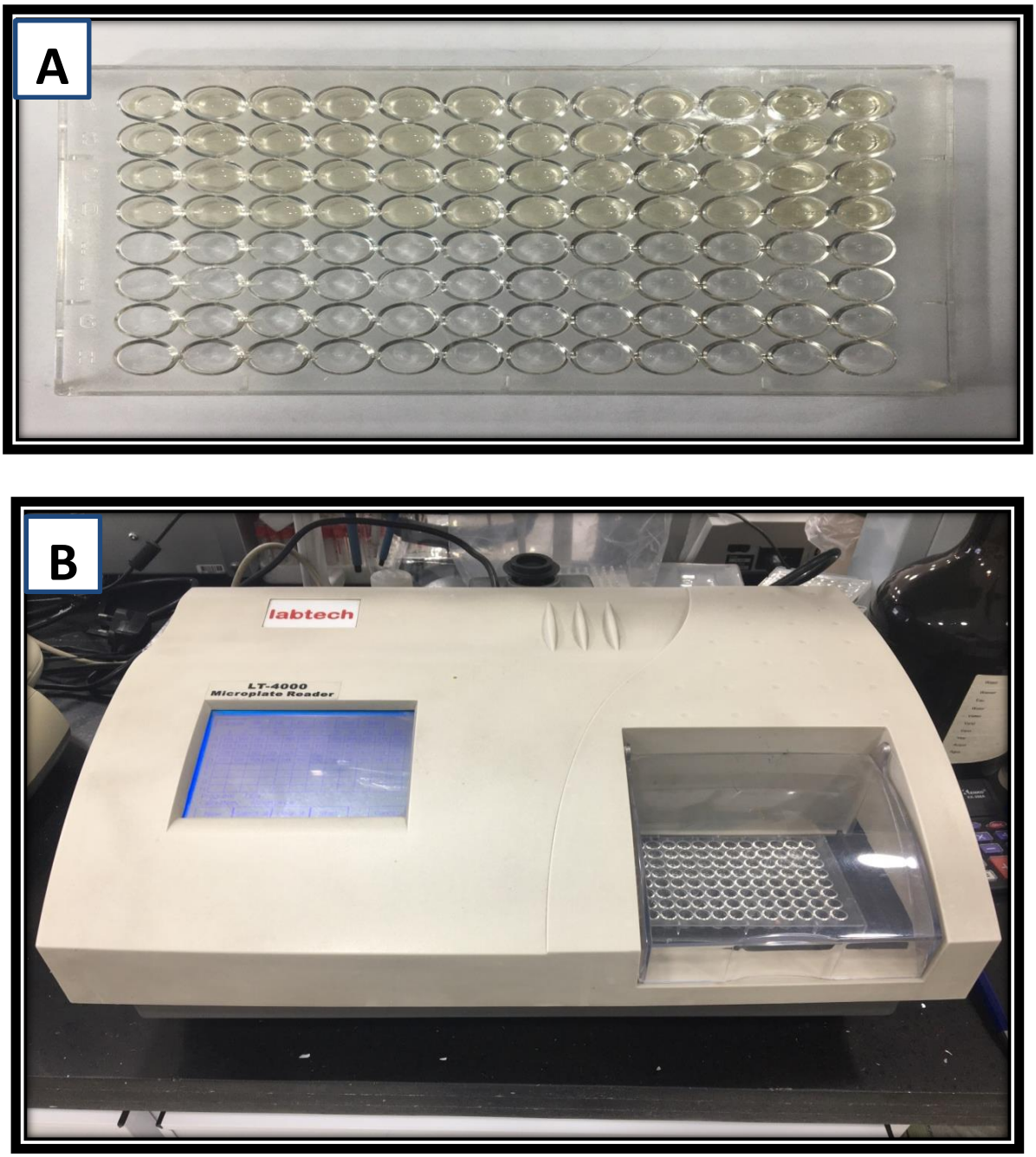

Figure (2.14) ELISA techniques : (A) optical 96- well plate (B) ELISA Reader

2.13 Evaluation of the Antibacterial activity for AgNPs and ZnONPs.

2.13.1 Well diffusion method

Antibacterial of green synthesis for AgNPs and ZnONPs was evaluated using a well-diffusion method against bacterial strains of gram-negative (Escherichia coli) and gram-positive (Staphylococcus aureus). Microorganisms were grown at 37 ° C in the medium of Uti chromagar (UCA) and Mannitol salt agar (MSA), which is shown in figure (2.15). For the preparation of bacterial suspension with a turbidity of 0.5 McFarland (equal to 1.5×108 colony-forming units (CFU)/ml), eighteen to 24 hours of single colonies on agar plates were used. Holes of 8 mm in diameter were filled with 80 µl impregnated with equal concentrations of Ashwagandha plant extract, AgNO3 solution, synthesized AgNPs, Zinc acetate solution, synthesized ZnO NPs, and meropenem, and kept at 37 ° C. The diameter of the growth inhibition zones was measured in millimeters (mm) after the 24-hour incubation time.

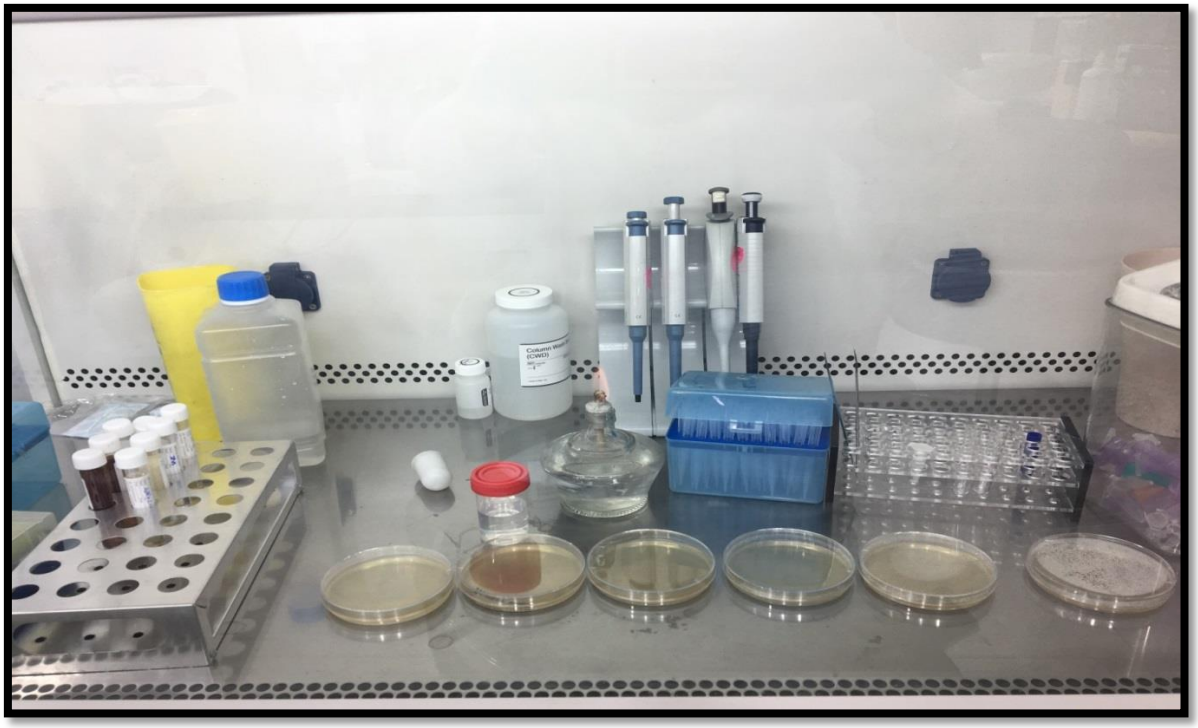

Figure (2.15) Showing all instruments and samples used in the study

2.14 Laser Systems

2.14.1 Diode Laser (410nm)

A continuous wave Diode Laser (410nm) was used in this study. It is compact, long lifetime, low cost and easy to operate. It is usually used in measurement, communication and spectral analysis. Figure (2.16) shows an arrangement with which the laser is fixed on.

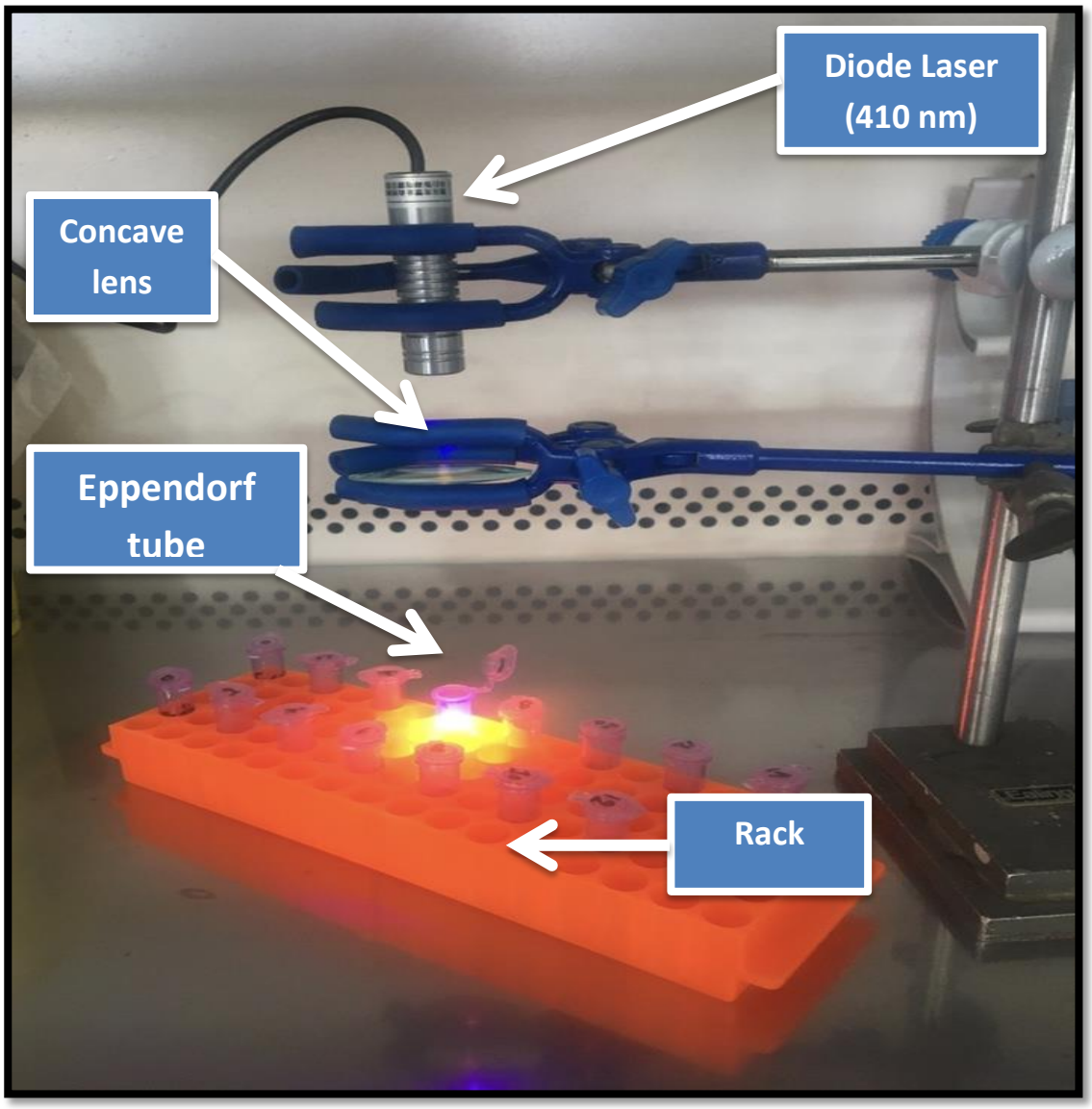

Figure (2.16): Diode laser (410 nm) set-up.

The Characteristics of the diode laser (410nm) are listed in Table (2.7). The parameters to be applied were chosen according to pilot experiments. The exposure time was varied depending on the bacterial response.

Table (2.7) : Parameters of Diode laser (410nm)

Fundamental wave length	410 nm
Mode	Continuous
Optical output power	100 mW
Operating current	140 mA
Operating voltage	3.5-5 V
Laser medium	Gallium Nitride (GaN).
Exposure time used for (*Escherichia coli*)	0 , 3, 5 ,7 ,9, 11, 13,15 minutes
Exposure time used for *(staphylococcus aureus).*	0 , 3, 5 ,7 , 9, 11, 13, 15 minutes

2.15 Preparation of Escherichia coli and staphylococcus aureus for irradiation experiments

The selected two bacterial strains were grown on McConkey agar at 37 ºC for 18-24 hours for *E.coli* and Mannitol salt agar at 37 ºC for 18-24 hours for *S.aureus*. The OD measurement for the bacterial suspension was repeated for the selected isolate before each trial.

A suspension of each bacterial growth with a dilution of 10^{-5} was chosen according to preliminary trials of viability count. The experimental sample was prepared by placing 0.5 ml of bacterial suspension with an equal volume of a 0.5 ml sterile physiological saline solution in each one of two Eppendorf tubes. The samples were then subjected to a laser irradiation experiment.

The laser beam was focused on the surface of the suspension at a distance of 21 cm, and a beam diameter of 1 cm using a concave lens. The exposure time was from 3 to 15 minutes for two bacterial strains at two minute interval. After irradiation, all samples were then incubated at 37 °C for 24 hours. The number of colony-forming units were calculated.

2.17 Statistical Analysis

The Statistical Analysis System- SAS (2012) program was used to detect the effect of different factors in study parameters. The least significant difference –the LSD test (Analysis of Variation-ANOVA) was used to significantly compare between means. An estimate of the correlation coefficient between variables in this study [69].

A probability value (P) is limited as:

- Non-significant at $P > 0.05$.
- Highly significant at $P \leq 0.01$.
- Significant at $P \leq 0.05$.

Chapter Three

Results & Discussions

3.1 Introduction

This chapter includes the results and discussions about the green synthesis of Ag and ZnO nanostructured material using Ashwagandha roots. Also, it includes the optical properties results, the structural results, and morphologies properties results.

The biological work includes the bacterial isolates and the bacterial activity of nanostructured material was tested against Gram-positive and Gram-negative bacterial strains.

Finally, the statistical results about using a laser (410nm) with bacteria interaction and the discussion about it.

3.2 Optical properties

The optical properties of silver (Ag) nanoparticles and zinc oxide (ZnO) nanoparticles that extracted using Ashwagandha were presented. This involves the UV - VIS absorption.

3.2.1 The UV–VIS absorption spectrum of Ashwagandha

The UV–VIS absorption spectrum of the control Ashwagandha root extract is shown in Figure (3.1). The absorption spectrum was ranged between 200-1100 nm. The wavelength for the absorption maxima (λmax) of Ashwagandha root extract was at 310 nm. As can be observed from the figure, the resultant absorption peak at 310 nm is corroborated with the pale yellow color for Ashwagandha root. This result proved that plant extract absorption spectrum in UV. The plants' absorption peak at the UV region while the spectrum region is at a minimum at the visible. This result agrees with M. Kumar Trivedi [70].

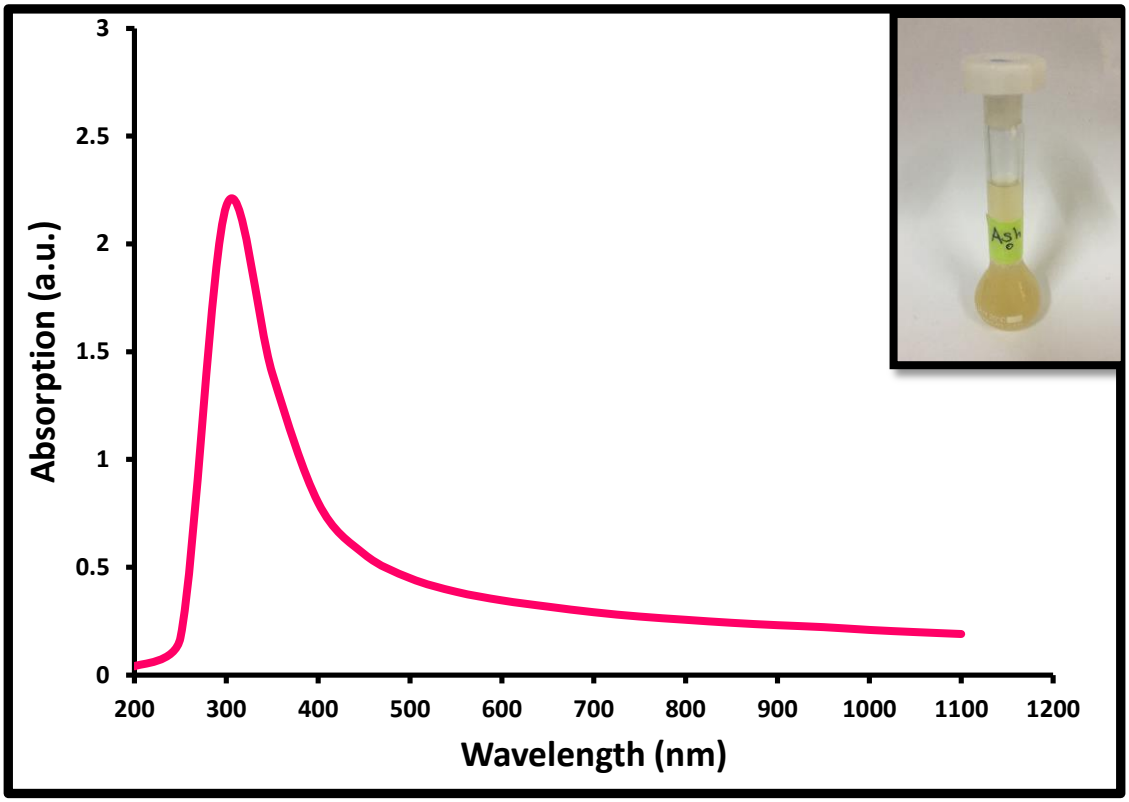

Figure (3.1): shows the UV–Vis absorption spectrum of the Ashwagandha root.

3.2.2 The UV–VIS absorption spectra of Silver Nanoparticles

UV–Vis spectra for different mixing times were achieved.The synthesized silver nanoparticles were analyzed in the range of 200-700 nm. In order to know the forming of Ag nanoparticles from mixing Ashwagandha roots with $AgNO_3$ solution.

All results were shown in Figure (3.2), the reduction of the silver ions was observed by measuring the UV-visible spectrum of the reaction mixture for 0 hours, 4 hours, 24 hours, 28 hours, 48 hours, and 72 hours. The absorption spectrum at 72 hours was similar to the absorption spectrum at 48 hours. For all our experimental work, 48 hours condition was chosen. When colorless $AgNO_3$ solution mixed with Ashwagandha roots at 0 hour time watery pale yellow color was shown. The mixed solution color at time 4 hours,

24 hours, 28 hours, 48 hours and 72 hours, was gradually from light yellow to dark reddish-brown. As can be seen from figure (3.2) absorption spectra for the Ag NPs five absorption peaks appear at 395 nm, 400 nm, 410 nm, 415 nm and 430 nm.

The change in color indicates the synthesis of different concentrations and particles of AgNPs. Broad absorption was observed for AgNPs between 375 and 450 nm. The peak at these regions confirms the presence of silver nanoparticles. In figure (3.2) the surface plasmon resonance peak at 430 nm has confirmed the synthesis of AgNPs. The optical properties of silver nanoparticles (AgNPs) change which depends upon the collective oscillation of free-electron when particles aggregate and the conduction electrons near each particle surface become delocalized and are shared amongst neighboring particles. Due to the combined oscillation of AgNPs electrons in resonance with the incident light wave, these electrons produce a surface plasmon resonance (SPR) band.

The result, observes the spectrum shifts the surface plasmon resonance (SPR) to lower energies. i.e. The absorption peaks move to red shift of plasmon resonance (increases intensity of wavelength at which plasmon resonance occurs) with wide and lower intensity spectrum towards blue shift because of the accumulation effect. When spherical AgNPs were present in the reaction solution, a single SPR band was observed, while more than one SPR band was present in the case of other shapes. The increase of color intensity and SPR band sharpness clearly indicates the reduction of Ag^{+}into Ag^{0}.These results are in good agreement with M.Gregory et.al. [71]

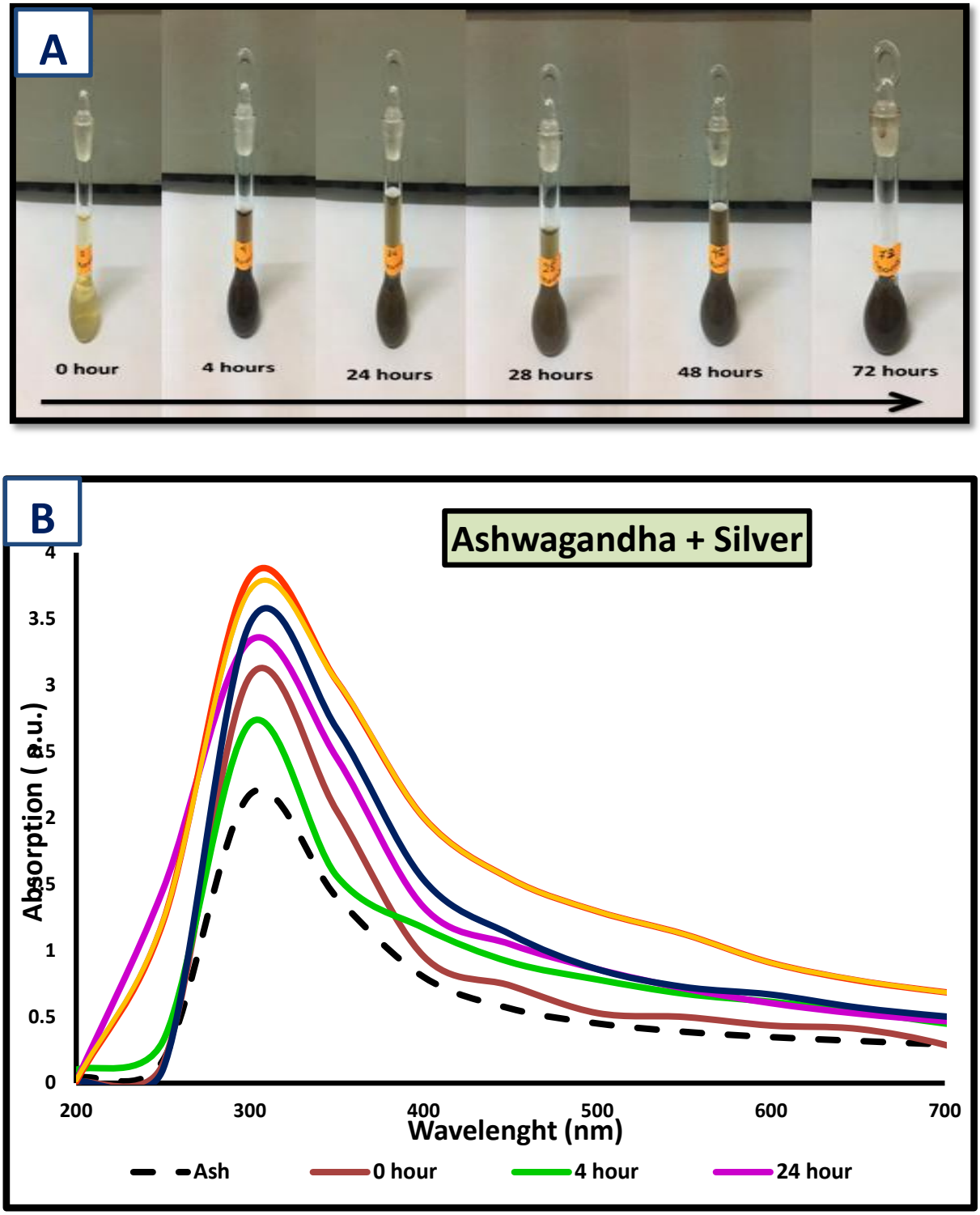

Figure (3. 2) Synthesis of AgNPs by using Ashwagandha roots extract: (A) Gradual visible color change during AgNPs synthesis and (B) UV-visible spectra of Sliver Nanoparticles with Ashwagandha at different times.

The optical band gap of silver nanoparticles (AgNPs) was calculated from Figure (3.2) as in figure (3.3), which is obtained when $(\alpha hv)^2$ is plotted against photon energy (hv). The intercept of the straight line of hv axis corresponds to the optical band gap (Eg),which shows the direct transitions between the valence and the conduction bands of the silver nanoparticles (AgNPs) where it is 2.3 eV at the time of 48 hours.

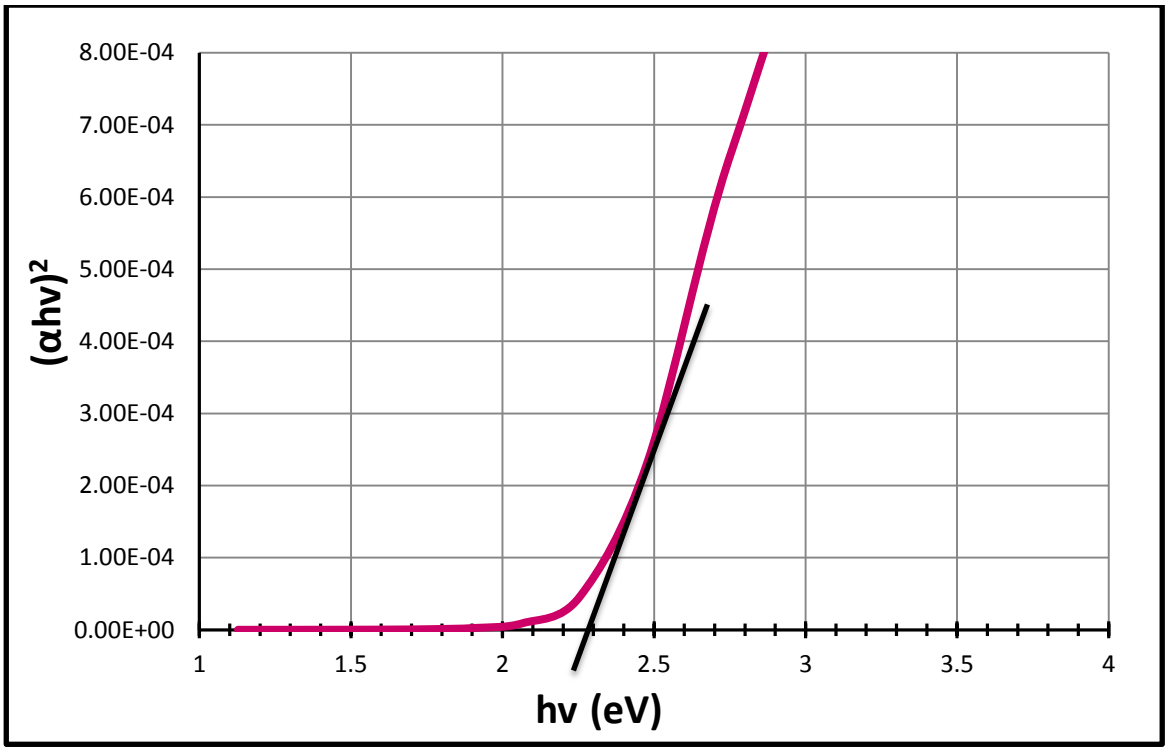

Figure (3.3): The band gab of silver nanoparticles (AgNPs).

3.2.3 The UV–VIS absorption spectrum of Zinc Oxide Nanoparticles

The reaction mixture of the extract roots of Ashwagandha and Zinc Acetate Dehydrate (ZAD) in solution produced a strong change of color after 24 hours from white to yellowish-brown. Where the observed change in color confirmed the ZnO NPs figuration. The color change monitored was due to ZnO NPs surface plasmon resonance excitation.

The UV-VIS spectrum of biosynthesized zinc oxide nanoparticles using Ashwagandha showed a strong absorption peak at 300 nm within the

absorption orange 200-600 nm, which is a characteristic signature for ZnONPs as shown in Figure (3.4). Intense and broad absorption further shows the individual distribution of nanoparticles.

The optical band gap of the zinc oxide nanoparticles (ZnO NPs) has been calculated as shown in Figure (3.5), which is obtained when $(\alpha h\nu)^2$ is plotted against photon energy ($h\nu$). The intercept of the straight line of the $h\nu$ axis corresponds to the optical band gap (Eg) that indicates the direct allowed transitions between valence and conduction bands.The band gap of ZnO was 3.4 eV. This result agrees with M. Manokari et.al.[72]

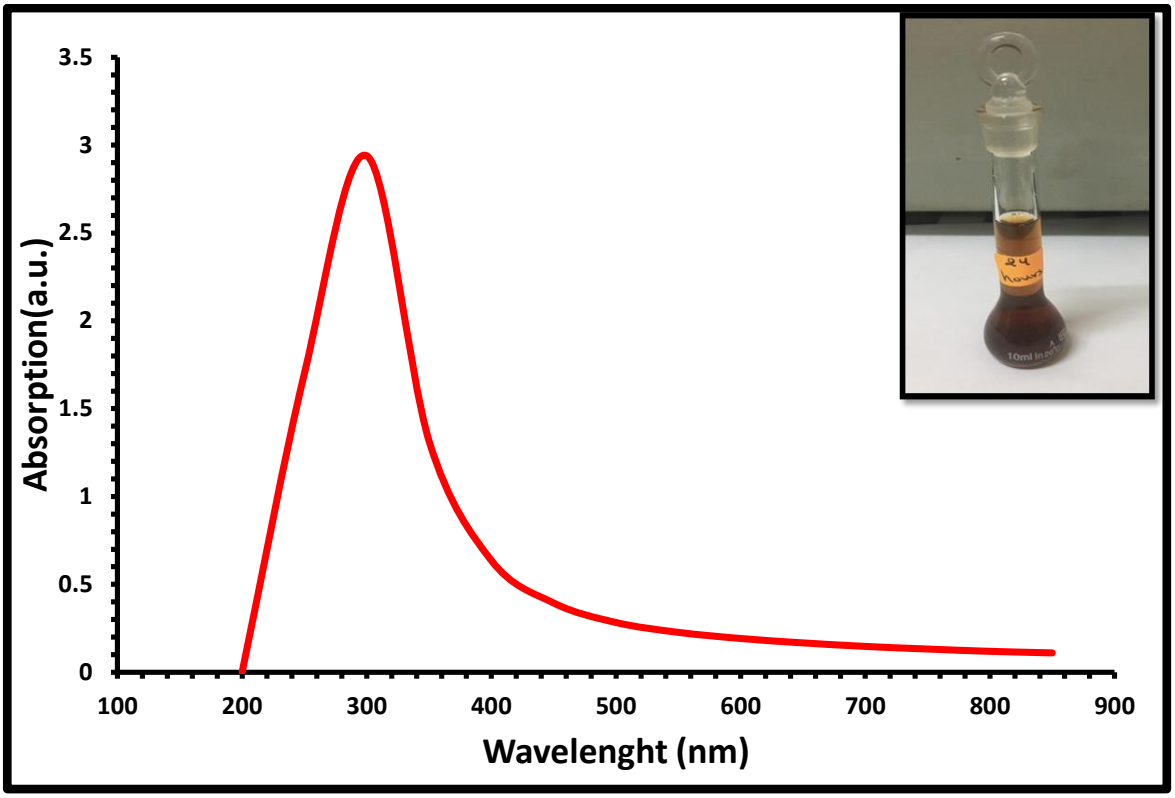

Figure (3.4): The absorption spectrum of ZnO nanoparticle.

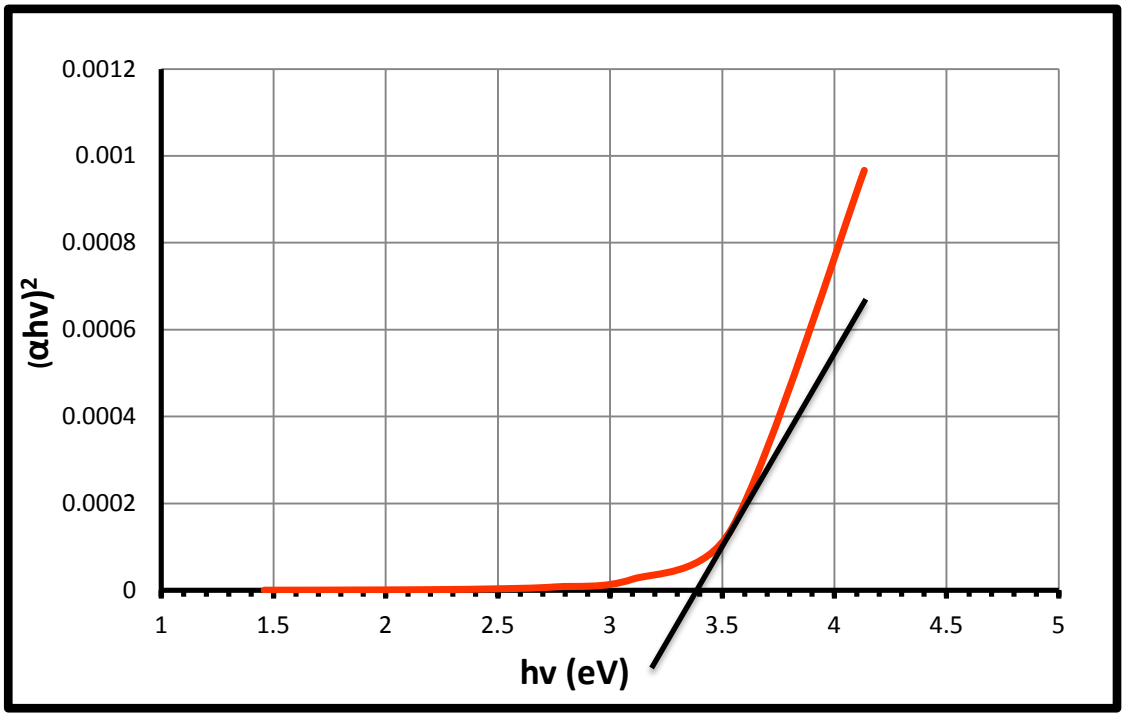

Figure (3.5): The band gab of ZnO nanoparticle

3.2.4 Fourier Transformation Infrared Spectrometer (FTIR)

The Fourier Transformation Infrared Spectrometer (FTIR) analysis of the ashwagandha root extract was done and the functional groups associated were determined as in figure (3.6). The broad absorption band observed at ~3421 cm^{-1} corresponds to the O-H stretching, while the absorbance band found at ~2920 cm^{-1} is related to stretching vibration of CH_3– groups, so it can be directly correlated with the presence of alkane groups in the plant extract.

The peak at 1618 cm^{-1} attributed to the stretching vibration of the C = C due to deformation in the aromatic ring of flavonoids where as the peaks at 1460 cm^{-1} and 1394 cm^{-1} peak are attributed to C– H bending. At 1078 cm^{-1} peak in the FTIR spectrum might be due to – C– O stretching of phenolic acid or polysaccharides of plant extract. The crest forms that appear between 838 cm^{-1} to 524 cm^{-1} are assigned to the C-H aromatic bending.

From the figure analysis, there chemicals can be indicated the number of chemicals such as Bromide, Iodide, Chloride, Fluoride, Alkanes, Imines, Oxine, Aromatic (C=C), Aldehyde, Amines, which all were found in all Ashwagandha roots extract.This result agrees with M. K.Trivedi et.al. [73].

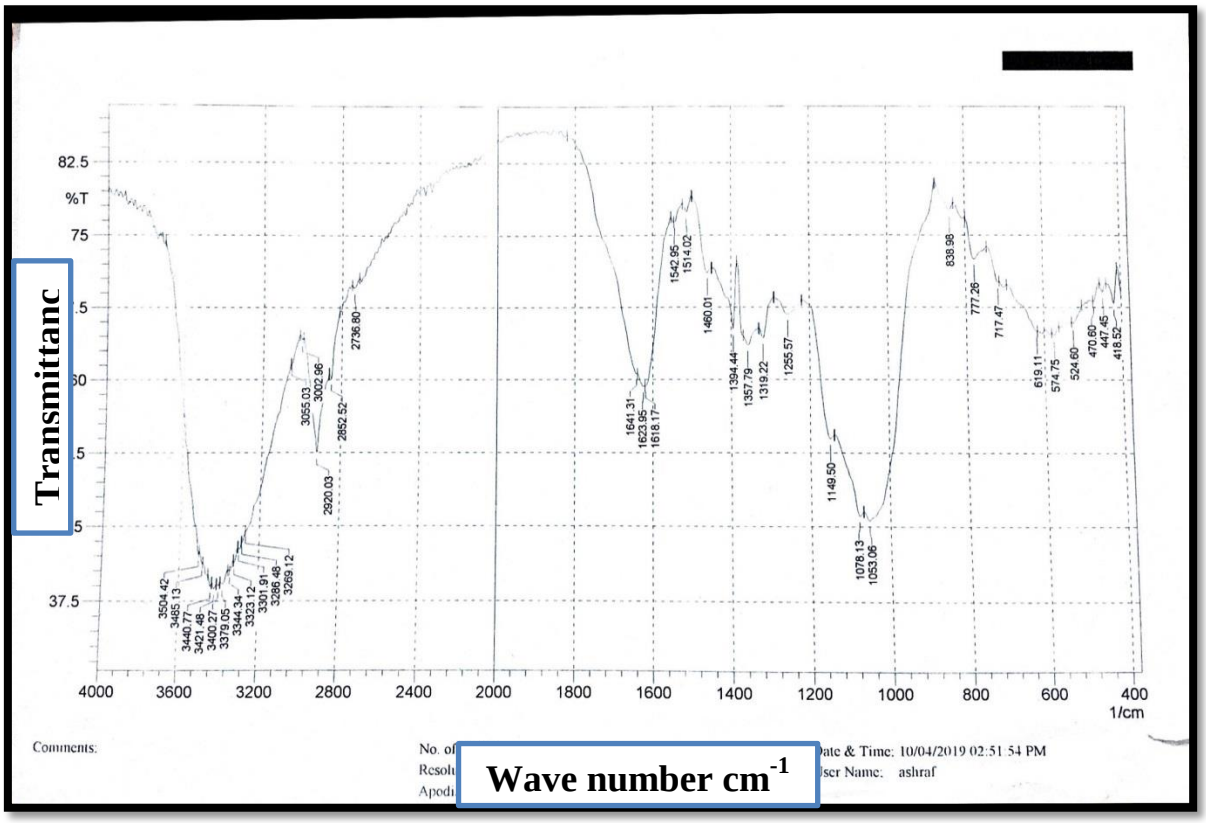

Figure (3.6): FTIR spectra for Ahwagandha roots.

The FTIR spectrum of AgNPs in Figure (3.7) provides information about the functional groups of the synthesized AgNPs using the Ashwagandha root extract. The observed main peak at 495 cm^{-1} corresponds to metal confirms the formation of (Ag).

The strong flexural band of 3413 cm^{-1} belongs to the -OH functional group on the root extract surface of the maize shifted due to the interaction between the Ashwagandha root extract and the silver metal. The medium peaks of 1460 cm^{-1} and 1394 cm^{-1} indicate the C−H and C≡H of alkanes and alkynes,

respectively. The peak at 1635 cm^{-1} is a signal of N−H bond vibrations from amide groups of the proteins.

Further, FTIR spectrum exposed a peak at 1290 cm^{-1} is due to the presence of the C−N-like amine groups. C-N stretching , vibrations peak were also appeared in the spectral range of 1384 cm^{-1} to 962 cm^{-1}. This result agrees with C. I. Nosiri et.al [74].

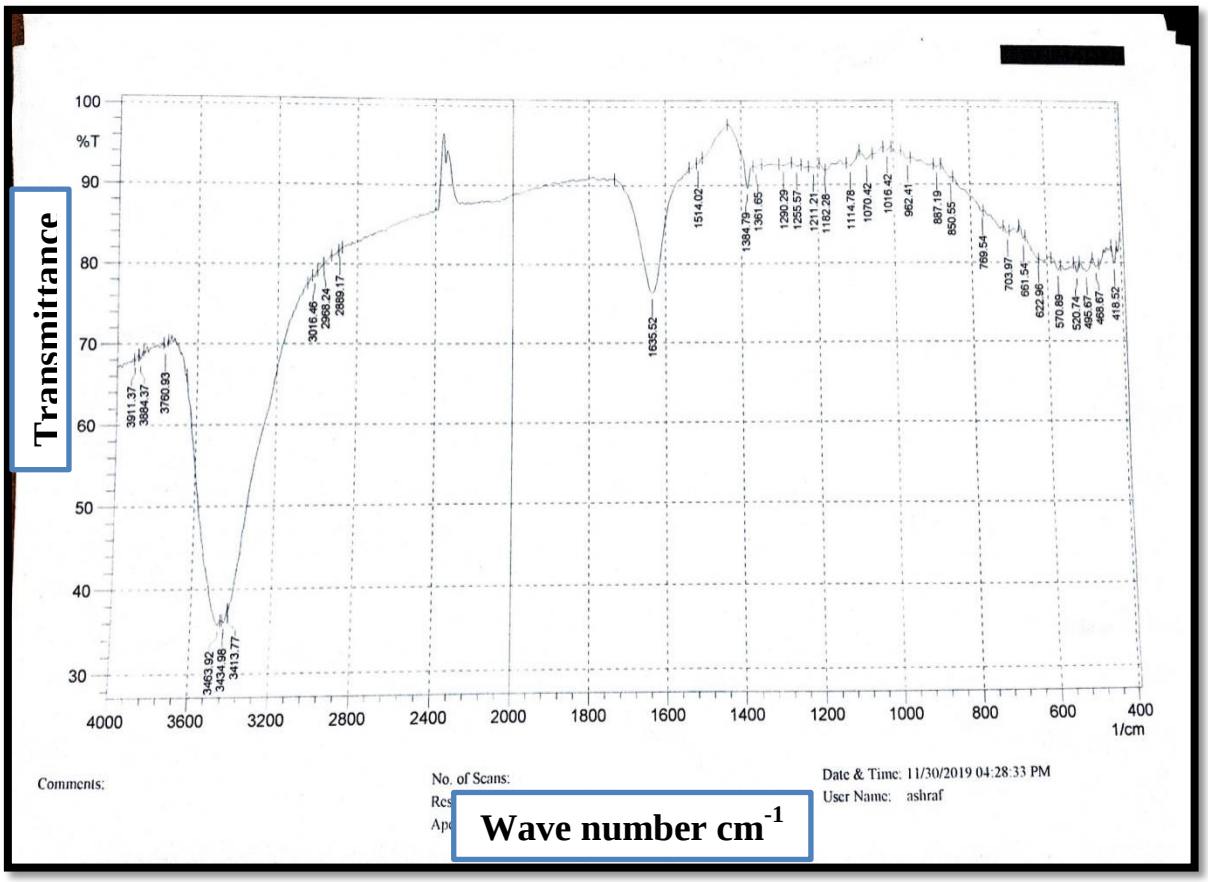

Figure (3.7): FTIR spectra of green synthesized AgNPs using Ashwagandha root extract.

Figure (3.8) represents the FTIR spectra for the green synthesized of ZnO nanoparticles were spectra recorded in the series of absorption band 4000 cm^{-1} to 500 cm^{-1}. The broad absorption band observed at ~3483 cm^{-1} corresponds to the O–H stretching vibrations of adsorbed water. The peaks at 2977 $cm^{-1}$and

2424cm^{-1}, which corresponds to C-H stretching vibration.The higher absorption band that appeared at 1382 cm^{-1} in the spectrum has corresponded to C=O stretching vibration. Where the absorption at 821 cm^{-1} is due to the formation of tetrahedral coordination of Zn.

The spectrum also reveals a peak around 1043 cm^{-1} is due to the C-O stretching vibration. The peaks that appear between 400 cm^{-1} to 600 cm^{-1} are assigned to the metal-oxygen (M–O) stretching mode. The Peak at 522 cm^{-1} is the characteristic absorption of the Zn-O bond confirms the formation of ZnO , which is agree with N. Jayarambabu et.al [75].

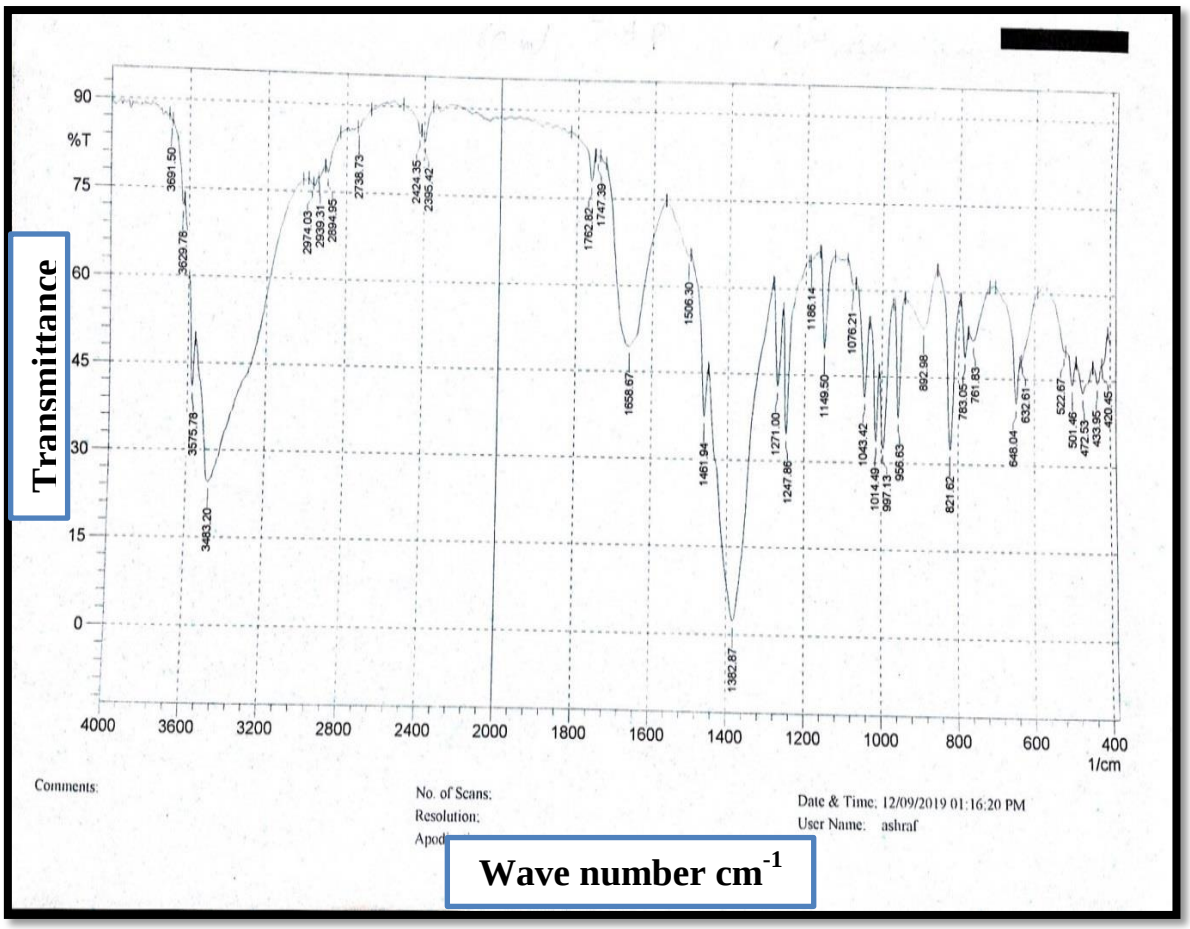

Figure (3.8): FTIR of green synthesized ZnO nanoparticles using Ashwagandha root extract.

3.3 X-Ray Diffraction of Sliver Nanoparticales and Zinc Oxide Nanoparticles Results

The X-Ray spectra were done for Ag and ZnO material which prepared by coating deposition technique on glass substrates with annealing temperature at 350°C were analyzed to identify and measure the crystainality and particle size of them.

The crystalline nature of silver nanoparticles (AgNPs) that extracted from mixing $AgNo_3$ with Ashwagandha was confirmed by X-ray diffraction analysis as in figure (3.9). The sharp diffraction peaks indicate the good crystallinity of the prepared AgNPs. The intense and narrow peaks (111), (200), (220), (311), (222), (400), (331), (420) and (422) were assigned at 2θ = 38.11°, 44.27°, 64.42°, 77.47°, 81.53°, 97.88°, 110.49°, 114.92° and 134.88°,respectively. The sample indicated a face centered cubic structure (FCC) of silver structure with the lattice constants (a = b = c = 4.086 Å), which are consistent with the values in the standard card.

Figure (3.9) shows that silver nanoparticles (111) diffraction peak is the strongest one which it indicates that formed silver particles have a preferential crystallographic (111) orientation. This is due to the organic compounds present in the extract, which are responsible for the reduction and stabilization of the resulting nanoparticles by silver ions. The silver nanoparticles synthesized using the Ashwagandha root were crystalline in nature, conforming to this observation.

The average crystallite size (D) for synthesized sliver particles was calculated according to the Debye Scherrer equation and was equal 21 nm. Similar results were obtained by B.E. Kedi1 et.al. [76].

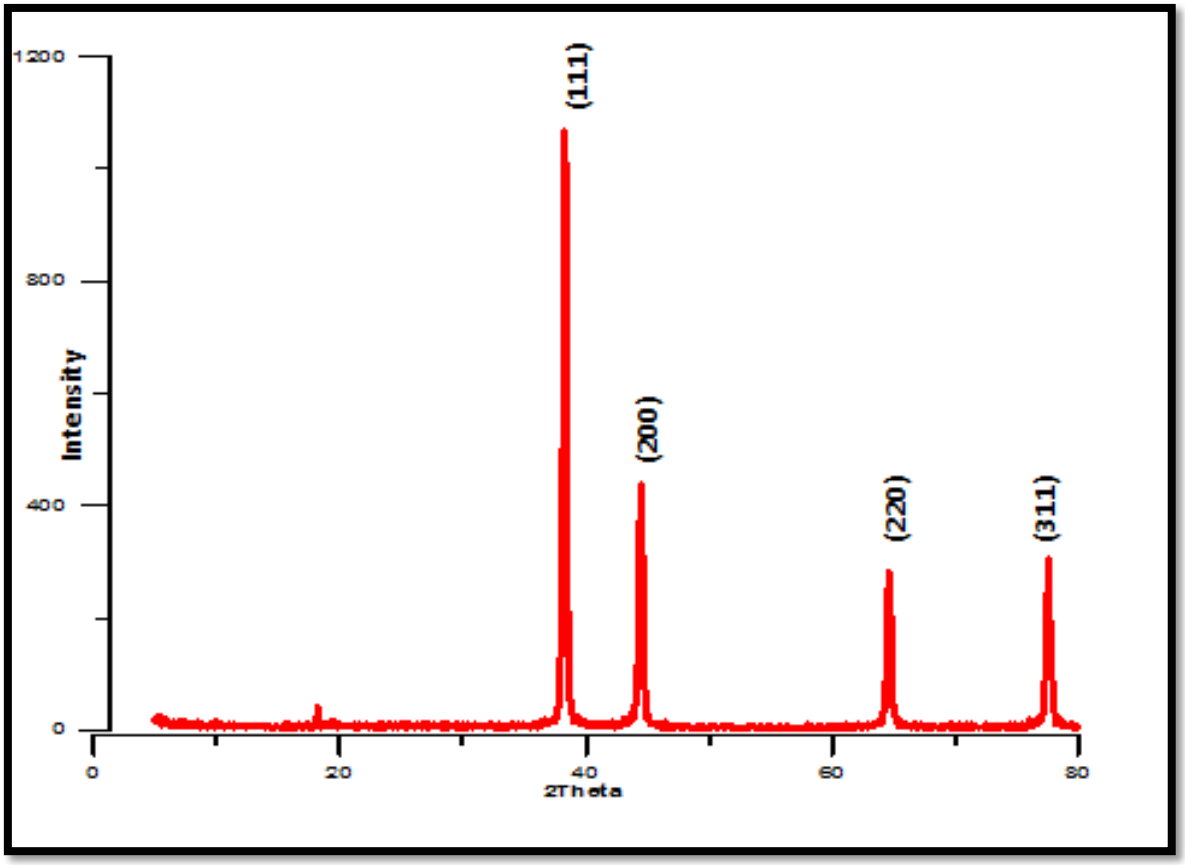

Figure (3.9): XRD pattern of synthesized AgNPs using Ahwagandha roots.

On the other side the phase characteristics and crystal structure pattern of annealed ZnO thin films at 350°C are exhibited in Figures (3.10). The sharp diffraction peaks indicate the good crystallinity of the prepared thin film. The intense and narrow peaks (100), (002), (101), (102), (110), (103), (200), (112) and (201) were assigned at 2θ = 31.69°, 34.38°, 36.18°, 47.45°, 56.46°, 62.75°, 66.21°, 67.80° and 68.92° , respectively. The sample indicated a hexagonal wurtzite ZnO structure with the lattice constants (a = b = 3.257 Å and c = 5.213 Å), which are consistent with the values in the standard card.

Figure (3.10) shows the XRD pattern a different line width for different diffraction peaks of ZnO which corresponding to the crystal nature of the morphology. Great diffraction was (100) and (101) the best diffraction peaks.

This indicates that the formed ZnO particles have a preferential crystallographic (100) and (101) orientation.The average crystallite size (D) for synthesized ZnO particles was calculated according to Debye Scherrer equation and was equal 29 nm. The range crystallite size calculated from the highest (100) and (101) XRD peak width was between 29 nm and 36 nm respectively, which is in agreement with J. Suresh et.al. [77].

The peak broadening in the XRD pattern clearly indicates that nanocrystals present in the samples. The manufacturing of ZnO in a noncrystalline form is a major way to increase its activity. There is no evidence of bulk remnant materials and impurities , this suggests that the high purity nanostructured ZnO was obtained from the chemical bath deposition method.

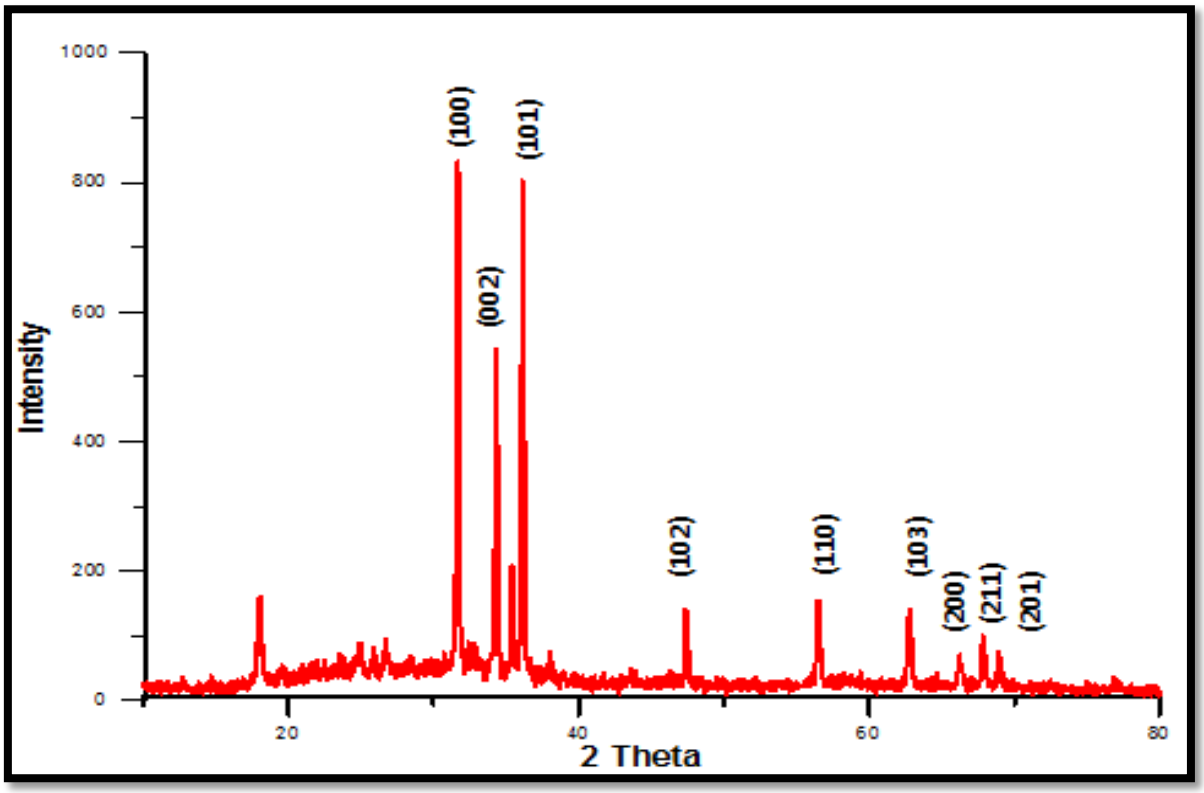

Figure (3.10) : X-Ray diffraction pattern of ZnO powder.

3.4 Morphological Analysis

3.4.1 Atomic Force Microscopy (AFM)

The topological properties of the Ashwagandha roots extract sample were investigated using Atomic Force Microscopy (AFM). Figure (3.11), is standard AFM images of Ashwagandha roots, it shows images calculated with size = 2139 X 2155 nm, and capacity analytical pixel = 404,407. The calculated values of surface roughness and the average particle size distrbution are in Table (3.1).

Avg. Diameter:72.24 nm						<=10% Diameter:40.00 nm		
<=50% Diameter:75.00 nm						<=90% Diameter:90.00 nm		
Diameter(nm)<	Volume(%)	Cumulation(%)	Diameter(nm)<	Volume(%)	Cumulation(%)	Diameter(nm)<	Volume(%)	Accumulation(%)
35.00	1.91	1.91	60.00	3.18	26.11	85.00	12.74	69.43
40.00	5.73	7.64	65.00	8.28	34.39	90.00	10.19	79.62
45.00	2.55	10.19	70.00	7.01	41.40	95.00	10.83	90.45
50.00	7.64	17.83	75.00	7.01	48.41	100.00	7.64	98.09
55.00	5.10	22.93	80.00	8.28	56.69	105.00	1.91	100.00

Table (3.1): The average particles size and roughness of Ashwagandha roots.

Figure (3.11 A) is the AFM image in the two- dimensional (2D), it is found that the average roughness are (24.2 nm),and the Root mean square (RMS) is (27.9nm).

Figure (3.11 B) represents a three-dimensional (3D) image, which explains the structure shape for grain. Ashwagandha roots AFM image reveals that the Ashwagandha is a rod shape with a length of roughly is 94.57 nm.

Figure (3.11 C) shows the granularity distribution charts, the distribution of particle size was Gaussian curve in the range between 40 and 100 nm. The highest percentage diameter of 85 nm.

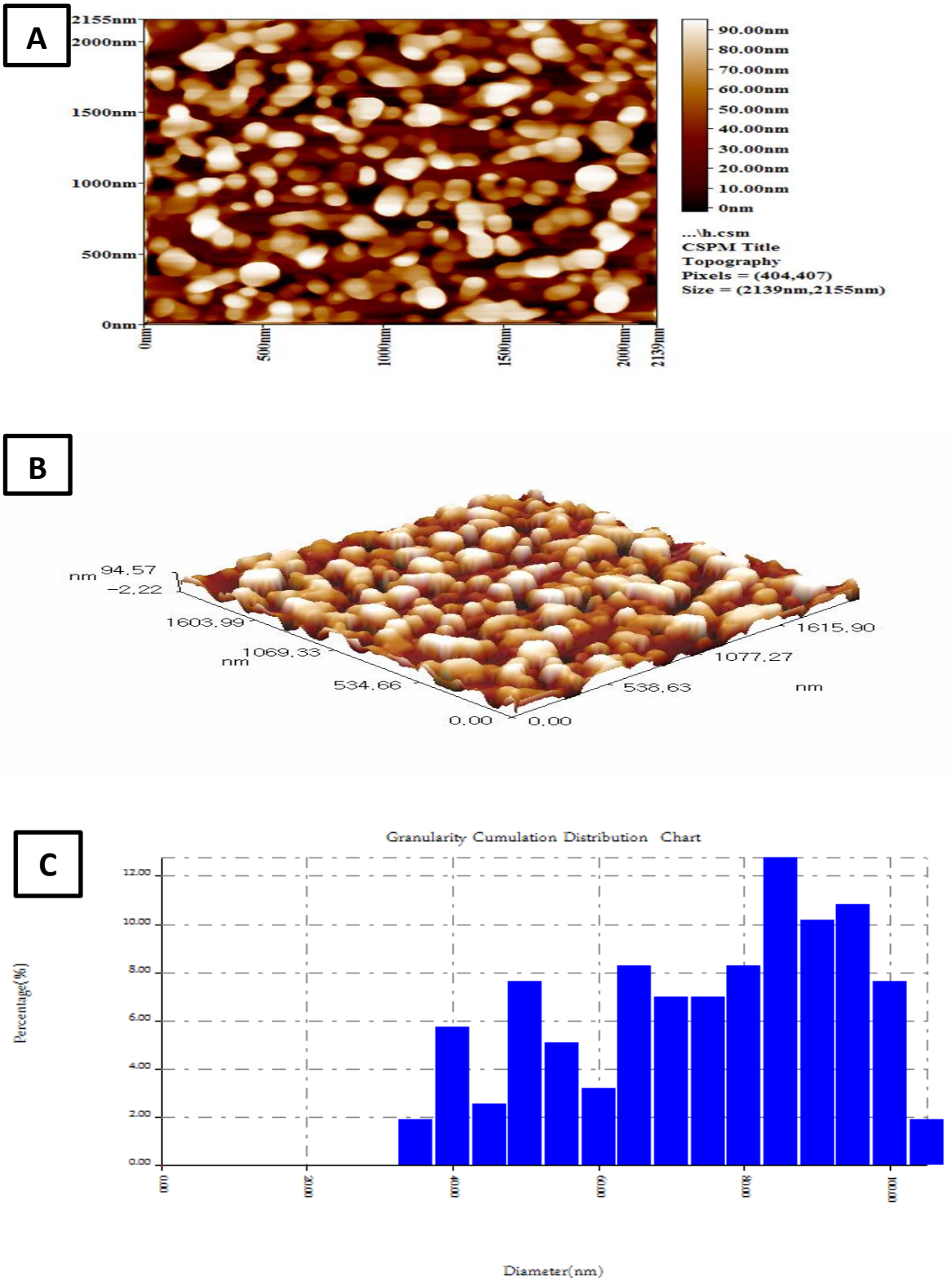

Figure (3.11): AFM images for Ashwaghandha roots thin film :

(A)Two-dimensional (B) Three-dimensional and (C) Size distribution histogram.

3.4.2 Field Emission Scanning Electron Microscope (FESEM) characteristics

The morphological analysis of the prepared nanostructured thin films that made by the green synthesis method using Field Emission Scanning Electron Microscopy. FESEM to test examines the shape and size of Ashwagandha, Ag NPs and ZnO NPs.

Figure (3.12) shows the FESEM images of Ashwagandha roots that recorded at 200nm -10µm. Figure (3.12 A) appears that Ashwagandha roots have a different size between (21- 53) nm , while the figure (3.12 B) represents that Ashwagandha roots almost have rod shape.

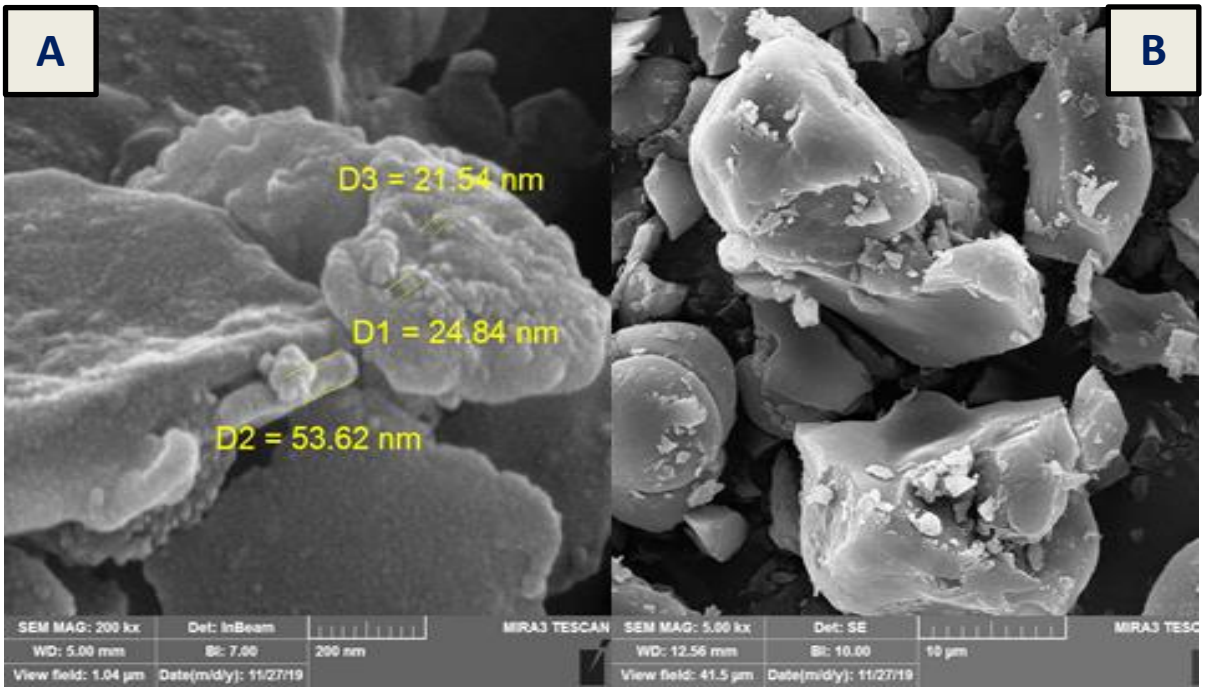

Figure (3.12) : The FESEM images of Ashwagandha roots different magnification.

FESEM is used to analyze the shape of the Ag NPs synthesized by a green method using Ashwagandha root extract. Figure (3.13) a,b,c,d shows FESEM images of silver nanoparticles (AgNPs) with different magnification ranges at 500 nm - 1 µm. Its clearly demonstrate that AgNPs nanoparticle

covered the substrates uniformly and grow on the substrates with uniform thickness continuous on all surfaces of the substrate. The morphology of the films was homogeneous and appears almost spherical in the shape of AgNP, which greater numbers of the agglomerated spherical particles within the diameter of 5.06 nm. Therefore ,the nanoparticle aggregation is dominant over the process of reduction and primary nucleation of reduced atoms. This may perhaps be related to the fact that a larger number of functional groups of Ashwagandha roots extract bind and nucleate. This result agrees with S. Chandrasekaran and S. P. Sivasamy [78]

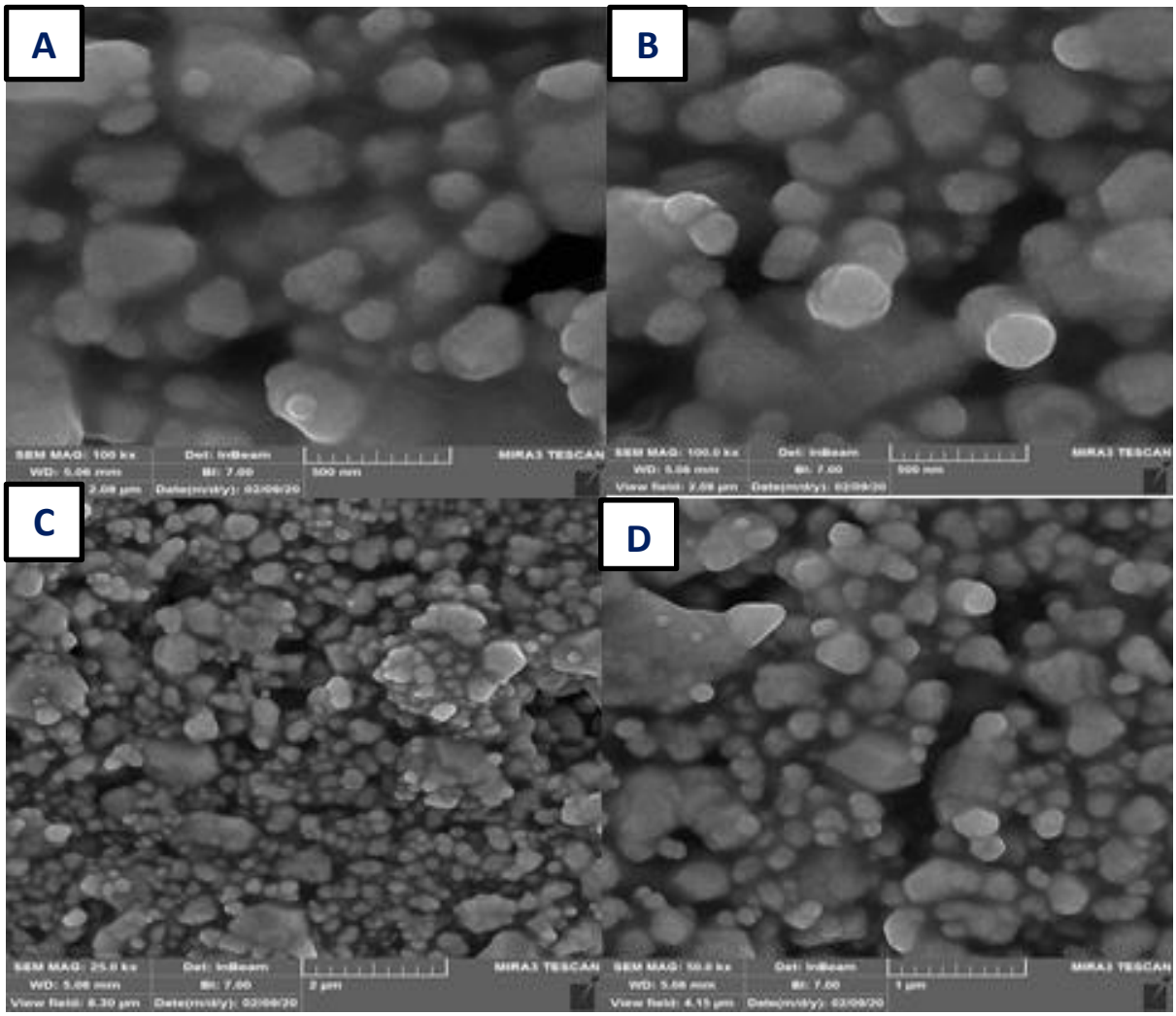

Figure (3.13): The FESEM images of AsAgNPs in different magnification ranges from 500 nm -1µm .

The morphology of the ZnO nanoparticles was investigated by using FESEM which is an important technique to study the surface morphology at the nanoscale . The FESEM image of the ZnO nanoparticles grown on glass substrate was demonstrated in figure (3.14) a,b,c,d with different magnification range from 200 nm -2 μm , which clearly demonstrate that ZnO nanoparticles covered the substrates uniformly and grow perpendicular to the substrates with uniform thickness continuous on all surfaces of the substrate. The morphology of the films was homogeneous and appears as nanoflowers shape of ZnO formed from concentrated rods nanoparticles with a length of rod (40 mm) and width diameter (5 mm).

Figure (3.14) shows the FESEM images of the annealed ZnO nanoparticles sample at 85 °C annealing temperatures. The whole surface looks smooth and uniform in the annealed samples, that the ZnO films formed micro aggregates composed of the growth of vertically aligned ZnO NR arrays through the Chemical Bath Deposition (CBD) method with the addition of PVA in the seeding solution ZAP. This result agrees with J. Sen Chang et al.[79].

It suggests that with increasing annealing temperatures, small crystallites start to coalesce together to form larger crystallites. It may be attributed to the annealing-induced coalescence of small grains by grain boundary diffusion, Also the PVA plays an important role in the formation of the structure of ZnO NR. SEM images also indicate that the hexagonal crystal phase is less distinct for the grown sample. The distinct phase appears gradually with increasing annealing temperatures. Together with previous x-ray results, it implies that the Chemical Bath Deposition (CBD) is an excellent method for the deposition of thin films of metallic oxides with optimum annealing temperature to get high-quality.

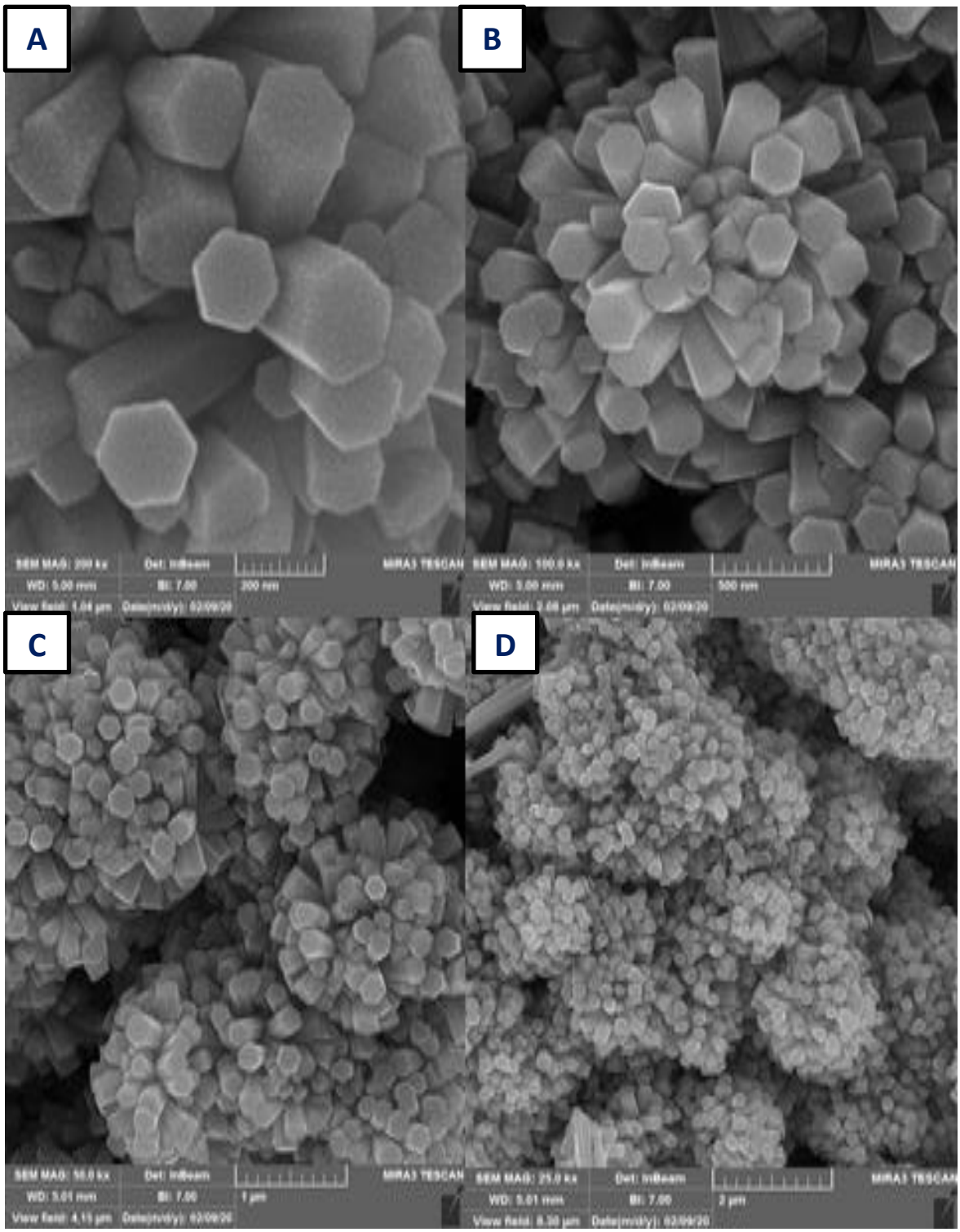

Figure (3.14) : The FESEM Images of ZnO NPs in different magnification ranges from 500 nm -2µm.

3.5 Energy Dispersive X-ray Analysis (EDX)

Energy Dispersive X-ray Analysis (EDX) is a chemical analysis method used in combination with SEM to determine the elemental composition of the Ashwagandha root extract sample.

Figure (3.15) appears peaks in the EDX Spectrum ,which identifies the atom orresponds to a single element component in the sample. The EDX spectrum proves that the Ashwagandha sample was composed of Ca , Cu, C and O elements by the representation of different Calcium, Copper , Carbon and Oxygen peaks.The EDX analysis revealed the presence of the other elements such as K ,Cl. The atomic percentage of all elements are in Table (3.2).

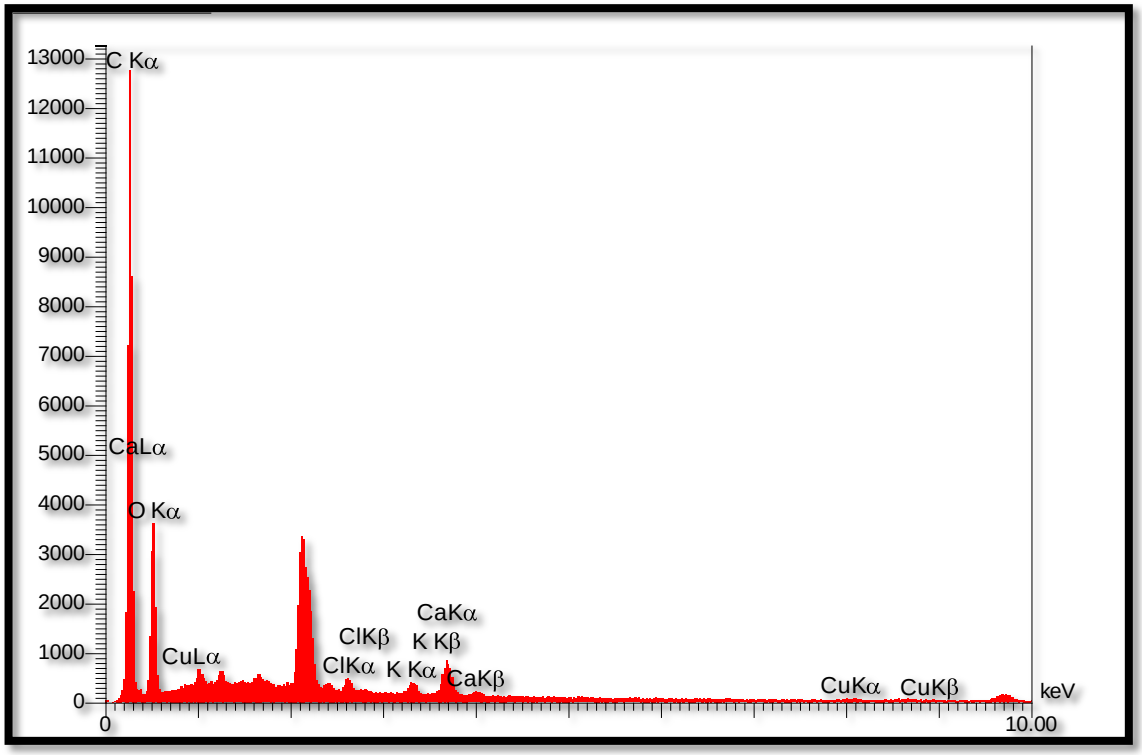

Figure (3.15) : EDX Spectrum of Ashwagandha root

Table (3.2) :The percentage of the elements present in the Ashwagandha roots.

Elt	Line	Int	K	Kr	W%	A%	ZAF
C	Ka	726.7	0.5713	0.2371	49.32	59.89	0.4807
O	Ka	245.1	0.1958	0.0813	39.34	35.86	0.2066
Cl	Ka	66.3	0.0602	0.0250	2.95	1.21	0.8471
K	Ka	58.4	0.0551	0.0229	2.66	0.99	0.8583
Ca	Ka	116.7	0.1125	0.0467	5.44	1.98	0.8583
Cu	Ka	4.4	0.0052	0.0021	0.30	0.07	0.7220

3.6 The biological activity results:

3.7 Isolation and Identification of *Escherichia coli* and *Staphylococcus aureus*.

Bacterial isolates were identified by a combination of cultural characteristics, Gram stain appearance, and finally confirmed by Vitek 2 compact system.

3.7.1 Cultural Characteristics

Escherichia coli (Gram-negative) isolates were identified depending on their colonial characteristics on MacConkey's Agar and UTI Agar .Gram negative bacteria usually grow well in the medium and are differentiated by their ability to ferment lactose. Lactose fermenting strains grow as red or pink and may be surrounded by a zone of acid precipitated bile as shown in figure (3.16).

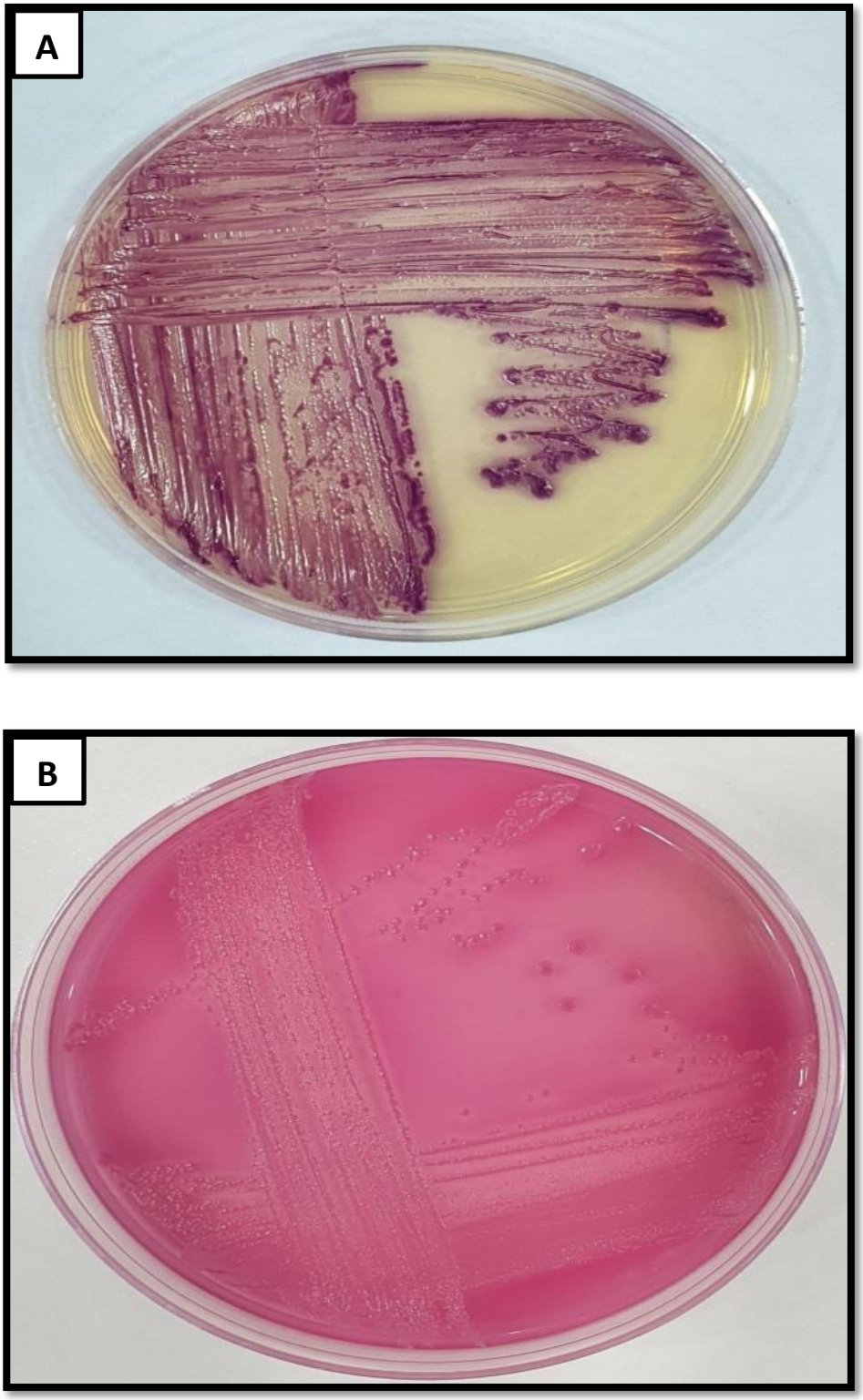

Figure (3.16): Cultural characteristics of *Escherichia coli* isolate on:

(A) UTI Agar (B) MacConkey's Agar.

Mannitol salt agar (MSA);can be used as a selective and differential medium for the isolation of staphylococci and to distinguish the bacteria based on the ability to ferment the sugar mannitol. The colonies of Mannitol fermentors *Staphylococcus aureus* (Gram-positive) appear yellow with yellow zones in the media (positive) as shown in figure (3.17).

While non-mannitol fermentors appear pink to red colonies with no yellow color change in the medium (negative).

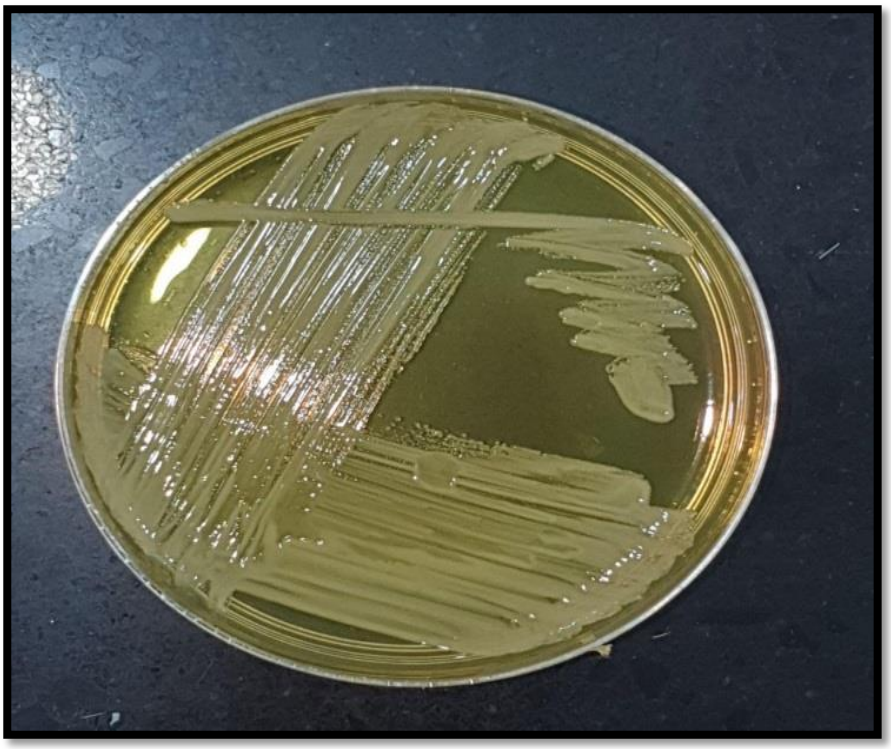

Figure (3.17)*: Staphylococcus aureus* isolate on Mannitol Salt Agar.

3.7.2 Gram Stain Morphology

Both bacteria were identified according to their color, shape, size and arrangements after Gram staining .

3.7.2.1 Gram stain morphology of *Escherichia coli*

Under the compound light microscope, Gram-stained smears of Escherichia coli appeared as gram-negative red color, bacilli, arranged in a single or short chain as shown in figure (3.18).

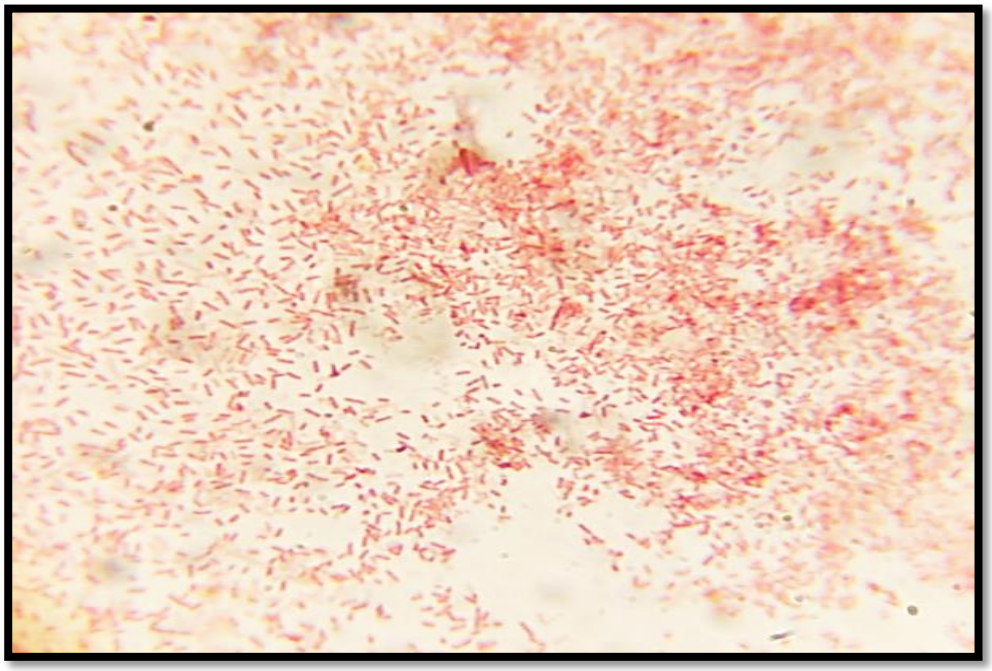

Figure (3.18): Gram-stained photomicrograph of *Escherichia coli* (100X magnification).

3.7.2.2 Gram stain morphology of *Staphylococcus aureus*

Microscopic examination of *Staphylococcus aureus* showed a gram-positive purple color, cocci arranged in a grape-like cluster , non-spore forming as shown in figure (3.19).

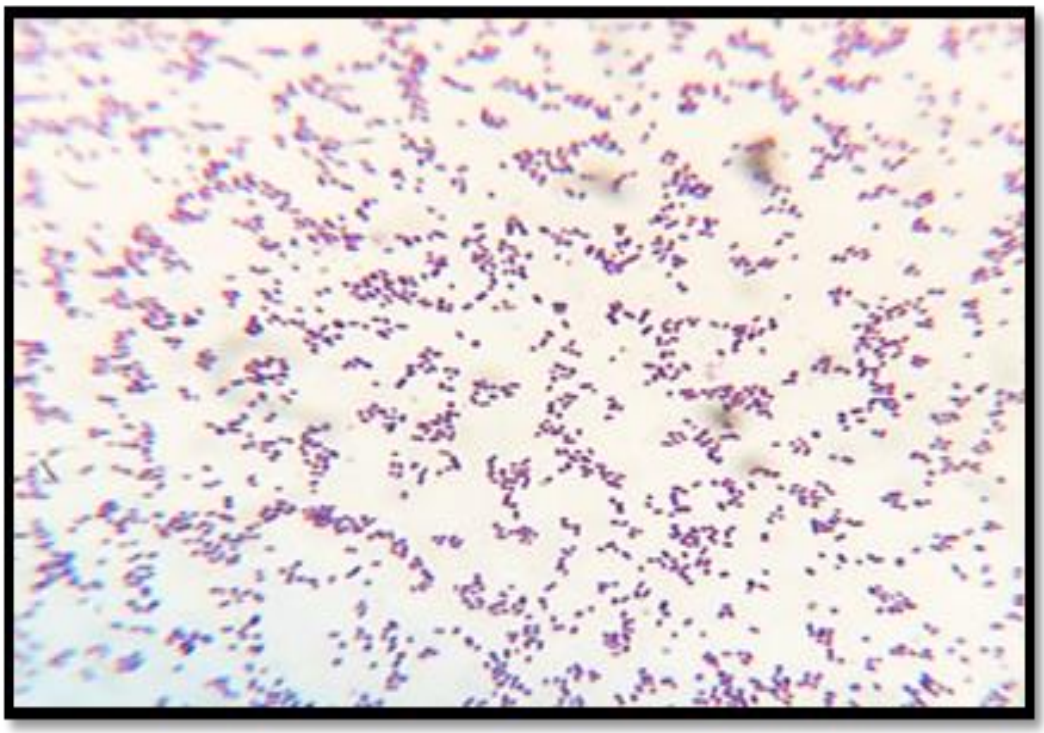

Figure (3.19): Gram-stained photomicrograph of *Staphylococcus aureus* (100X magnification).

3.7.3 VITEK® 2 Compact System Test for *Escherichia coli* and *Staphylococcus aureus*.

VITEK Compact 2 Systems are automated microbial identification systems utilizing growth-based technology. It was used in this study for its accuracy to confirm bacterial identification. Figure (3.20A) and (3.20B) illustrates the Vitek test results for *E.coli* and *S. aureus*.

A

bioMérieux Customer: Microbiology Chart Report Printed Jun 18, 2020 14:05 CDT

Patient Name: Hiba, . Patient ID: Hiba
Location: . Physician: Teeba
Lab ID: Hiba Isolate Number: 2

Organism Quantity:
Selected Organism : Escherichia coli

Source: Urine **Collected:**

Comments:	

Identification Information	**Analysis Time:**	3.88 hours	**Status:**	Final
Selected Organism	99% Probability **Bionumber:**	**Escherichia coli** 0005610540004611		
ID Analysis Messages				

Biochemical Details

2	APPA	-	3	ADO	-	4	PyrA	-	5	IARL	-	7	dCEL	-	9	BGAL	-
10	H2S	-	11	BNAG	-	12	AGLTp	-	13	dGLU	+	14	GGT	-	15	OFF	+
17	BGLU	-	18	dMAL	+	19	dMAN	+	20	dMNE	+	21	BXYL	-	22	BAlap	-
23	ProA	-	26	LIP	-	27	PLE	-	29	TyrA	+	31	URE	-	32	dSOR	+
33	SAC	-	34	dTAG	-	35	dTRE	+	36	CIT	-	37	MNT	-	39	5KG	-
40	ILATk	-	41	AGLU	-	42	SUCT	-	43	NAGA	-	44	AGAL	-	45	PHOS	-
46	GlyA	-	47	ODC	-	48	LDC	+	53	IHISa	-	56	CMT	+	57	BGUR	+
58	O129R	+	59	GGAA	-	61	IMLTa	-	62	ELLM	+	64	ILATa	-			

Figure (3.20A): The printout of the Vitek test results for the identification of E.coli

bioMérieux Customer: Microbiology Chart Report Printed Jun 17, 2020 12:18 CST

Patient Name: Hiba, . Patient ID: Hiba
Location: . Physician: Zahraa
Lab ID: Hiba Isolate Number: 1

Organism Quantity:
Selected Organism : Staphylococcus aureus

Source: Urine **Collected:**

Comments:	

Identification Information	**Analysis Time:**	3.87 hours	**Status:**	Final
Selected Organism	99% Probability **Bionumber:**	**Staphylococcus aureus** 050402022663031		
ID Analysis Messages				

Biochemical Details

2	AMY	-	4	PIPLC	-	5	dXYL	-	8	ADH1	+	9	BGAL	-	11	AGLU	+
13	APPA	-	14	CDEX	-	15	AspA	-	16	BGAR	-	17	AMAN	-	19	PHOS	+
20	LeuA	-	23	ProA	-	24	BGURr	-	25	AGAL	-	26	PyrA	+	27	BGUR	-
28	AlaA	-	29	TyrA	-	30	dSOR	-	31	URE	-	32	POLYB	+	37	dGAL	-
38	dRIB	-	39	ILATk	+	42	LAC	-	44	NAG	-	45	dMAL	+	46	BACI	+
47	NOVO	-	50	NC6.5	+	52	dMAN	+	53	dMNE	+	54	MBdG	+	56	PUL	-
57	dRAF	-	58	O129R	-	59	SAL	-	60	SAC	+	62	dTRE	+	63	ADH2s	-
64	OPTO	+															

Figure (3.20B): The printout of the Vitek test results for the identification of S. aureus.

3.8 Evaluation of different parameters for antibacterial activity

3.8.1 Antibacterial activity of AgNPs against *Escherichia coli* (Well Diffusion Method)

The antibacterial activity of AgNPs showed positive results against gram-negative bacterial pathogenic strains. The plant extract (Ashwagandha) solution was no effect against *E. coli*, while $AgNO_3$ solution was showed little effect against *E. coli* with a zone of inhibition=11mm, but AgNPs showed a greater effect against *E. coli* with a zone of inhibition =17 mm compared to Meropenem was effective against *E. coli* with a zone of inhibition=11mm as shown in figure (3.21).

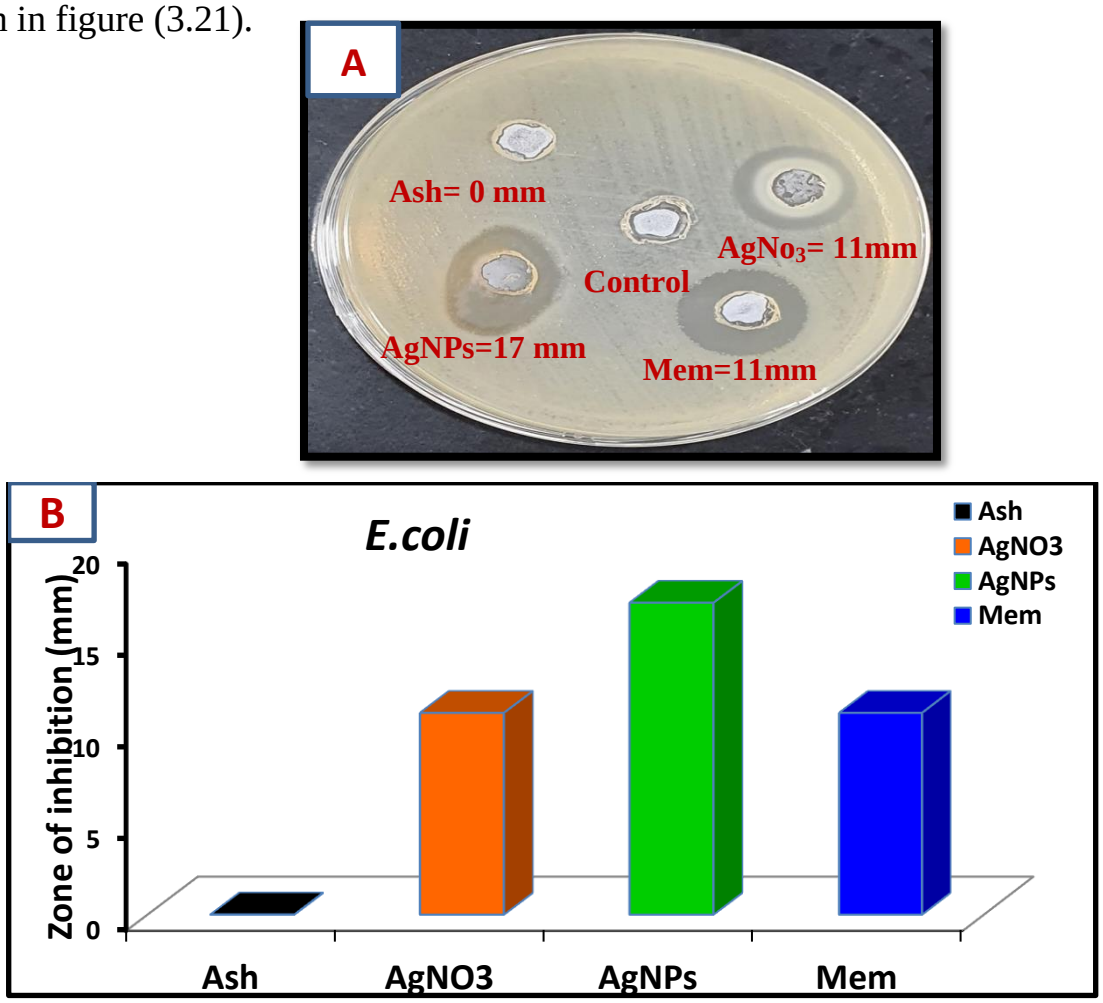

Figure (3.21): Antibacterial activity of AgNPs Against *Escherichia coli* By well diffusion method (Ashwagandha,$AgNO_3$ solution, AgNPs, Meropenem) .

3.8.2 Antibacterial activity of AgNPs against *Staphylococcus aureus* (Well Diffusion Method)

Figure (3.22) showed the AgNPs effect against *S. aureus* with a zone of inhibition = 8 mm, than the silver nitrate (AgNO3) against *S. aureus* with a zone of inhibition = 7 mm. But the Meropenem was showed the highest effect against *S. aureus* with a zone of inhibition = 16 mm.

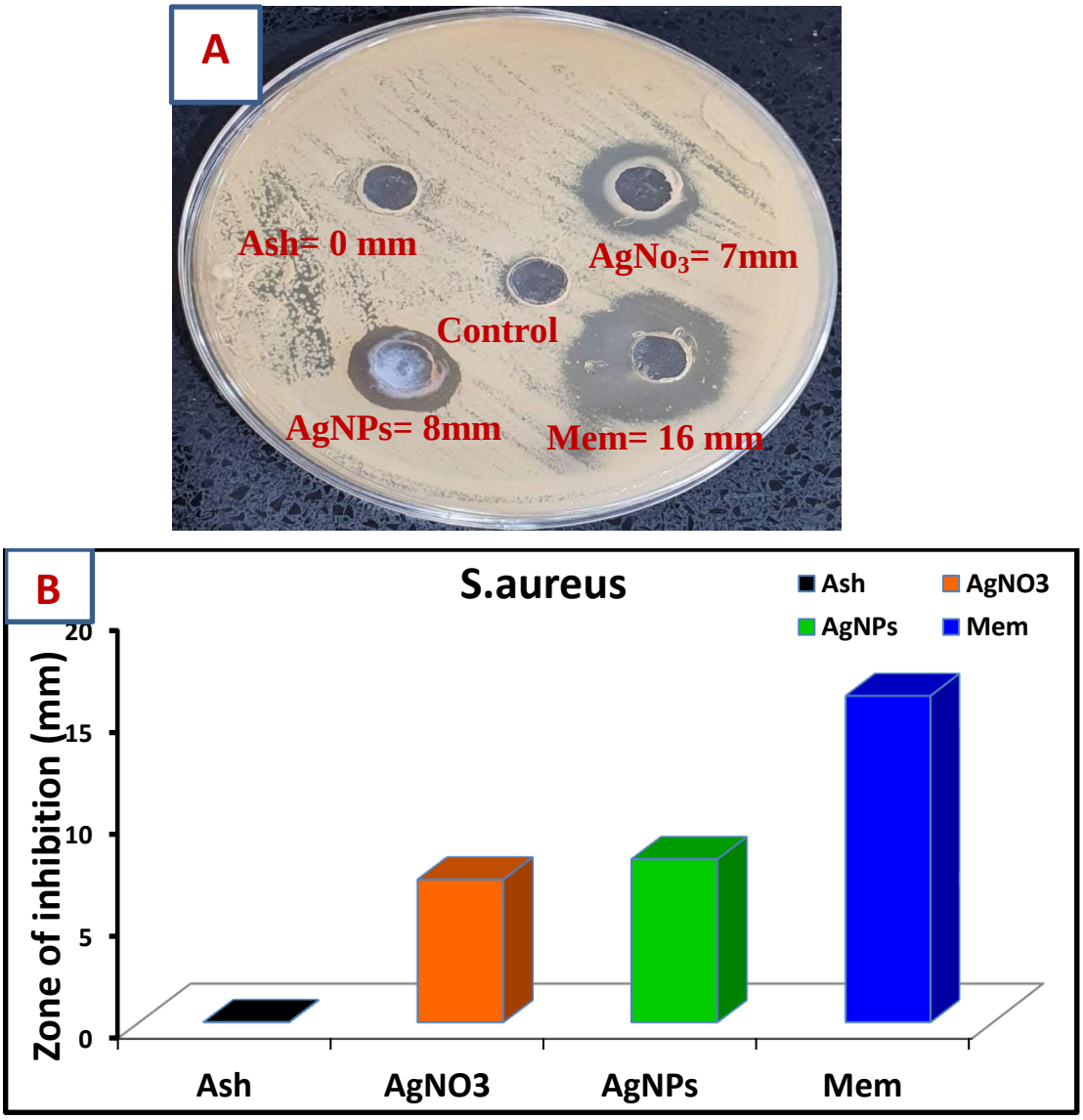

Figure(3.22):Antibacterial activity of AgNPs Against *Staphylococcus aureus* By well diffusion method (Ashwagandha,$AgNO_3$ solution, AgNPs, Meropenem).

However, the antibacterial activity of green synthesis AgNPs has been prepared using the Ashwagandha root extract. Figure (3.23) AgNPs showed positive results against both gram-positive and gram-negative bacterial pathogenic strains. While the Ashwagandha roots extract did not exhibit any effect on both bacteria the dose of the plant equal to 0.05 mg/ml.

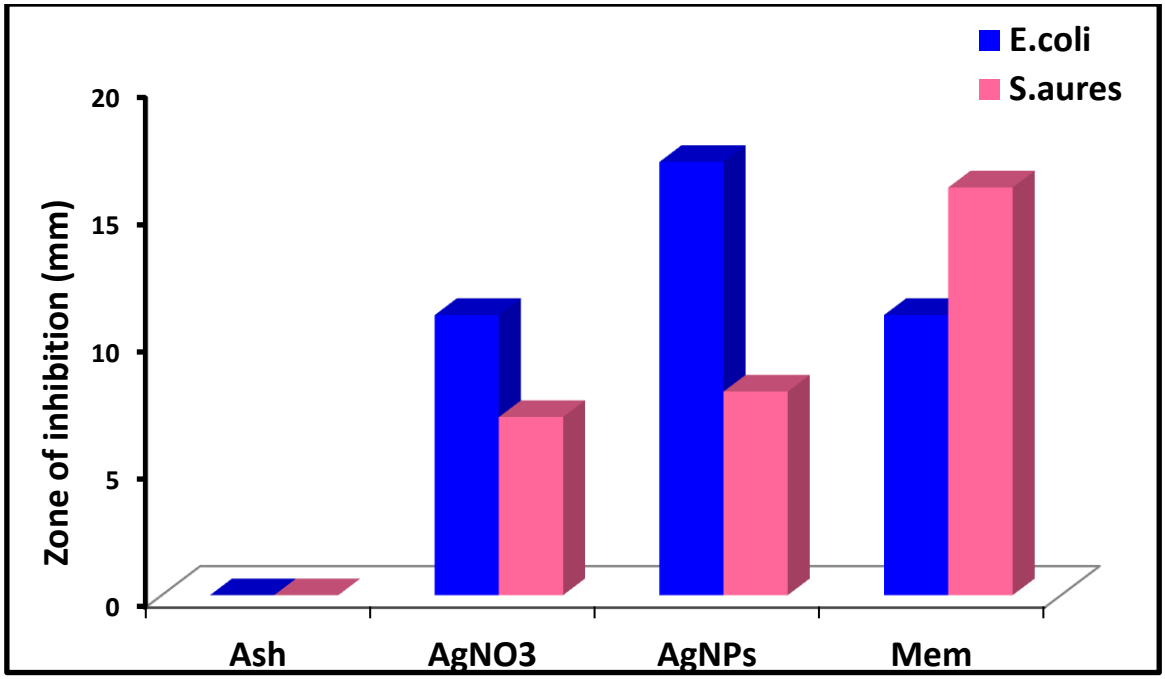

Figure (3.23): Antibacterial activity of AgNPs against pathogenic bacteria.

3.8.3 Antibacterial effects of ZnONPs Against *Escherichia coli* (Well Diffusion Method)

Zinc oxide nanoparticles have exhibited the effect against E. coli with a zone of inhibition = 9 mm ,than the Meropenem showed a greater effect against E. coli with a zone of inhibition =10 mm when Zinc acetate showed a greater effect against E. coli with a zone of inhibition = 8 mm. But Ashwagandha roots was showed non effect against E. coli with a zone of inhibition = 0 mm as shown in the figure (3.24).

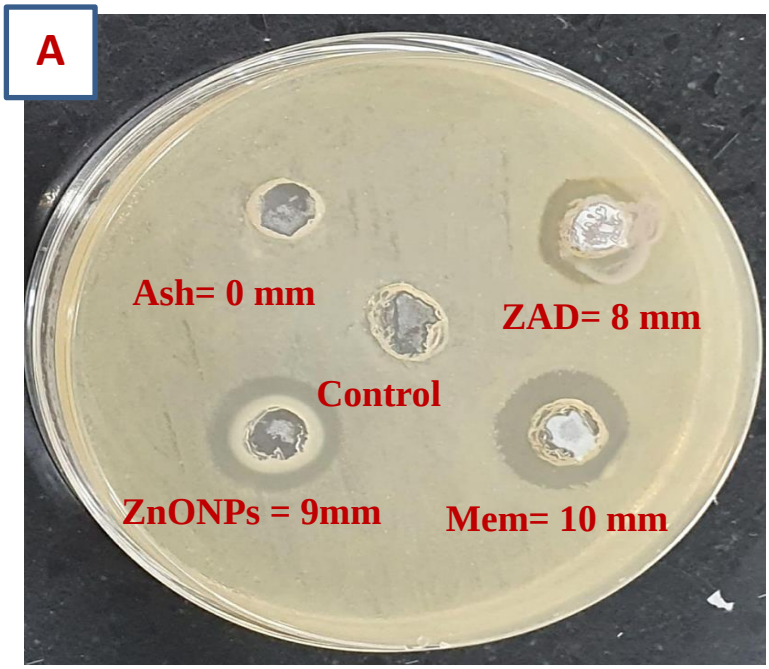

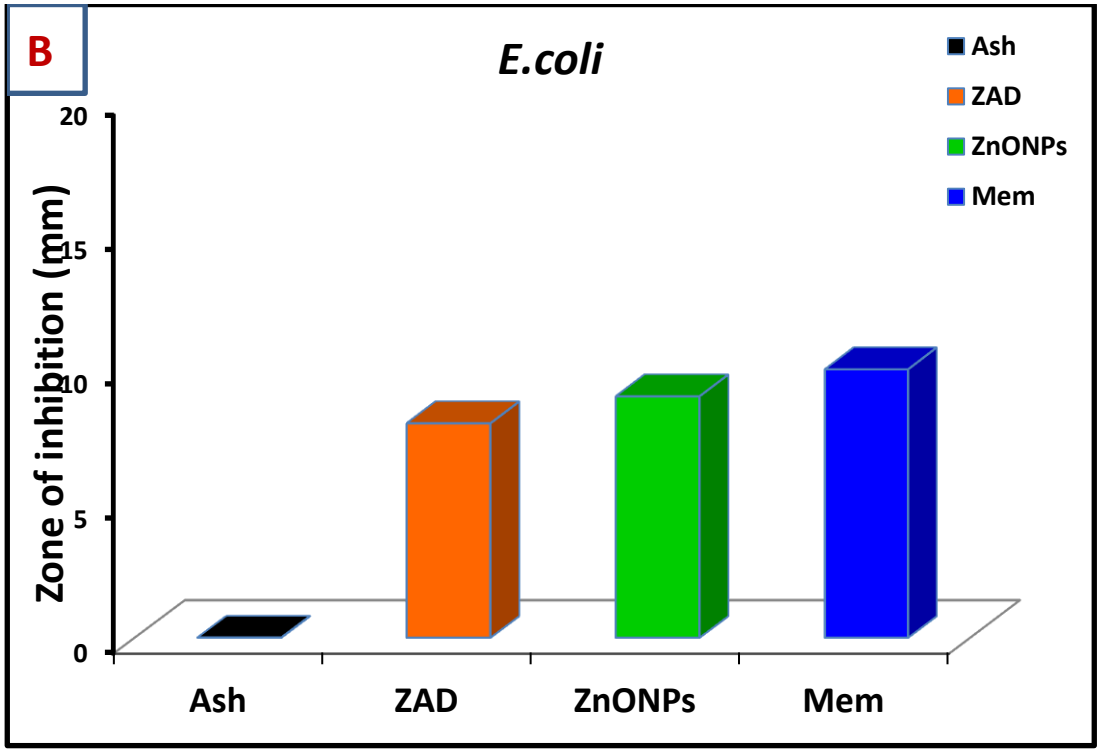

Figure (3.24): Antibacterial activity of ZnoNPs Against *Escherichia coli* by well diffusion method (Ashwagandha, ZAD solution, ZnONPs, Meropenem).

3.8.4 Antibacterial effects of ZnONPs Against *Staphylococcus aureus* (Well Diffusion Method)

Zinc acetate showed the effect against S. aureus with a zone of inhibition = 11 mm, but ZnOPNs was showed less effect against S. aureus with a zone of inhibition = 9 mm compared to the Meropenem stronger effect against S. aureus with a zone of inhibition = 21 mm shown in figure (3.25).

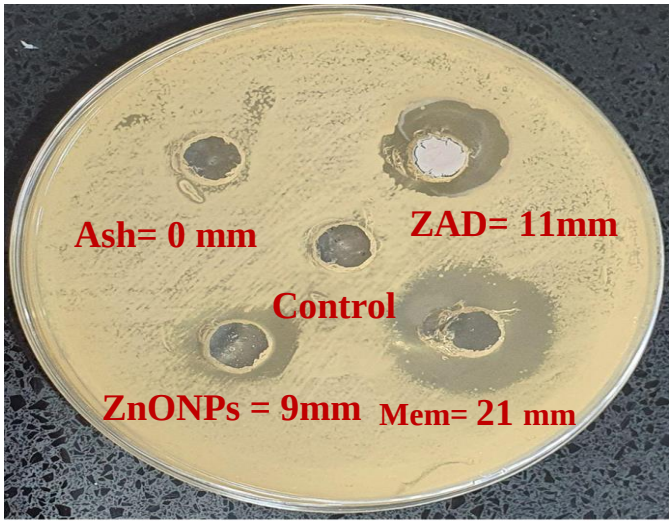

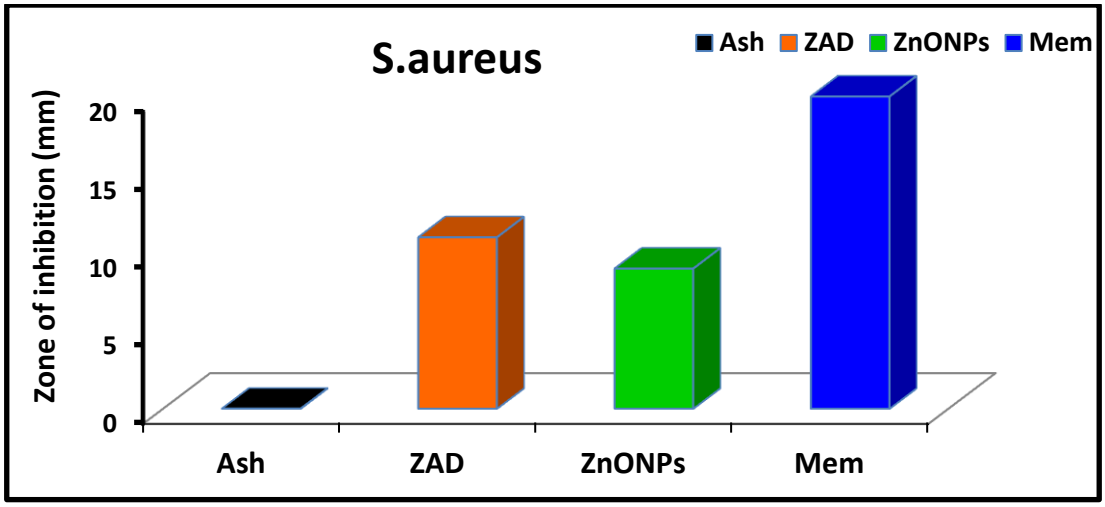

Figure (3.25) :Antibacterial activity of ZnoNPs Against *Staphylococcus aureus* by well diffusion method (Ashwagandha, ZAD solution, ZnONPs, Meropenem).

Figure (3.26) shows the antibacterial activity of the biosynthesized ZnO nanoparticles. Antibacterial activity was measured against grams of positive bacteria (*S.aureus*)and gram of negative bacteria (*E. coli*), that have the same effect on this bacterial pathogen.

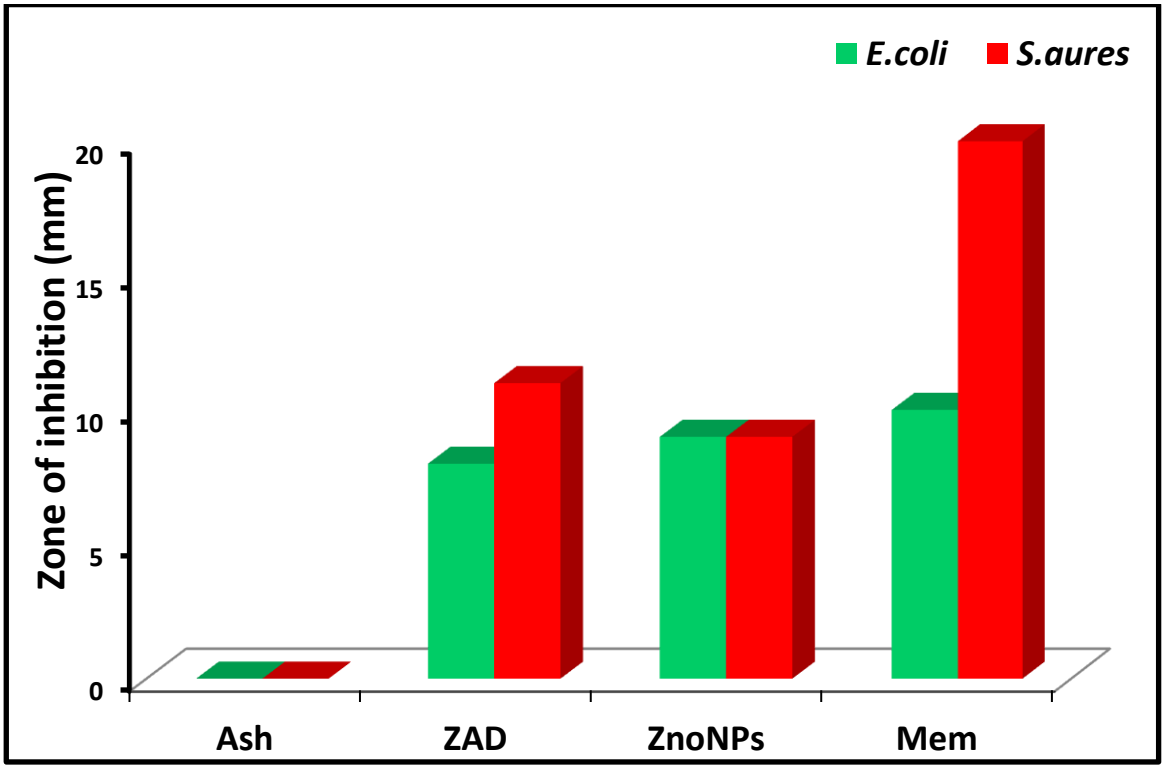

Figure (3.26): Antibacterial activity of ZnoNPs against pathogenic bacteria.

S.aureus and *E.coli* are the major causes of hospital-acquired infections and the environment. These organisms occur naturally in the human body. However, certain strains can lead to infections and are becoming resistant to antibiotics. The preliminary results of this study indicate that lower sensitivity (or resistance) of Gram positive strains (*S.aureus)* than Gram negative strains (*E. coli*) depending on outer membrane inhibits and/or retards the penetration. Also, another reason is their possession of multi drug resistance (MDR) pumps, which extrude amphipathic toxins across the outer membrane.

Moreover, AgNPs have strong antibacterial activity more than ZnONPs to the selected bacteria due to the cell structure. These silver nanoparticles might be used as antibiotics in the future due to non-toxic, cheap, eco-friendly, and highly effective against the bacteria.

3.9 Laser Irradiation Eeffect

3.9.1 The effect of irradiation of Diode laser (410nm)

The effect diode laser (410nm), at a power density of 0.128 W/cm^2, at different exposure times is shown in Table (3.3). The Statistical Analysis System-SAS (2012) software was used to detect the effects of various factors on the parameters of this study. The least significant difference – the LSD test (Analysis of Variation-ANOVA),was used to make a significant distinction between the means in this study. A probability value (P) is limited as:

1- Non- significant value at (P) > 0.05.
2- Highly significant at (P) ≤ 0.01.
3- Significant at (P) ≤ 0.05.

The results from laser irradiation in a show that no significant reduction in the mean number of log CFU/ml of *E.coli* was noted following 3 minutes laser irradiation except for the 5 minutes irradiation time, significant ($p<0.05$) reduction was recorded. Whereas, highly significant ($p<0.01$) reduction in the log CFU/ml (0.641) was observed at 9 min (99.53%) and above compared with the control group (0.599) (Figure 3.27 and Table 3.3). However, a 100% reduction in the number of CFU/ml for *E.coli* was achieved after 15 minutes of exposure to 410 nm laser irradiation as shown in Figure (3.27).

Table (3.3): Mean, standard deviation of log CFU/ml .

Time(minutes)	*E.coli*	*S.aureus*	LSD value
0	0.599 ± 0.063 ab	0.411 ± 0.021 a	0.079 **
3	0.459 ± 0.052 bc	0.394 ± 0.024 a	0.073 NS
5	0.525 ± 0.019 b	0.381 ± 0.008 a	0.094 **
7	0.398 ± 0.036 c	0.371 ± 0.017 a	0.055 NS
9	0.641 ± 0.041 a	0.367 ± 0.027 a	0.082 **
11	0.269 ± 0.009 e	0.357 ± 0.032 a	0.072 **
13	0.380 ± 0.044 d	0.338 ± 0.020 a	0.057 NS
15	0.196 ± 0.08 e	0.340 ± 0.012 a	0.087 **
LSD value	0.112 **	0.0963 NS	---
Means having with the different letters in same column differed significantly. ** (P≤0.01).			

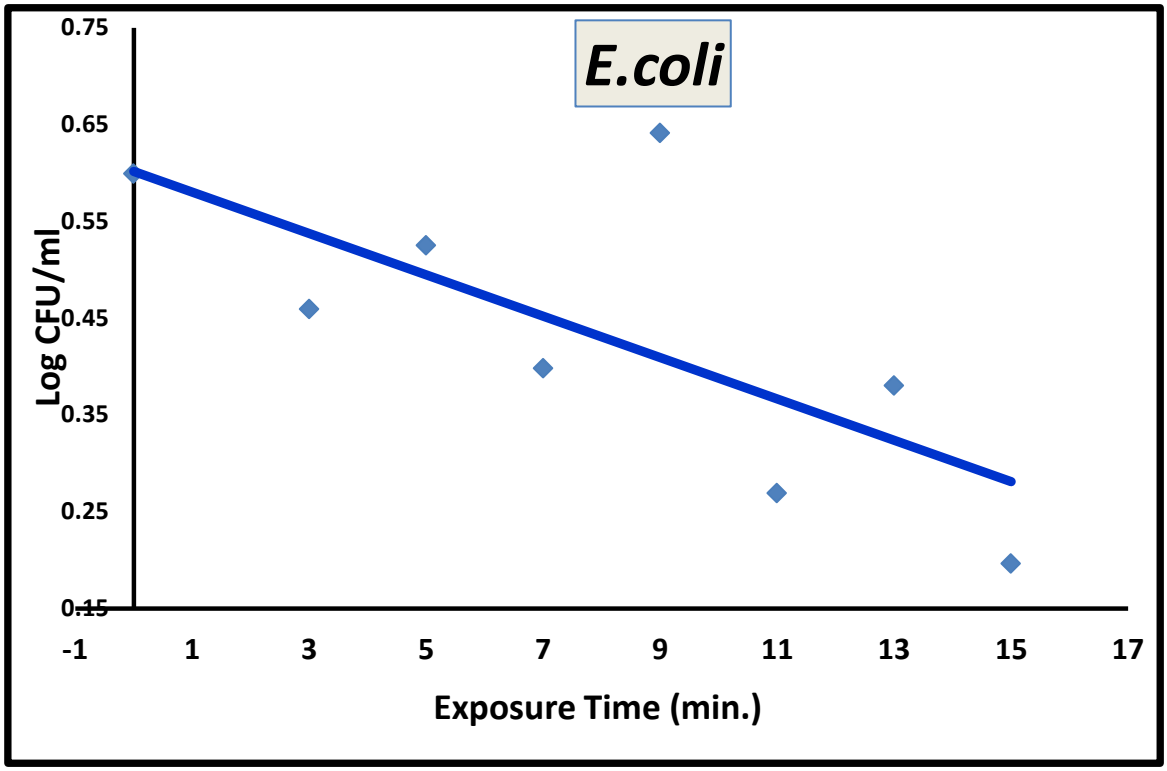

Figure (3.27) : Mean Log CFU/ml obtained for E.coli irradiated with 410 nm diode laser at 0.128 W/cm2 power density and different exposure time.

Figure (3.28) and Table (3.3) show the effect of diode laser (410nm) irradiation inhibited the growth of S. aureus at different exposure times. Similar to the previous experiment on E.coli, The results showed that there was a significant reduction (P<0.01) in the number of log CFU/ml (0.394) was observed following exposure to 410 nm laser light for 3 minutes compared with the control group (0.411) .The number of log CFU/ml continued not decreased with increasing the time of exposure to laser light. However, no complete mortality was reached after 15 minutes as shown in Figure (3.28).

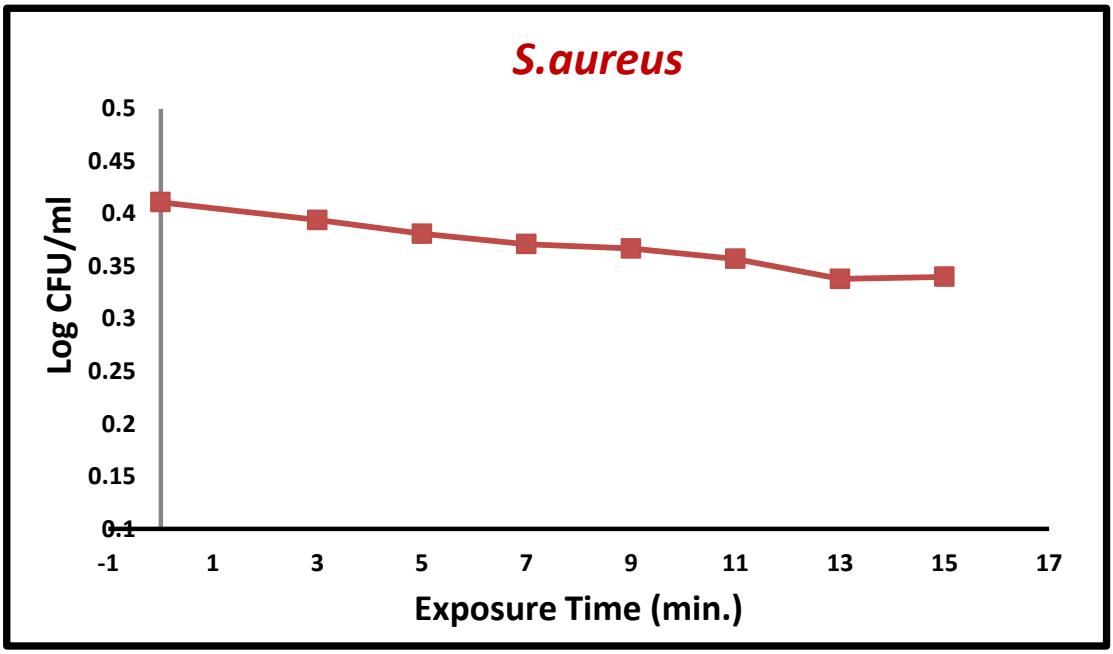

Figure (3.28) : Mean Log CFU/ml obtained for S.aureus irradiated with 410 nm diode laser at 0.128 W/cm^2 power density and different exposure time.

The percentage of reduction in the growth of *E.coli* and *S. aureus* is shown in Figure (3.29).Laser Irradiation experiments showed that the number of CFU/ml of *E.coli* and S. aureus was significantly reduced with increasing exposure times, reaching a100% bacterial mortality at 15 min for Gram-negative *(E.coli)* , while the exposure time (15 minutes) for Gram-positive

S.aureus no significant differences in the number of log CFU/ml , just at the exposure time 3 minutes number of log CFU/ml was a significant reduction (P<0.01) compared with the control group.

Accordingly, the blue laser irradiation seems to have a more bactericidal effect on Gram-negative *(E.coli)*, than Gram-positive bacteria *(S. aureus).*The bactericidal effect of laser photodynamic therapy (PDT) depends upon wavelength, power density, bacterial viable number, and bacteria species.

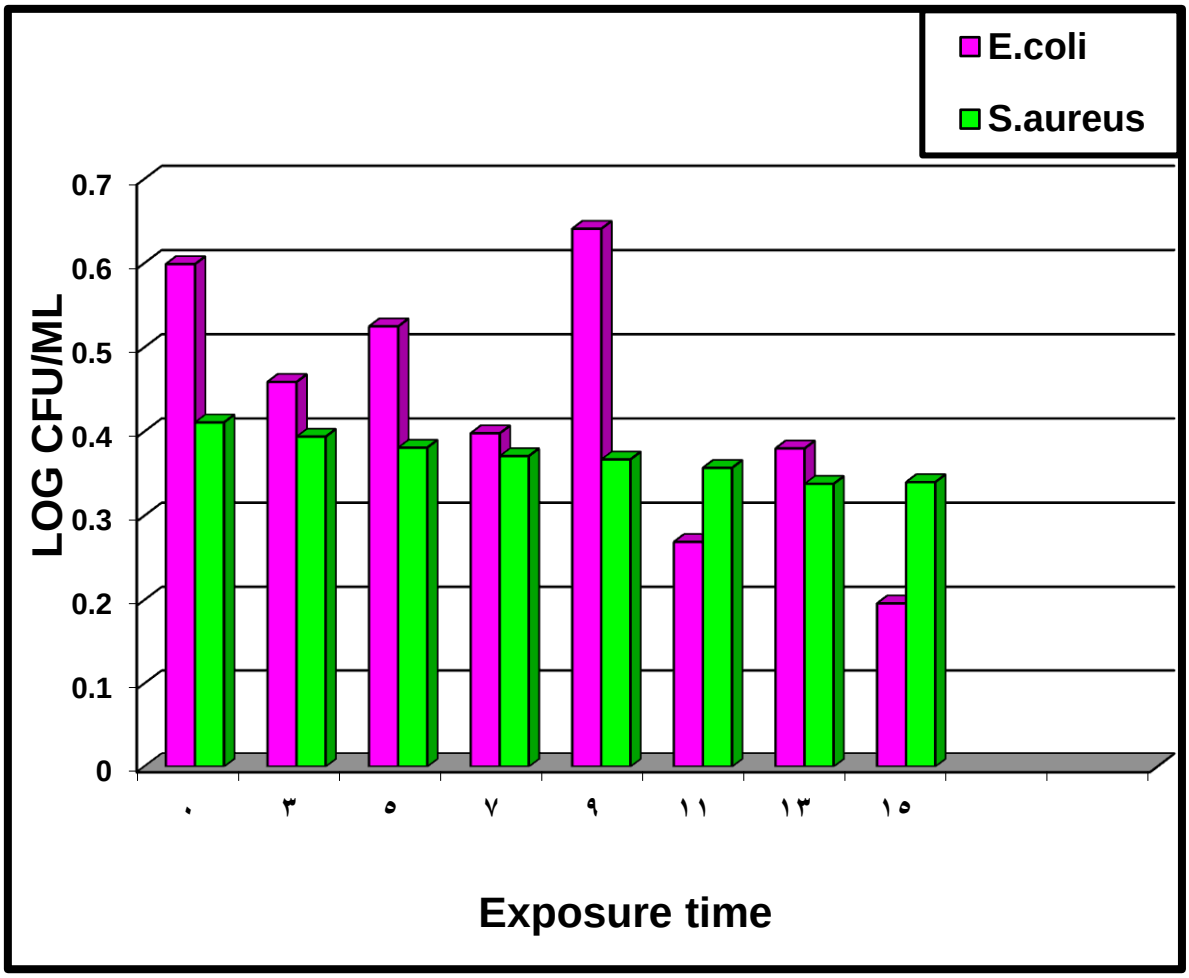

Figure (3.29): Percentage of reduction of Mean values of CFU/ml obtained for E.coli and S.aureus irradiated with (410 nm) diode laser at 0.128 W/cm^2 power density and different exposure time.

3.10 Conclusion:

Based on the results of the present work, the following conclusions are reached:

-Green synthesis is a successful eco-friendly technique to create nanoparticle materials.

- Green synthesis of silver nanoparticles using Ashwagandha roots extract with properties to reduce AgNO3 solution, also the biosynthesized of AgNPs were spherical in shape. Synthesized AgNPs have shown the ability to function as a strong antioxidant agent and have antibacterial activity against both gram-positive and gram-negative bacteria.

-Zinc oxide nanoparticles have been synthesized by using the green synthesis method using Ashwagandha root extract, zinc oxide nanoparticles were rod in shape.

- Ashwagandha is a powerful plant that can be used reducing agents.

-ELISA using to calculate the colonies-forming units of bacteria.

-The blue diode laser irradiation at a wavelength of 410 nm with a power density of 0.128 W/cm2 showed a significant reduction in bacterial number Gram-negative Escherichia coli more than Gram-positive Staphylococcus aureus.

-*S.aureus* is more resistant bacteria than *E.coli* due to the cell structure. Also, Meropenem is an antibiotic wide range activity of both bacteria.

3.11 Future Work

- Using the same parameters with wide different sides.

-Examine the combined effect of 410 nm diode laser and dyes (photosensitizers) on *Escherichia coli* and *Staphylococcus aureus* can be considered at different doses to achieve the best bactericidal effect.

-Investigate the effects of diode laser irradiation at 410 nm on other types of bacteria.

- Investigating the effects of other types of laser with nanoparticles on bacteria.

-Using other plants as reducing agent and anti-bacterial activity.

References

References:

[1] S. D. Gan, K. R. Patel, " Enzyme immunoassay and enzyme-linked immunosorbent assay ", Journal of Investigative Dermatology, Vol 133, No. 9, pp. 12-14; (2013).

[2] S. X. Leng , J. E. McElhaney, J. D. Walston , D. Xie, N. S. Fedarko , and G. A. Kuche, J Gerontol , ELISA AND MULTIPLEX TECHNOLOGIES FOR CYTOKINE MEASUREMENT IN INFLAMMATION AND AGING RESEARCH A Biol Sci Med Sci. August ; 63(8): 879–884,(2008).

[3] N. Jayarambabu, K. V. Rao, and Y. T. Prabhu, "BENEFICIAL ROLE OF ZINC OXIDE NANOPARTICLES ON GREEN CROP PRODUCTION Introduction : Nanotechnology is the term given to those areas of science and," *Int. J. Multidiscip. Adv. Res. Trends*, no. April 2016, 2015, [Online].

[4] R. Vivek, R. Thangam, K. Muthuchelian, P. Gunasekaran, K. Kaveri, and S. Kannan, "Green biosynthesis of silver nanoparticles from Annona squamosa leaf extract and its in vitro cytotoxic effect on MCF-7 cells," *Process Biochem.*, vol. 47, no. 12, pp. 2405–2410, 2012, doi: 10.1016/j.procbio.2012.09.025.

[5] S.P Chandran, M. Chaudhary, R. Pasricha, A. Ahmad, M. Sastry, Synthesis of Gold Nanotriangles and Silver Nanoparticles Using Aloe Vera Plant Extract, Biotechnol Prog. 2006; 22: 577-583.

[6] Palaniselvam Kuppusamy, Mashitah M Yusoff, Gaanty Pragas Maniam, Natanamurugaraj, Govindan. Biosynthesis of Metallic Nanoparticles Using Plant Derivatives and their Avenues in Pharmacological Applications-An Updated Report, Soudi *Pharmaceutical Journal*. 2016; 24: 473-484.

[7] V. Pareek, A. Bhargava, R. Gupta, N. Jain, and J. Panwar, "Synthesis and Applications of Noble Metal Nanoparticles: A Review," *Adv. Sci. Eng. Med.*, vol. 9, no. 7, pp. 527–544, 2017, doi: 10.1166/asem.2017.2027.

[8] J. Vega-Baudrit, S. M. Gamboa, E. R. Rojas, and V. V. Martinez, “Synthesis and characterization of silver nanoparticles and their application as an antibacterial agent,” *Int. J. Biosens. Bioelectron.*, vol. 5, no. 5, 2019, doi: 10.15406/ijbsbe.2019.05.00172.

[9] R. Janardhanan, M. Karuppaiah, N. Hebalkar, and T. N. Rao, “Synthesis and surface chemistry of nano silver particles,” *Polyhedron*, vol. 28, no. 12, pp. 2522–2530, 2009, doi: 10.1016/j.poly.2009.05.038.

[10] L. F. and D. Sutherland, *Nanotechnologies: Principles, Applications, Implications and Hands-on Activities*. 2012.

[11] H. Nadaroglu, A. Alayli, H. Nadaroğlu, A. Alayli Güngör, and S. İnce, “Synthesis of Nanoparticles by Green Synthesis Method,” *Int. J. Innov. Res. Rev.*, vol. 1, no. 1, pp. 6–9, 2017.

[12] M. Rafique,A. Shaikh,R. Rasheed and M. Bilal, “A Review on Synthesis, Characterization and Applications of Copper Nanoparticles Using Gree Method,” *Nano*, vol. 12, no. 4, 2017, doi: 10.1142/S1793292017500436.

[13] Frattini, N. Pellegri, D. Nicastro, de Sanctis O (2005) Effect of amine groups in the synthesis of Ag nanoparticles using aminosilanes Mater. Chem. Phys. 94 148-152.

[14] L. Wei, J. Lu, H. Xu, A. Patel, Z. S. Chen, and G. Chen, “Silver nanoparticles: Synthesis, properties, and therapeutic applications,” Drug Discov. Today, vol. 20, no. 5, pp. 595–601, 2015, doi: 10.1016/j.drudis.2014.11.014.

[15] S. Lin, R. Huang, Y. Cheng, J. Liu, B. L. T. Lau, and M. R. Wiesner, “Silver nanoparticle-alginate composite beads for point-of-use drinking water disinfection,” Water Res., vol. 47, no. 12, pp. 3959–3965, 2013, doi: 10.1016/j.watres.2012.09.005.

[16] R. Kumar, V. P. Singh, D. Maurya, A. K. Pandey," Bionanoparticles: A Green Nanochemical Approach; Pharma Tutor", 3(9); pp 28-35, (2015).

[17] J. Pulit, M. Banach, L. Tymczyna, A. Chmielowiec-Korzeniowska, "State of research and trends in the preparation of nanostructured silver", Przemys Chemiczny, 91, pp 929–936 (2012).

[18] M. Rai, A. Yadav, and A. Gade, "Silver nanoparticles as a new generation of antimicrobials," *Biotechnol. Adv.*, vol. 27, no. 1, pp. 76–83, 2009.

[19] S. Kameswara Srikar, D. D. Giri, D. B. Pal, P. K. Mishra, and S. N. Upadhyay, "Green Synthesis of Silver Nanoparticles: A Review," *Green Sustain. Chem.*, vol. 6, no. 6, pp. 34–56, 2016.

[20] B. Sadeghi and F. Gholamhoseinpoor, "A study on the stability and green synthesis of silver nanoparticles using Ziziphora tenuior (Zt) extract at room temperature," *Spectrochim. Acta Part A Mol. Biomol. Spectrosc.*, vol. 134, pp. 310–315, Jan. 2015.

[21] M. Zhang, K. Zhang, B. De Gusseme, W. Verstraete, and R. Field, "The antibacterial and anti-biofouling performance of biogenic silver nanoparticles by *Lactobacillus fermentum*," *Biofouling*, vol. 30, no. 3, pp. 347–357, Mar. 2014.

[22] A. S. Dehnavi, A. Raisi, and A. Aroujalian, "Control Size and Stability of Colloidal Silver Nanoparticles with Antibacterial Activity Prepared by a Green Synthesis Method," *Synth. React. Inorganic, Met. Nano-Metal Chem.*, vol. 43, no. 5, pp. 543– 551, Jan. 2013.

[23] S. Chanda, "Silver nanoparticles (medicinal plants mediate): A new generation of antimicrobials to combat microbial pathogens- a review," *Formatex*, pp. 1314–1323, 2013.

[24] S. Ahmed, M. Ahmad, B. L. Swami, and S. Ikram, "A review on plants extract mediated synthesis of silver nanoparticles for antimicrobial applications: A green expertise," *J. Adv. Res.*, vol. 7, no. 1, pp. 17–28, 2016.

[25] S. Rajeshkumar and L. V Bharath, "AC," 2017, doi: 10.1016/j.cbi.2017.06.019.

[26] K. K. Y. Wong and X. Liu, "Silver nanoparticles - The real 'silver bullet' in clinical medicine?," *Medchemcomm*, vol. 1, no. 2, pp. 125–131, 2010, doi: 10.1039/c0md00069h.

[27] G. Amin, Ph.D. thesis, Department of Science and Technology, Linköping University, Sweden (2012).

[28] W. C. Lee, "Photoelectrochemical water splitting and gas ionisation sensing using metal oxide nanostructures," no. November, 2015, doi: 10.13140/RG.2.1.4480.6483.

[29] R. Dobrucka and J. Długaszewska, "Biosynthesis and antibacterial activity of Zno nanoparticles using Trifolium Pratense flower extract," SAUDI J. Biol. Sci., 2015, doi: 10.1016/j.sjbs.2015.05.016.

[30] M. Li, L. Zhu, and D. Lin, "Toxicity of ZnO Nanoparticles to Escherichia coli : Mechanism and the Influence of Medium Components," pp. 1977–1983, 2011.

[31] Y. H. Leung *et al.*, "Antibacterial activity of ZnO nanoparticles with a modified surface under ambient illumination," *Nanotechnology*, vol. 23, no. 47, 2012, doi: 10.1088/0957-4484/23/47/475703.

[32] S. Sarwar, S. Chakraborti, S. Bera, I. A. Sheikh, K. M. Hoque, and P. Chakrabarti, "The antimicrobial activity of ZnO nanoparticles against Vibrio cholerae: Variation in response depends on biotype," *Nanomedicine Nanotechnology, Biol. Med.*, vol. 12, no. 6, pp. 1499–1509, 2016, doi: 10.1016/j.nano.2016.02.006.

[33] J. Jiang, J. Pi, and J. Cai, 'The Advancing of Zinc Oxide Nanoparticles for Biomedical Applications,' vol. 2018, 2018.," *Bioinorg. Chem. Appl.*, vol. 2018, p. 18, 2018.

[34] R. P. Chauhan, C. Gupta, and D. Prakash, "Methodological Advancements in Green Nanotechnology and Their Applications in Biological Synthesis of Herbal Nanoparticles," Int. J. Bioassays, vol. 1, no. 07, pp. 6–10, 2012.

[35] X. Li, H. Xu, Z. S. Chen, and G. Chen, "Biosynthesis of nanoparticles by microorganisms and their applications," *J. Nanomater.*, vol. 2011, 2011, doi: 10.1155/2011/270974.

[36] S. V. Ganachari et al., "Green nanotechnology for biomedical, food, and agricultural applications," Handb. Ecomater., vol. 4, pp. 2681–2698, 2019, doi: 10.1007/978-3-319-68255-6_184.

[37] R. Roushan, "Ashwagandha (Withania Somnifera); A potential aphrodisiac drug in Ayurveda Received : 5 July Revised : 13 July Accepted : 22 July," no. February, 2019.

[38] S. Rajasekar and R. Elango, "Estimation of alkaloid content of Ashwagandha (Withania somnifera) with HPLC methods," J. Exp. Sci., vol. 2, no. 5, pp. 39–41, 2011.

[39] P. Sengupta, A. Agarwal, M. Pogrebetskaya, S. Roychoudhury, D. Durairajanayagam, and R. Henkel, "Role of Withania somnifera (Ashwagandha) in the management of male infertility," Reprod. Biomed. Online, vol. 36, no. 3, pp. 311–326, 2018, doi: 10.1016/j.rbmo.2017.11.007.

[40] G. Singh, P. K. Sharma, R. Dudhe, and S. Singh, "Biological activities of Withania somnifera," *Ann. Biol. Res.*, vol. 1, no. 3, pp. 56–63, 2010, [Online]. Available: http://scholarsresearchlibrary.com/ABR-vol1-iss3/ABR-2010-1-3-56-63.pdf.

[41] N. J. Dar, A. Hamid, and M. Ahmad, "Pharmacologic overview of Withania somnifera, the Indian Ginseng," Cell. Mol. Life Sci., vol. 72, no. 23, pp. 4445–4460, 2015, doi: 10.1007/s00018-015-2012-1.

[42] N. Khanchandani, P. Shah, T. Kalwani, A. Ardeshna, and D. Dharajiya, "Antibacterial and Antifungal Activity of Ashwagandha (Withania somnifera L.): A review," J. Drug Deliv. Ther., vol. 9, no. 5-s, pp. 154–161, 2019, doi: 10.22270/jddt.v9i5-s.3573.

[43] Baron S. (1996). Medical Microbiology, 4th edition. University of Texas Medical Branch at Galveston.

[44] Collee J. G., Fraser A. G., Marmison B. P., Simmon, S. A. (1996). Mackie and MaCathneys. Practical medical microbiology. 14th edition, Churchill Livingstone, U. K.pp.978.

[45] Kaper JB, Nataro JP, Mobley HL. Pathogenic Escherichia coli. Nat Rev Microbiol. 2004;2:123–40.

[46] Nakazato G, Tatiana A, Eliana G, Marcelo B, Wanderley D. Virulence factors of avian pathogenic Escherichia coli Pesq. Vet Bras. 2009;29:479–86.

[47] L. G. Harris, S. J. Foster, R. G. Richards, P. Lambert, D. Stickler, and A. Eley, “An introduction to Staphylococcus aureus, and techniques for identifyingand quantifying S. aureus adhesins in relation to adhesion to biomaterials:Review,” Eur. Cells Mater., vol. 4, pp. 39–60, 2002, doi: 10.22203/ecm.v004a04.

[48] Irving. W, Ala’Aldeen. D and Boswell. T (2005). Medical Microbiology.

[49] P. k. Das, "Laser and Optical Engineering ", Springer, (1991).

[50] S. Chopra, H.M. Chawla," Laser in Chemical and Biological Sciences", Wiley Eastern Ltd.; (1992).

[51] M. Bedrym, "A study of interaction of XeCl excimer laser with human tissue". Ph.D. Thesis, Baghdad University, (1997).

[52] H. S. Ashour," Tuning semiconductor laser diode lasing frequency and narrowing the laser linewidth using external oscillating driving field". J. Applied Sci., Vol 6, No. 10, pp. 2209-2216; (2006).

[53] M. H. Niemz, " Laser Tissue Interaction". Springer; (1996).

[54] N. R. M. Mosaad," Laser Technology and Laser Applications in Medicine and Surgery". IESCO; (1997).

[55] D .J .Elliott, " Ultraviolet Laser Technology and Applications". Academic Press, (1995).

[56] J. E. Julia, V. Aboites, M.A. Casillas, " CO2 laser interaction with biological tissue". Instrum. Dev., 3: 53-59, (1998).

[57] M. A. Ansari, E. Mohajerani, " Mechanisms of laser-tissue interaction: optical properties of tissue ", Journal of Lasers in Medical Sciences ", Vol 2, No. 3, pp. 119-125; (2011).

[58] S. K. Verma and A. Kumar, "Therapeutic uses of withania somnifera (Ashwagandha) with a note on withanolides and its pharmacological actions," *Asian J. Pharm. Clin. Res.*, vol. 4, no. SUPPL. 1, pp. 1–4, 2011.

[59] M. P. Srivastava, R. Tiwari, N. Sharma, and P. P. Division, "Manuscript Info," *Int. J. Adv. Res.*, vol. 1, no. 8, pp. 1–6, 2013.

[60] A. K. Singh, V. Rathod, D. Singh, S. Ninganagouda, and P. Kulkarni, "ISSN 2277-3851 Original Article Bioactive Silver Nanoparticles from Endophytic Fungus Fusarium sp . Isolated from an Ethanomedicinal Plant Withania somnifera (Ashwagandha) and its Antibacterial Activity," vol. 5, no. 1, pp. 15–19, 2015.

[61] A. Tereshchenko *et al.*, "Optical biosensors based on ZnO nanostructures: Advantages and perspectives. A review," *Sensors Actuators, B Chem.*, vol. 229, pp. 664–677, 2016, doi: 10.1016/j.snb.2016.01.099.

[62] M. G. Mohammed and A. M. Maki, "Effect of 410 nm Diode Laser Irradiation on the Growth of Burn Wounds-associated Bacteria , Pseudomonas Aeruginosa and Staphylococcus Aureus," vol. 16, pp. 11–19, 2017.

[63] C. Zhou, H. Zou, M. Li, C. Sun, D. Ren, and Y. Li, "Fiber optic surface plasmon resonance sensor for detection of E. coli O157:H7 based on antimicrobial peptides and AgNPs-rGO," *Biosens. Bioelectron.*, vol. 117, pp. 347–353, 2018, doi: 10.1016/j.bios.2018.06.005.

[64] I. Uddin, G. Kavya, G. Soundarya, G. Ropa, and S. Ch, "Anti-Diabetic Activity of Silver Nanoparticles Synthesized," vol. 7, no. 2, 2018.

[65] S. Rahman , L. Rahman , A. Khalil ,N.Ali . D.Zia and M.Ali, "Endophyte-

mediated synthesis of silver nanoparticles and their biological applications," *Appl. Microbiol. Biotechnol.*, vol. 103, no. 6, pp. 2551–2569, 2019, doi: 10.1007/s00253-019-09661-x.

[66] B. Malaikozhundan, J.Vinodhini, M.Kalanjiam,V. Vinotha, S. Palanisamy and S.Vijayakumar ,"High synergistic antibacterial, antibiofilm, antidiabetic and antimetabolic activity of Withania somnifera leaf extract-assisted zinc oxide nanoparticle," *Bioprocess Biosyst. Eng.*, vol. 43, no. 9, pp. 1533–1547, 2020, doi: 10.1007/s00449-020-02346-0.

[67] U. Holzwarth and N. Gibson: 'The Scherrer equation versus the 'DebyeScherrer equation', Nature Nanotech. 2011, 6, 534. 5.

[68] Instruction Manual System User's Guide UV-1800 SHIMADZU Spectrophotometer (SHIMADZO CORRORAT) 206-97040A Feb. 2008.

[**69**] Statistical Analysis System SAS. (2012)., User's Guide. Statistical. Version 9.1th ed. SAS. Inst. Inc. Cary. N.C. USA.

[70] M. Kumar Trivedi, "Evaluation of the Physico-chemical, Thermal and Behavioral Properties of Ashwagandha Root Extract: Effects of Consciousness Energy Healing Treatment," *Int. J. Pharm. Chem.*, vol. 3, no. 3, p. 41, 2017, doi: 10.11648/j.ijpc.20170303.13.

[71] M. Gregory, R. Selvakesavan, G. Franklin, B. Sarmento, and A. Dias, "Green synthesis of silver nanoparticles using Withania somnifera extract and their incorporation into a cream with antibacterial activity," *Planta Med.*, vol. 80, no. 16, 2014, doi: 10.1055/s-0034-1394514.

[72] M. Manokari, C. P. Ravindran, and M. S. Shekhawat, "Production of Zinc Oxide Nanoparticles using aqueous extracts of a medicinal plant Micrococca mercurialis (L Benth .," vol. 30, pp. 117–128, 2016.

[73] B. Properties *et al.*, "Influence of the Biofield Energy Healing Treatment on Physicochemical , Influence of the Biofield Energy Healing Treatment on Physicochemical , Thermal and Behavioral Properties of Ashwagandha

Withania somnifera) Root Extract," no. April, 2017, doi: 10.11648/j.ajbio.20170502.12.

[74] C. I. Nosiri, U. O. Arunsi, A. C. Ngwogu, J. Idume, and O. C. Atasie, "International Journal of Green and Proximate and preleminaryphytochemical analysis of leaves of Cassine Glauca plant," *Int. J. Green Herb. Chem.*, vol. 8, no. 1, pp. 30–36, 2019, doi: 10.24214/IJGHC/GC/8/1.

[75] N. Jayarambabu, K. V. Rao, and Y. T. Prabhu, "BENEFICIAL ROLE OF ZINC OXIDE NANOPARTICLES ON GREEN CROP PRODUCTION Introduction : Nanotechnology is the term given to those areas of science and," *Int. J. Multidiscip. Adv. Res. Trends*, no. April 2016,2015.

[76] P. Belle Ebanda Kedi *et al.*, "Biosynthesis of Silver Nanoparticles from Microsorum Punctatum (L.) Copel Fronds Extract and an In-vitro Anti-Inflammation Study," *J. Nanotechnol. Res.*, vol. 02, no. 02, pp. 25–41, 2020, doi: 10.26502/jnr.2688-85210014.

[77] J. Suresh, G. Pradheesh, V. Alexramani, M. Sundrarajan, and S. I. Hong, "Green synthesis and characterization of zinc oxide nanoparticle using insulin plant (Costus pictus D. Don) and investigation of its antimicrobial as well as anticancer activities," *Adv. Nat. Sci. Nanosci. Nanotechnol.*, vol. 9, no. 1, 2018, doi: 10.1088/2043-6254/aaa6f1.

[78] S. Chandrasekaran and S. P. Sivasamy, "Biosynthesis and Characterization of silver nanoparticles by Fusarium sp . and it ' s antimicrobial and antioxidant activity," vol. 5, no. 9, pp. 1–10

[79] J. Sen Chang, J. Strunk, M. N. Chong, P. E. Poh, and J. D. Ocon, "Multi-dimensional zinc oxide (ZnO) nanoarchitectures as efficient photocatalysts: What is the fundamental factor that determines photoactivity in ZnO?," *J. Hazard. Mater.*, vol. 381, no. August 2019, p. 120958, 2020, doi: 10.1016/j.jhazmat.2019.120958.

الخلاصـــة

استخدام طريقة التخليق الأخضر لتحضير الجسيمات النانوية المعدنية والتي تعتبر طريقة سريعة ، بسيطة ، صديقة للبيئة ، اقتصادية وغير سامه. في هذه الطريقة ، تم استخدام مستخلص جذور نبات اشواغاندا مع أوكسيد الزنك والفضة كنشاط مضاد للبكتيريا.

في هذا البحث تم فحص بنية وخصائص المواد ذات البنية النانوية المصنوعة من الفضة وأكسيد الزنك باستخدام تحليل حيود الأشعة السينية (XRD) لتحديد وقياس التبلور وحجم الجزيئات. واثبتت النتائج التركيب مكعب الوجه للفضة والتركيب السداسي لاوكسيد الزنك ، حيث ان حجم البلورة كان 21 نانومتر و 29 نانومتر للفضة وأكسيد الزنك على الترتيب. اما باستخدام FTIR فقد لوحظ وجود الفضة واوكسيد الزنك .

فحصت الخواص البصرية باستخدام مطياف الاشعة الفوق البنفسجية – المرئية ، حيث تم قياس طيف الامتصاص للمواد المستخدمة. اظهر طيف الامتصاص لمستخلص جذور اشواغاندا واوكسيد الزنك عند المنطقة الفوق البنفسجية ، بينما امتدت الاستجابة الضوئية لمادة الفضة بعد خلطها مع اشوغندا باتجاه المنطقة المرئية.

تم دراسة الخصائص السطحية لمستخلص جذوراشواغاندا باستخدام مجهر القوة الذرية (AFM) بمعدل حجم الحبيبة للعينة وتساوي 72.24 نانومتر.

أوضحت نتيجة EDX أن التركيب الكيميائي وكمية جذور أشواغاندا تتطابق تمامًا مع المادة الأساسية المستخدمة ، حيث يثبت طيف EDX أن جذور الأشواغاندا تتكون من الكالسيوم والنحاس والكربون والأكسجين.

اثبتت نتائج FESEM أن العينات المحضرة على شكل زهرة مكونه من عدة قضبان لاوكسيد الزنك ، في حين ان الفضة على شكل جسيمات كروية .

عزلت وشخصت البكتريا اعتمادا على زراعتها على اوساط اختيارية ، وخصائصها الزرعية ، ومظهرها الخارجي في صبغة غرام ، واكدت أخيرًا بواسطة نظام اختبار Vitek 2 المدمج.

تم تطبيق الجسيمات النانوية المحضرة بطريقة التخليق الاخضر على نمو بكتريا سالبة الجرام وإيجابية الجرام. وأيضا تأثير إشعاع ليزر دايود ذو الطول الموجي 410 نانومتر على نمو الإشريكية القولونية سالبة الجرام والمكورات العنقودية الذهبية إيجابية الجرام . بعد التشعيع ، حسبت اعداد وحدات تكوين المستعمرة في المليتر باستخدام الاليزا (ELISA).

أظهرت تجارب التشعيع بالليزر أن عدد وحدات تكوين المستعمرة في الملتر للإشريكية القولونية سلبية الجرام والمكورات العنقودية الذهبية إيجابية الجرام انخفض بشكل ملحوظ مع زيادة أوقات التعرض ، ووصل إلى معدل وفيات جرثومي 100 ٪ قتل للبكتريا الإشريكية القولونية عند دقيقة 15 ، بينما كان وقت التعرض (15 دقيقة) للمكورات العنقودية الذهبية لا توجد فروق ذات دلالة إحصائية في عدد تكوين المستعمرات ، فقط في وقت التعرض 3 دقائق كان عدد سجل CFU / مل انخفاضًا كبيرًا (P <0.01) مقارنة بمجموعة التحكم. وفقًا لذلك ، يبدو أن إشعاع الليزر الأزرق له تأثير اكثر حساسية على سالبة الجرام (الإشريكية القولونية) من البكتيريا موجبة الجرام (المكورات العنقوديه).

من كل ما تم ذكره سابقًا ، فإن اوكسيد الزنك وجسيمات الفضة النانوية المحضرة بطريقة التخليق الاخضر وتشعيع ليزر دايود ذو الطول الموجي 410 نانومتر على نمو سالبة الجرام وإيجابية الجرام هي طريقة فعالة للنشاط المضاد للبكتيريا.

وزارة التعليم العالي والبحث العلمي

جامعه بغداد

معهد الليزر للدراسات العليا

دراسة تأثير اوكسيد الزنك والفضة النانويه على البكتريا بوجود وعدم 410 nm دايود ليزر

رسالة مقدمة الى

معهد الليزر للدراسات العليا / جامعة بغداد /لاستكمال متطلبات نيل شهادة

ماجستير علوم في الليزر/ الفيزياء

من قبل

هبة تقي صالح

بكالوريوس علوم فيزياء طبية – 2008

بأشراف

الاستاذ المساعد الدكتورة زينب فاضل مهدي

1442هـ 2020 م